WASHINGTON UNIVERSITY
SEVER INSTITUTE OF TECHNOLOGY
DEPARTMENT OF CIVIL ENGINEERING

RESPONSE MODIFICATION OF BUILDINGS AND BRIDGES: COMPARATIVE STUDIES IN SEISMIC CONTROL

by

Laura M. Jansen

Prepared under the direction of Professor Shirley J. Dyke

A thesis presented to the Sever Institute of
Washington University in the partial fulfillment
of the requirements of the degree of

MASTER OF SCIENCE

December, 2000

Saint Louis, Missouri

WASHINGTON UNIVERSITY
SEVER INSTITUTE OF TECHNOLOGY
DEPARTMENT OF CIVIL ENGINEERING

ABSTRACT

RESPONSE MODIFICATION OF BUILDINGS AND BRIDGES:
COMPARATIVE STUDIES IN SEISMIC CONTROL

by Laura M. Jansen

ADVISOR: Professor Shirley J. Dyke

December, 2000
Saint Louis, Missouri

This thesis presents the results of research to evaluate the effectiveness of modern control strategies for the mitigation of earthquake induced hazards in building and bridge structures. Through a numerical example, a six story building structure with magnetorheological (MR) dampers on the lower two floors is used to evaluate the performance of a number of recently proposed semi-active control algorithms. The semi-active control algorithms considered include the Lyapunov controller, decentralized bang-bang controller, modulated homogenous friction algorithm, and a clipped optimal controller. Through simulation of the building structure using the El Centro earthquake, the reductions in inter-story

drifts, absolute accelerations, and relative displacements are examined and compared for each semi-active control algorithm.

In addition to the application of control for a building structure, control of a bridge structure is studied using purely passive, active, and semi-active control strategies. Linear and nonlinear models are developed for a multi-span simply supported bridge. For the nonlinear bridge model, two models, the bilinear and the Bouc-Wen, are considered to represent the nonlinear behavior of the bearings. Through simulation, the behavior of each bearing model is compared. A linear bridge model as well as a nonlinear bridge model using the bilinear bearing model are used for the control study. Several device placement location cases are considered to determine the most effective placement of devices. Using synthetic ground motion records generated based on a modified approach to the spectrum compatible ground acceleration approach, the bridge models are simulated for each control strategy. Furthermore, bridge structural responses and bearing and control forces are compared for each control algorithm. The most effective device placement is chosen and the effectiveness of the purely passive, active, and semi-active control devices are compared.

To my husband, Andy; my daughter, Sarah;
and especially my mom, dad, and sister.

Contents

Tables

Figures

Chapter 1

Introduction

1.1 General Remarks

Catastrophic failures occur in civil engineering structures, such as buildings and bridges, during seismic events. The costs of repairing and restoring these structures can be enormous. For example, during the 1989 Loma Prieta Earthquake (6.9 Mw) approximately 21,500 building structures and 71 bridge structures were damaged resulting in 8.3 billion dollars in direct losses (DIS, Inc., 2000). More recently, during the 1999 Izmit, Turkey (M7.4) Earthquake it is estimated that at least 20,000 building structures collapsed or suffered severe damage along with isolated bridge collapses at the fault crossing locations (EQE, 1999).

There is a need within the civil engineering community to develop mitigation methods that will be effective in reducing these earthquake hazards and costs. The application of modern control strategies to civil engineering structures is being researched for use in controlling structural responses due to seismic loading. In particular, passive, active, and semi-active control strategies are being investigated.

The focus of this thesis is on the application of various control strategies for building and bridge structures. In particular, a number of semi-active control algorithms are examined for use with multiple MR dampers to control a building structure. In addition, the effectiveness of the addiction of control to a bridge structure is investigated using ideal passive, active, and semi-active control strategies.

1.2 Literature Review

For building structures, semi-active control systems have received a great deal of attention in recent years. Semi-active devices are attractive because they combine the best features of passive and active systems. Semi-active devices are characterized by their ability to dynamically vary their properties with a minimal amount of power (Housner *et al*., 1997; Spencer and Sain, 1997). Because semi-active devices can only absorb or store vibratory energy in a structure by reacting to its motion, they are considered to be stable (in a bounded-input, bounded-output sense). Thus, semi-active devices are expected to offer effective performance over a variety of amplitude and frequency ranges.

Within the class of semi-active control devices, one of the most promising devices is the magnetorheological (MR) damper. Magnetorheological (MR) dampers have, over the last several years, been recognized as having a number of attractive characteristics for use in vibration control applications (Kamath and Wereley, 1995, 1997a-b; Gordaninejad, 1999; Weiss, et. al., 1994; Ginder, et. al., 1996; Spencer et al., 1997b; Spencer and Sain, 1997; Dyke and Spencer, 1996; Dyke et al., 1998). MR fluids were developed in the 1940's (Winslow, 1947; Rainbow, 1948), and consist of a suspension of iron particles in a carrier medium such as oil. Application of a magnetic field to the fluid causes the particles to align and interparticle bonds increase the resistance of the fluid, turning the fluid into a semi-solid (Weiss, et. al., 1994; Ginder, et. al., 1996). MR dampers are relatively inexpensive to manufacture because the fluid properties are not sensitive to contaminants. Other attractive features include their small power requirements, reliability, and stability. Requiring only 20–50 watts of power, these devices can operate with a battery, eliminating

the need for a large power source or generator. Because the device forces are adjusted by varying the strength of the magnetic field, no mechanical valves are required, making a highly reliable device. Additionally, the fluid itself responds in milliseconds, which allows for the development of devices with a high bandwidth.

MR dampers have demonstrated promise for civil engineering applications in both analytical and experimental studies. Spencer *et al.*, (1997d) developed a phenomenological model for an MR damper based on the Bouc-Wen hysteresis model (Wen, 1976). This model was subsequently used to demonstrate the capabilities of MR dampers (Dyke *et al.*, 1996a–d). Further, Dyke, *et al.* (1998) conducted an experiment using a single MR damper to control a three-story structure. An evaluation of these control strategies was conducted for use with a single MR damper (Dyke and Spencer, 1997). In a numerical example, a linear multi-story building was controlled with a single MR damper. The results demonstrated that the performance of the controlled system is highly dependent on the choice of algorithm. Further studies have examined the effectiveness of the clipped-optimal controller for multi-input MR control systems (Yi et al., 1998, 1999a,b; Dyke et al., 1999; Dyke and Spencer, 1996). Additionally, a 20-ton MR damper is being tested at the University of Notre Dame (Spencer et al., 1997b; Carlson and Spencer, 1996b).

One challenge in the use of semi-active technology is in developing nonlinear control algorithms that are appropriate for implementation in full-scale structures. A number of control algorithms have been adopted for semi-active systems. In one of the first examinations of semi-active control, Karnopp *et al.* (1974) proposed a “skyhook” damper control algorithm for a vehicle suspension system and demonstrated that this system offers improved performance over a passive system when applied to a single-degree-of-freedom system. Feng and Shinozukah (1990) developed a bang-bang controller for a hybrid controller on a bridge. More recently a control strategy based on Lyapunov stability theory has been proposed for ER dampers (Brogan, 1991; Leitmann, 1994). The goal of this algorithm is to reduce the responses by minimizing the rate of change of a Lyapunov function. McClamroch and Gavin (1995) used a similar approach to develop a decentralized bang-

bang controller. This control algorithm acts to minimize the total energy in the structure. A modulated homogeneous friction algorithm (Inaudi, 1997) was developed for a variable friction device. Clipped-optimal controllers have also been proposed and implemented for semi-active systems (Sack and Patten, 1994; Sack et al., 1994; Dyke, 1996a–d).

The effective utilization of multiple control devices is an important step in the examination of semi-active control algorithms. A typical control system for a full-scale structure is expected to have control devices distributed throughout a number of floors. Because of the inherent nonlinear nature of these devices, one of the challenging aspects of utilizing this technology to achieve high levels of performance is in the development of appropriate control algorithms. The proper selection of a control algorithm may be dependent on the type of nonlinearity present in the semi-active device, the available feedback measurements, or the number of devices to be implemented in the structure.

Promising research is also being conducted for the application of modern control strategies to bridge structures. Bridges in the US are being used well beyond their design lifetime, and inexpensive and effective techniques are needed for maintaining the reliability of such structures. For the protection of bridges, an important goal is to protect both superstructure (deck, girder) and supporting structure (column, pier). Both analytical and experimental studies have been conducted to evaluate the performance of numerous control techniques for bridges.

Base isolation systems (passive systems), such as sliding isolation and elastomeric systems, have been used frequently in bridge structures. Base isolation systems have been shown to reduce bridge deck acceleration responses and limit damage to piers supporting the bridge deck (Nagarajaiah et al., 1993). A drawback of the sliding isolation systems, however, is that for large earthquakes larger forces are transmitted with excessive bearing displacement. One method that has proven effective in reducing bridge response from earthquake motion is the use of hybrid protective systems, a combination of passive isolation systems and active devices. In a hybrid system, the passive isolation system is used to

reduce the ground motion transmitted to the bridge girder, while the active devices are used to further control the bridge responses (Yang et al., 1995). One type of hybrid protective system, rubber bearings and variable dampers, has been demonstrated to be very effective for protecting seismically-excited bridges (Kawashima et al., 1991, 1992; Kawashima and Unjoh, 1994; Feng and Shinozuka, 1990; Yang et al., 1993, 1995). Furthermore, another hybrid protective system, sliding bearings and variable dampers or actuators, has also been investigated for the protection of seismically-excited structures (Feng et al., 1991; Nagarajaiah et al., 1992, 1993; Riley et al., 1992; Reinhorn et al., 1993a, 1993b; Yang et al., 1993, 1995).

Through a numerical simulation, Feng and Shinozuka (1990) compared the effectiveness between the use of a passive isolator and a hybrid controller using a variable damper to reduce bridge vibration under earthquake loading. For the study, the hybrid system was modeled as an elastic spring in parallel with a damper having a controllable viscous damping coefficient. Both a bang-bang and an instantaneous optimal semi-active controller were developed for the hybrid controller. The results show that while the passive isolator is able to reduce the response acceleration of the bridge girder, at the same time large relative displacements between the girder and the piers are produced. However, using the hybrid system and the proposed semi-active controllers, the displacements can be decreased significantly over the passive control system with a slightly larger decrease in acceleration also over the passive control system. Kawashima and Unjoh (1994) also investigated the use of a variable damper to control bridge responses induced by an earthquake. Analytical and experimental studies with two variable dampers installed between the deck and piers, with the deck supported by elastic isolators (rubber bearings), were conducted to examine the effectiveness of the variable damper. The analytical study revealed that the variable damper was able to significantly reduce peak deck displacement and acceleration and peak bending moment at the bottom of the piers over the uncontrolled case. The experimental tests also confirmed the effectiveness of the variable damper in reducing bridge responses induced by earthquakes.

Through analytical and experimental studies, Nagarajaiah et al. (1993) investigate the use of a hybrid control system for bridges using sliding bearings, with recentering springs, in parallel with servo hydraulic actuators. A new control law with absolute acceleration feedback was developed to control the hybrid system. The results show that the hybrid system is able to produce significantly reduced deck acceleration response while still maintaining the sliding displacements within an acceptable range. Furthermore, these reductions are evident regardless of the frequency content of the earthquake and for both large and moderate earthquakes. When comparing the hybrid system to the passive system, Nagarajaiah et al. (1993) show that the hybrid system is able to achieve greater reductions in deck acceleration, however, deck relative displacement is slightly increased but still within an acceptable range. Also, by lowering the coefficient of friction of the sliding bearings for the passive case, a greater reduction in deck acceleration can be achieved, but at the expense of much larger deck relative displacements. Finally, through comparison with experimental tests, Nagarajaiah et al. (1993) confirm that the analytical model is able to reliably predict the responses of the system.

The advantages of two types of protective systems, (i) rubber bearings and variable dampers and (ii) sliding bearings and actuators are presented through simulation in Yang et al. (1995). Through a numerical example, a multi-degree of freedom bridge model using each protective system is controlled using newly developed control methods. The results show that the effectiveness of the sliding isolation system is improved greatly with the use of actuators. In addition, the hybrid system consisting of rubber bearings and variable dampers also significantly improves the performance of seismically-excited bridges. However, in comparison with the variable dampers, when replacing the variable dampers with passive viscous dampers, the optimal passive damper is quite effective.

Recently, there has been promising research on the effectiveness of “smart” (semi-active) devices, in particular the MR damper to control seismically induced bridge responses (Liu et al., 2000; Nagarajaiah et al., 2000; Ramallo et al., 2000). Nagarajaiah et al. (2000) studied the performance of MR dampers in sliding isolated bridges subjected to near fault

earthquake ground motions. Through experimental testing, a scaled single span sliding isolated bridge model with four sliding bearings and one MR damper connected between one pier and the deck was tested. Five different earthquakes, some of which were near source, were used for the tests. In addition, the test cases included MR damper off (constant 0 V), MR damper on (constant 4 V), and the controlled case where the voltage was switched between 0 and 4 V. A new sliding mode controller was developed by the authors to control the MR damper. The results showed that with the MR damper off the total force, which is composed of the frictional force in the sliding isolation system, the MR damper force, and the spring force, is decreased but bearing displacement is increased. Furthermore, with the MR damper always on, bearing displacement decreases but energy dissipation increases significantly. For the controlled case, less energy is dissipated and both bearing displacement and total force are reduced.

The effectiveness of several base isolation strategies, including isolation systems with lead rubber bearings and with smart dampers, is discussed in Ramallo et al. (2000). From the results, the lead rubber bearing isolation systems, or passive systems, were shown to effectively isolate the building in many cases, but were not optimal for the wide range of ground motion. However, because of their ability to adapt to various excitations, the smart damping systems were able achieve better response reductions.

Lui et al. (2000) perform open and closed loop control experimental tests, under both simple harmonic and simulated earthquake excitation, on a scaled bridge structure to demonstrate the effectiveness of the MR dampers in suppressing bridge deck displacement with respect to the base. The experimental structure is a 1/12-scaled two-span bridge with two abutments at the base and MR dampers mounted on the underside of the bridge deck, attached to one of the abutments. The results show that semi-active control is able to reduce the relative displacement between the deck and the abutment, while also limiting peak damper forces and deck acceleration.

This research will expand upon and compliment the previous research in the field in several ways. For example, the examination of semi-active control algorithms for the utilization of multiple-control devices for implementation in a building structure will be investigated. In particular, two MR dampers will be implemented in a building structure and various semi-active control algorithms will be compared for their effectiveness in reducing building responses due to earthquake loading. In addition, purely passive, active, and semi-active control strategies will be studied for use in a bridge. Furthermore, both a linear and nonlinear bridge model will be used for the control study.

1.3 Objectives and Scope

The objective of this research is to investigate the effectiveness of various control strategies for building and bridge structures in order to reduce seismic structural responses. The background for the development of the ground motion records used in the control study of a bridge structure as well as the control strategies used in the both the building and bridge control studies will be discussed in Chapter 2. Chapter 3 presents a comparison of a number of recently proposed control algorithms to control a six story structure with MR dampers on the lower two floors. In Chapter 4, the linear and nonlinear bridge models used in the control study will be formulated. In addition, two nonlinear bearing models, a bilinear model and a Bouc-Wen model (Wen, 1976) will be compared in Chapter 4. The effectiveness of the control strategies for the linear and nonlinear bridge models will be addressed in Chapter 5. Finally, Chapter 6 summarizes the research and gives recommendations for future investigations.

Chapter 2

Background

For the bridge study, synthetic ground motion records were used to evaluate and compare the effectiveness of the passive, active, and semi-active control strategies. The ground motion records were generated based on a modified approach to the spectrum compatible ground acceleration approach (Clough and Penzien, 1993). The steps used in generating the ground motion records will be described in this chapter along with background relating to the control strategies implemented in the building and bridge control studies.

2.1 Modified Spectrum Compatible Approach

The modified spectrum compatible approach generates ground motion records that are compatible with a model response spectrum. The following steps were used to generate the ground motion records:

1. Determine model response spectrum to be used.

   For this study, the California Department of Transportation (CALTRANS) spectrum C, shown in Fig. 2-1, was used as the model response spectrum.

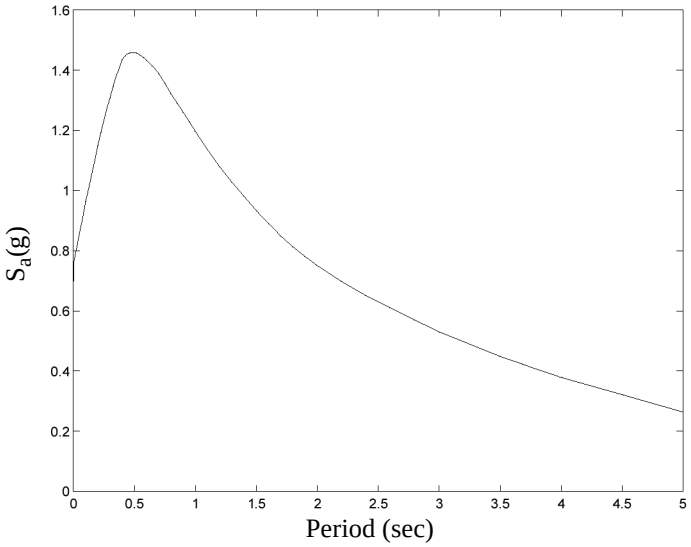

FIGURE 2-1 CALTRANS-C Response Spectrum

2. Calculate two filtering functions, $H_1(iw_k)$ and $H_2(iw_k)$, given by

$$H_1(i\omega_k) = \frac{\left[1 + 2 \cdot i \cdot x_1 \cdot \left(\frac{w_k}{w_1}\right)\right]}{\left[\left(1 - \left(\frac{w_k}{w_1}\right)^2\right) + 2 \cdot i \cdot x_1 \cdot \left(\frac{w_k}{w_1}\right)\right]} \text{ and} \tag{2-1}$$

$$H_2(iw_k) = \frac{\left(\frac{w_k}{w_2}\right)^2}{\left[\left(1 - \left(\frac{w_k}{w_2}\right)^2\right) + 2 \cdot i \cdot x_2 \cdot \left(\frac{w_k}{w_2}\right)\right]} \tag{2-2}$$

Where $w_k = k \cdot \Delta w$ and Δw are chosen based on the model response spectrum. Eq. (2-1) is the Kanai/Tajimi filter function which is a low-pass filter and Eq. (2-2) is a high-pass filter. The parameters w_1 and x_1 are some characteristic ground frequency and damping ratio, respectively. Also, the parameters w_2 and x_2 are chosen to produce the desired filtering of the very low frequencies (Clough and Penzien, 1993).

3. Calculate the power spectral density of the absolute ground acceleration, $S_a(w_k)$, by

$$S_a(w_k) = H_1(iw_k) \times H_1^*(iw_k) \times H_2(iw_k) \times H_2^*(iw_k) \times S_o \tag{2-3}$$

where S_o is the intensity of the excitation and a (*) indicates complex conjugate.

4. Generate a synthetic time history using

$$a(t) = \sum_k \sqrt{4 \cdot S_a(w_k) \cdot \Delta w} \cdot \sin(w_k \cdot t + \theta_k) \qquad (2\text{-}4)$$

   Where θ_k is a random variable uniformly distributed between 0 and 2π and t is time.

5. Compute the pseudo-acceleration response spectrum of the generated time history for comparison with the model response spectrum.

2.1.1 Construction of Ground Motion Records

In constructing a time history, initial values for the parameters w_1, x_1, w_2, x_2, and S_o were first selected. In addition, Δw and k were chosen as 0.5 and 50, respectively.With all parameters defined, one synthetic time history was generated and its corresponding pseudo-acceleration response spectrum was computed, following steps 2-5 from above. The generated pseudo-acceleration response spectrum was compared to the CALTRANS-C model response spectrum given in step 1. Initially, the two spectrums were not an acceptable match. Therefore, the parameters w_1, x_1, w_2, x_2, and S_o were adjusted and the procedure (steps 2-5) was repeated until a reasonable match was obtained with respect to the model response spectrum. The final set of parameters was then used to generate a number of different synthetic time histories to ensure that all of the corresponding pseudo-acceleration response spectrum were indeed an acceptable match with the model response spectrum. Figure 2-2 shows two generated ground motions and a comparison of their psuedo-acceleration response spectrum to the CALTRANS-C model response spectrum

.

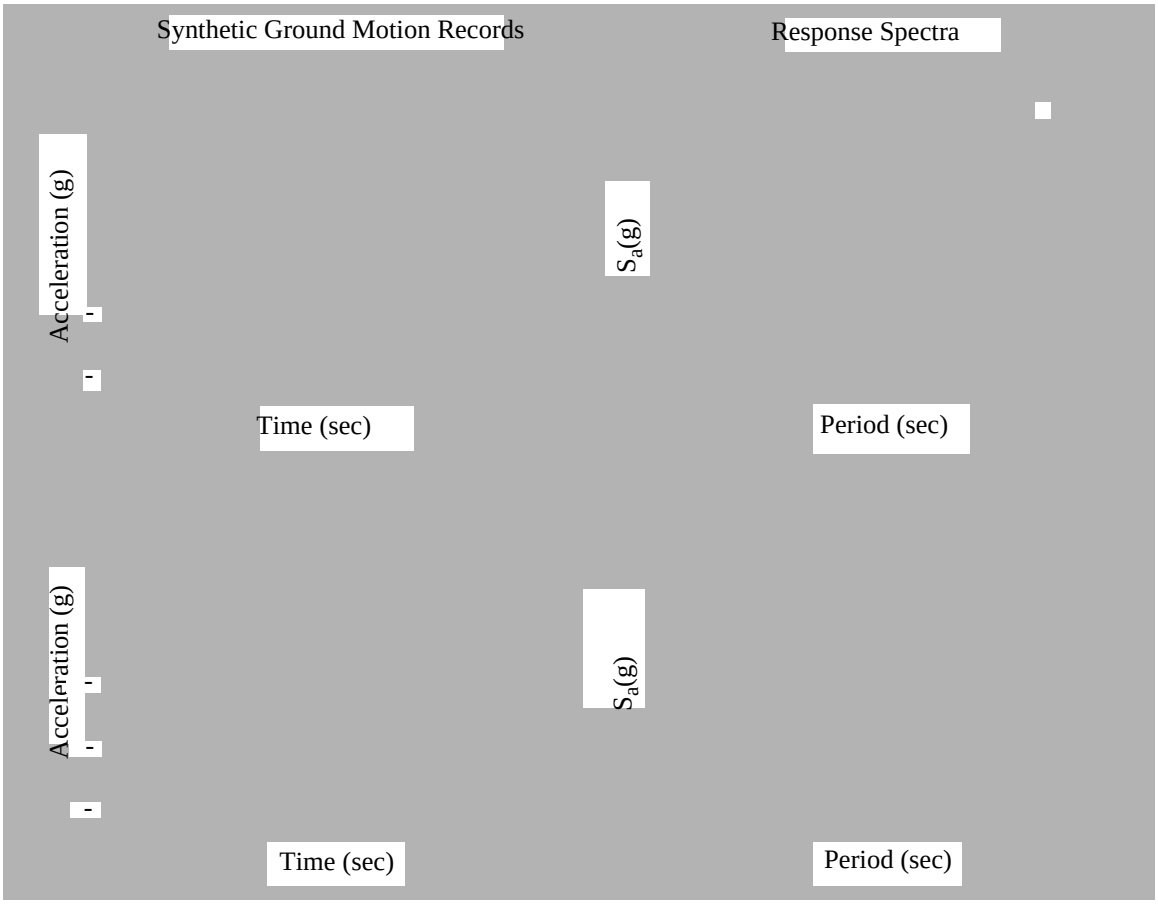

FIGURE 2-2 Comparison of CALTRANS-C Response Spectrum and Synthetic Psuedo-Acceleration Response Spectrum

The final set of parameters was w_1 = 10 radians/sec., x_1 = 0.4, w_2 = 0.1∗(2π) radians/sec., x_2 = 0.6, and S_o = 1/(45)^2. These parameters were used to generate all ground motion records used in the bridge control study.

2.2 Device Modeling and Control

Consider, for example, a seismically excited structure with *n* control devices. Assuming that the forces provided by the control devices are adequate to keep the response of the primary structure from exiting the linear region, the equation of motion can be written as

$$\mathbf{M}_s\ddot{\mathbf{x}} + \mathbf{C}_s\dot{\mathbf{x}} + \mathbf{K}_s\mathbf{x} = \mathrm{L}\mathbf{f} - \mathbf{M}_s\mathrm{G}\ddot{x}_g \tag{2-5}$$

where **x** is a vector of relative displacements of the floors of the structure, $\ddot{x}_g$ is a one-dimensional ground acceleration, $\mathbf{f} = [f_1, f_2, \ldots f_n]^T$ is the vector of measured control forces generated by the *n* control devices, Γ is a column vector of ones, and Λ is a vector determined by the placement of the control devices in the structure. The state-space form of this eqaution will take the following form

$$\dot{\mathbf{x}}_s = \mathbf{A}\mathbf{x}_s + \mathbf{B}\mathbf{f} + \mathbf{E}\ddot{x}_g \tag{2-6}$$

$$\mathbf{y} = \mathbf{C}_y\mathbf{x}_s + \mathbf{D}_y\mathbf{f} + \mathbf{F}_y\ddot{x}_g + \mathbf{v} \tag{2-7}$$

$$\mathbf{z} = \mathbf{C}_z\mathbf{x}_s + \mathbf{D}_z\mathbf{f} + \mathbf{F}_z\ddot{x}_g \tag{2-8}$$

where $\mathbf{x_s}$ is the state vector, **y** is the vector of measured outputs, **z** is the regulated output vector, **v** is a vector of measurement noises, and $\mathbf{A}$, $\mathbf{B}$, $\mathbf{E}$, $\mathbf{C}_y$, $\mathbf{D}_y$, $\mathbf{F}_y$, $\mathbf{C}_z$, $\mathbf{D}_z$, and $\mathbf{F}_z$ are matrices of appropriate dimension.

In the bridge control study, passive, active, and semi-active control systems are implemented and compared for a bridge structure. The passive, active, and semi-active devices considered for the bridge control study are all modeled as ideal devices. As a result, the device models do not included actuator dynamics or control-structure interaction. This modeling is appropriate because the purpose of the bridge control study is to examine the best possible performance for each class of systems. In addition, the control laws are based on readily measurable responses to ensure that the control laws are implementable on a physical system. For the seismically excited bridge structure this includes the absolute acceleration of each bridge mass. The forces provided by the actuators are also measured in the semi-active case to determine the control action. The approach used to model the ideal passive, active, and semi-active control devices for the bridge control study is described in the following sections.

2.2.1 Passive Control

A passive control device is a device that develops forces at the location of the device by utilizing the motion of the structure. Through the forces developed, a passive control device reduces the energy dissipation demand on the structure by absorbing some of the input energy (Soong and Dargush, 1997). Thus, a passive control device cannot add energy to the structural system. Furthermore, a passive control device does not require an external power supply. Examples of passive control devices, depicted in Figure 2-3, include viscous fluid dampers, tuned mass dampers, and base isolation systems.

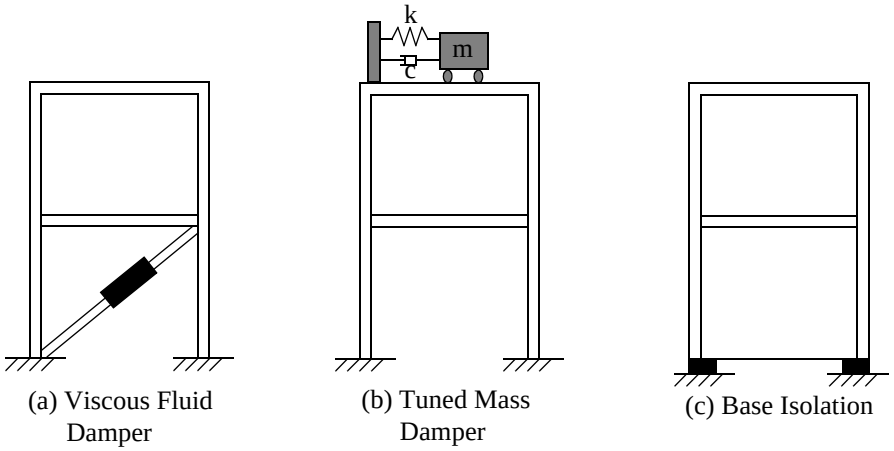

FIGURE 2-3 Passive Control System Examples

A viscous fluid damper uses the flow of fluids to achieve the needed energy dissipation. A tuned mass damper system consists of a spring and mass system attached to the main structure. By tuning the natural frequency of the tuned mass damper to that of the excitation, a tuned mass damper works to control unwanted vibration in the main structure. In a structure with a base isolation system, the typical fixed-base design is replaced with an isolation system, such as elastomeric (rubber) bearings, between the base of the building and the ground. The effect of the base isolation system is to be stiff under vertical loads and at the same time flexible under lateral loads. Therefore, the result is that the base isolation system will reduce forces transmitted to the structure.

In the bridge control study, an ideal viscous damper is used as the passive control device. A block diagram of an ideal viscous damper is shown in Figure 2-4 (Yi and Dyke, 2000).

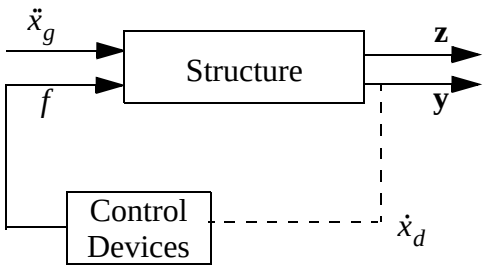

FIGURE 2-4 Block Diagram of Ideal Passive System

The force *f* generated by the ith viscous damper is defined by (Yi and Dyke, 2000)

$$f_i(t) = -c\dot{x}_d(t) \tag{2-9}$$

where *c* is the viscous damping coefficient and $\dot{x}_d(t)$ is the relative velocity at the location of the device. The damping coefficient *c* is varied to achieve optimal results.

2.2.2 Active Control

With an active control device, actuators are used to generate the desired control forces. In contrast to a passive control device, an active control device can add energy to the structural system. An active control device requires an external power supply to operate the actuators that will generate the forces to be applied to a structure. Feedback measurements of the excitation and/or structural responses are used by an active control system to develop the required control forces. The structural responses are measured using sensors mounted at certain locations on the structure. Furthermore, a control algorithm uses the feedback measurements to determine the appropriate control forces to be applied to the structure.

Some examples of active control devices, depicted in Figure 2-5, are active bracing systems, active mass damper systems, and active base isolation systems.

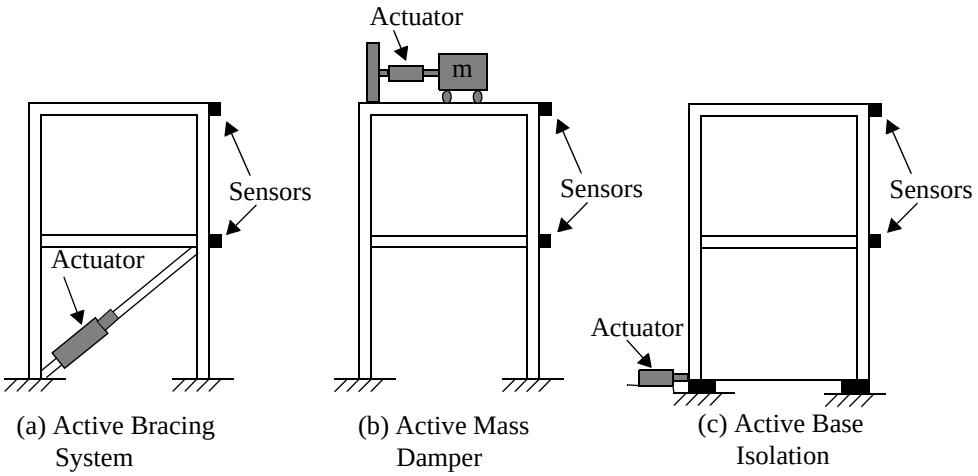

FIGURE 2-5 Active Control System Examples

For the bridge control study, the active devices are modeled as ideal force actuators. A block diagram of an ideal active system is shown in Figure 2-6 (Yi and Dyke, 2000).

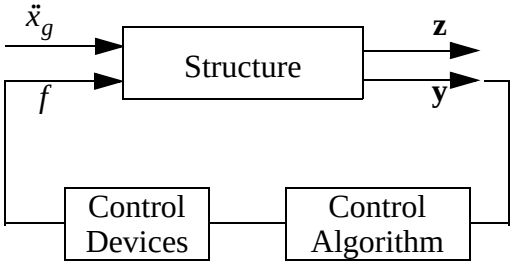

FIGURE 2-6 Block Diagram of Ideal Active System

The use of ideal active devices implies the ability of the actuators to instantaneously and exactly supply the force commanded by the control algorithm. Thus, the force provided by the ith active control device is given by (Yi and Dyke, 2000)

$$f_i(t) = u_{ic}(t) \tag{2-10}$$

where $u_{ic}(t)$ is the command force for the ith device determined by the control algorithm. It should be noted that although actuator dynamics and/or control-structure interaction

will occur in the physical system, they are not considered in the ideal model of the active device (Dyke *et al.*, 1995).

For seismically excited structures, the H_2/LQG control law has been shown to be an effective control algorithm for the active device (Dyke et al., 1996d,e). For this control law, the ground excitation $\ddot{x}_g$ is taken to be a stationary white noise. Furthermore, the regulated outputs, $\mathbf{z}$, are weighted with an infinite horizon performance index (cost function) given by

$$J = \lim_{\tau \to \infty} \frac{1}{\tau} \mathrm{E}\left[\int_0^{\tau} \{(\mathbf{C}_z\mathbf{x} + \mathbf{D}_z\mathbf{u})^{\mathrm{T}}\mathbf{Q}(\mathbf{C}_z\mathbf{x} + \mathbf{D}_z\mathbf{u}) + \mathbf{u}^{\mathrm{T}}\mathbf{R}\mathbf{u}\}(dt)\right] \tag{2-11}$$

where **R** is an identity matrix and the elements of the weighting matrix **Q** are selected to appropriately weight the regulated outputs (Yi and Dyke, 2000). The weighting cases for the regulated outputs and the corresponding **Q** matrices used for the bridge control study are given in Table 2-1. Also, the measurement noise is assumed to be a identically distributed, statistically independent Gaussian white noise process with $S_{\ddot{x}_g\ddot{x}_g} / S_{v_i v_i} = \gamma = 25$.

TABLE 2-1. Weighting Matrices for Control Designs in Bridge Study

Case	*Weighting Type*	*Regulated Output Vector,* $\mathbf{z}$	*Corresponding Weighting Matrix,* $\mathbf{Q}$
AA	**All bridge mass accelerations**	$\mathbf{z}^T = [\ddot{x}_{a1}\ddot{x}_{a2}\ddot{x}_{a3}\ddot{x}_{a4}\ddot{x}_{a5}]$	$\mathbf{I}_{5x5}$
AD	**All bridge mass displacements**	$\mathbf{z}^T = [x_1 x_2 x_3 x_4 x_5]$	$\mathbf{I}_{5x5}$
EN	**Energy**	$\mathbf{z}^T = [x_1 x_2 x_3 x_4 x_5 \dot{x}_1 \dot{x}_2 \dot{x}_3 \dot{x}_4 \dot{x}_5]$	$\begin{bmatrix} \mathbf{K} & \mathbf{0} \\ \mathbf{0} & \mathbf{M} \end{bmatrix}$
ID	**Bridge deck inter-mass displacements**	$\mathbf{z}^T = [x_1 x_2 - x_1 x_3 - x_2 x_3]$	$\mathbf{I}_{4x4}$

The control law is of the form (Spencer et al., 1998b)

$$\mathbf{u} = -\mathbf{K}_u\hat{\mathbf{x}} \tag{2-12}$$

where $\hat{\mathbf{x}}$ is the Kalman filter estimate of the state vector. The full state feedback gain matrix $\mathbf{K}_u$ for the deterministic regulator problem is given by

$$\mathbf{K}_u = \tilde{\mathbf{R}}^{-1}(\tilde{\mathbf{N}} + \mathbf{B}^T\underset{\sim}{\mathbf{P}}) \tag{2-13}$$

where $\underset{\sim}{\mathbf{P}}$ is the solution of the algebraic Riccati equation given by

$$\mathbf{0} = \underset{\sim}{\mathbf{P}}\tilde{\mathbf{A}} + \tilde{\mathbf{A}}^T\underset{\sim}{\mathbf{P}} - \underset{\sim}{\mathbf{P}}\mathbf{B}\tilde{\mathbf{R}}^{-1}\mathbf{B}^T\underset{\sim}{\mathbf{P}} + \tilde{\mathbf{Q}} \tag{2-14}$$

and

$$\tilde{\mathbf{Q}} = \mathbf{C}_z{}^T\mathbf{Q}\mathbf{C}_z - \tilde{\mathbf{N}}\tilde{\mathbf{R}}^{-1}\tilde{\mathbf{N}}^T \tag{2-15}$$

$$\tilde{\mathbf{N}} = \mathbf{C}_z{}^T\mathbf{Q}\mathbf{D}_z \tag{2-16}$$

$$\tilde{\mathbf{R}} = \mathbf{R} + \mathbf{D}_z{}^T\mathbf{Q}\mathbf{D}_z \tag{2-17}$$

$$\tilde{\mathbf{A}} = \mathbf{A} - \mathbf{B}\tilde{\mathbf{R}}^{-1}\tilde{\mathbf{N}}^T \tag{2-18}$$

The MATLAB (1999) routine *lqry.m* within the control toolbox were used to calculate $\mathbf{K}_u$.

The Kalman Filter optimal estimator is given by

$$\dot{\hat{\mathbf{x}}} = \mathbf{A}\hat{\mathbf{x}} + \mathbf{B}\mathbf{u} + \mathbf{L}(\mathbf{y}_m - \mathbf{C}_y\hat{\mathbf{x}} - \mathbf{D}_y\mathbf{u}) \tag{2-19}$$

$$\mathbf{L} = [\underset{\sim}{\mathbf{R}}^{-1}(\gamma\mathbf{F}_y\mathbf{E}^T + \mathbf{C}_y\mathbf{S})]^T \tag{2-20}$$

where $\mathbf{S}$ is the solution of the algebraic Riccati equation given by

$$\mathbf{0} = \mathbf{S}\underset{\sim}{\mathbf{A}} + \underset{\sim}{\mathbf{A}}^T\mathbf{S} - \mathbf{S}\underset{\sim}{\mathbf{G}}\mathbf{S} + \underset{\sim}{\mathbf{H}} \tag{2-21}$$

and

$$\underset{\sim}{\mathbf{A}} = \mathbf{A}^{\mathrm{T}} - \mathbf{C}_y{}^{\mathrm{T}}\underset{\sim}{\mathbf{R}}^{-1}(\gamma\mathbf{F}_y\mathbf{E}^{\mathrm{T}}) \tag{2-22}$$

$$\underset{\sim}{\mathbf{G}} = \mathbf{C}_y{}^{\mathrm{T}}\underset{\sim}{\mathbf{R}}^{-1}\mathbf{C}_y \tag{2-23}$$

$$\underset{\sim}{\mathbf{H}} = \gamma\mathbf{E}\mathbf{E}^{\mathrm{T}} - \gamma^2\mathbf{E}\mathbf{F}_y{}^{\mathrm{T}}\underset{\sim}{\mathbf{R}}^{-1}\mathbf{F}_y\mathbf{E}^{\mathrm{T}} \tag{2-24}$$

$$\underset{\sim}{\mathbf{R}} = \mathbf{I} + \gamma\mathbf{F}_y\mathbf{F}_y{}^{\mathrm{T}} \tag{2-25}$$

The MATLAB routine *lqew.m* within the control toolbox was used to calculate $\mathbf{L}$.

2.2.3 Semi-Active Control

A semi-active control device is a combination of passive and active control devices. Like passive control devices, semi-active control devices generate forces as a result of the motion of the structure and cannot add energy to the structural system. However, like with an active control device, feedback measurements of the excitation and/or structural system are used by a controller to generate an appropriate signal for the semi-active device (Symans and Constantinou, 1995). In addition, only a small external power source is required for operation of a semi-active control device. Examples of semi-active devices include variable orifice dampers, variable friction dampers, and magnetorheological dampers. These semi-active devices are implemented in the same manner as active control devices as shown in Figure 2-7.

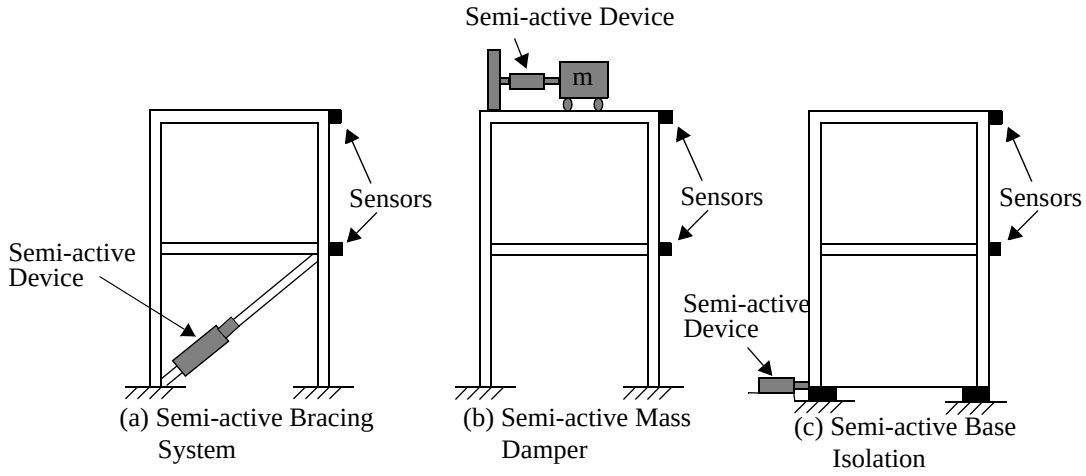

FIGURE 2-7 Semi-Active Control Device Examples

The semi-active devices used in the bridge control study are considered to be ideal semi-active devices. A block diagram of an ideal semi-active device is given in Figure 2-8 (Yi and Dyke, 2000). The dashed line in the diagram represents the control force feedback loop. This feedback loop is present because a semi-active control algorithm often uses a measure of the control force produced by the semi-active device to generate the command signal for the semi-active device.

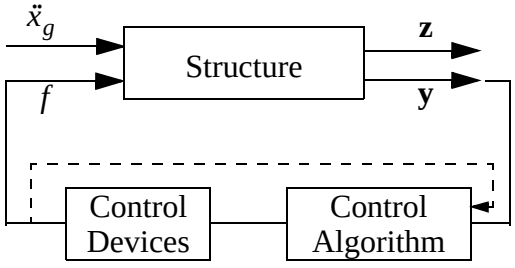

FIGURE 2-8 Block Diagram of Ideal Semi-Active Device

Ideal semi-active devices are considered to be purely dissipative devices and therefore capable of generating any control force that is in the second or fourth quadrants of the force velocity plane (see Figure 2-9).

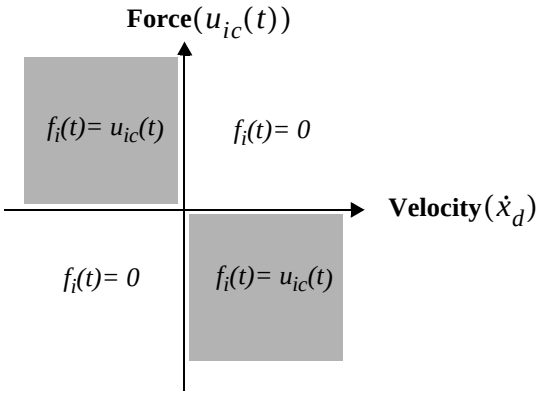

FIGURE 2-9 Graphical Representation of Control Force Determination

Thus the force provided by the ith semi-active device is given by (Yi and Dyke, 2000)

$$f_i(t) = \begin{cases} u_{ic}(t) & \text{when } \dot{x}_d u_{ic}(t) < 0 \\ 0 & \text{otherwise} \end{cases} \tag{2-26}$$

Numerous control algorithms have been developed for semi-active systems. The results of recent studies have demonstrated that the performance of semi-active systems is highly dependent on the choice of control algorithm (Dyke and Spencer, 1997; Jansen and Dyke, 1999, 2000). In chapter 3, various semi-active control algorithms will be developed and implemented to control a building structure with MR dampers.

2.3 Summary

For use with the bridge control study, described in detail later in chapters 4 and 5, synthetic ground motion records were generated using a modified spectrum compatible approach. The method of generating the synthetic time histories as well as the design of the ideal passive, active, and semi-active control devices used for the analytical bridge control study were described. In the next chapter, the development of a number of semi-active control algorithms to control semi-active MR devices in buildings will be presented along with a numerical example comparing and contrasting each algorithms effectiveness.

Chapter 3

Semi-Active Control Strategies for MR Dampers: A Comparative Study

The failure of building structures during earthquakes can be extremely devastating and costly. As a result, there is a need for the development of effective mitigation methods for application in buildings subjected to seismic loading. This chapter presents the results of a study to evaluate the performance of a number of recently proposed semi-active control algorithms for use with multiple MR dampers to control a seismically excited building structure (Jansen and Dyke, 1999, 2000). Four recently proposed semi-active control algorithms are discussed including the decentralized bang-bang controller, the Lyapunov controller, the clipped-optimal controller, and the modulated homogeneous friction controller. In addition to these, a related fifth algorithm, referred to herein as the maximum energy dissipation algorithm, is also considered. Each algorithm is formulated for use with the MR damper. Additionally, each algorithm uses measurements of the absolute acceleration and device displacements for determining the control action to ensure that the algorithms would be implementable on a physical structure.

In a numerical example, a six-story building model with MR dampers on the bottom two floors is used to compare the performance of the proposed control algorithms. This example was selected to represent the experimental system in the Washington University Struc-

tural Control and Earthquake Engineering Lab (http://www.seas.wustl.edu/research/quake/). An experimentally-verified phenomenological model based on the Bouc-Wen model is used to simulate the behavior of the MR damper. In simulation, an El Centro earthquake is used to excite the system, and the reduction in the drifts, accelerations, and relative displacements throughout the structure is examined.

3.1 Shear Mode Magnetorheological Damper Modeling

Magnetorheological dampers are semi-active devices that use magnetorheological fluids to construct a versatile damping device. Because the strength of the magnetic field controls the yield stress of the fluid, devices utilizing MR fluids are expected to be applicable for a wide range of situations. For civil engineering applications MR devices are attractive because they require only a battery for power and are quite reliable (Kamath and Wereley, 1995, 1997a-b; Kamath, et. al., 1996, 1997; Gordaninejad, 1999; Carlson and Spencer, 1996a-b; Spencer et al., 1997b; Yi et al., 1998, 1999; Dyke, et al. 1999a-b). Furthermore, they are relatively inexpensive to manufacture and maintain, and their insensitivity to temperature fluctuations makes them suitable for both indoor and outdoor applications (Carlson, 1994; Carlson and Weiss, 1994; Carlson, et. al. 1996).

In Yi et al. (1998, 1999a,b) and Dyke et al. (1999), a prototype shear mode MR damper obtained from the Lord Corporation was used for experimental testing (Jansen and Dyke, 2000). A schematic diagram of the prototype device is shown in Fig. 3-1.

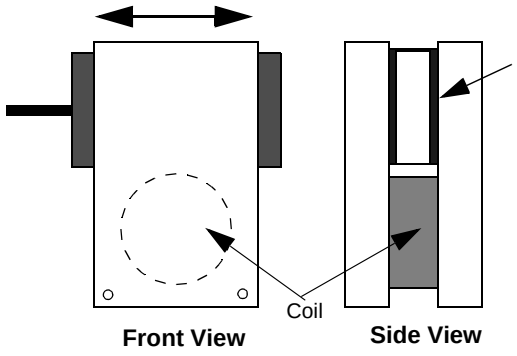

FIGURE 3-1 Schematic Diagram of a Shear Mode MR Damper

The device consists of two steel parallel plates. The dimensions of the device are $4.45\times1.9\times2.5$ cm^3 ($1.75\times0.75\times1.0$ in^3). The magnetic field produced in the device is generated by an electromagnet consisting of a coil at one end of the device. Forces are generated when the moving plate, coated with a thin foam saturated with MR fluid, slides between the two parallel plates. The outer plates of the device are 0.635 cm (0.25 in) apart, and the force capacity of the device is dependent on the strength of the fluid and on the size of the gap between the side plates and the center plate. A center plate with a thickness of 0.495 cm (0.195 in) is employed, resulting in a gap of 0.071 cm (0.028 in). Each of the control devices can generate a maximum force of 29 N, which is approximately 1.8% the weight of the structure.

Tests conducted on the experimental prototype MR damper are described in detail in Yi et al. (1998, 1999a,b) and Dyke et al. (1999). In their tests, a hydraulic actuator was used to drive the damper, and the displacement and force were measured. The velocities were calculated using a central differences approximation. Furthermore, sinusoidal, triangular, and square displacement command signals were used. Various constant and time-varying voltages were applied to the prototype MR damper to observe the characteristics of the MR damper. Yi et al. (1998, 1999a,b) and Dyke et al. (1999) obtained hysteresis loops for the shear mode MR damper through their experimental testing. An example of the typical hysteresis loops obtained from the experimental testing are provided in Figure 3-2. The response of the MR damper due to a 1.5 Hz sinusoid with an amplitude of 1.5 cm is shown

for constant voltage levels, 0 V, 1.0 V, 2.0 V, and 3.0 V, being applied to the pulse width modulation circuit used with the MR damper. The force-displacement hysteresis loop is shown in Fig. 3-2a and the force-velocity hysteresis loop is shown in Fig. 3-2b. Further details on the experimental behavior and testing of the MR damper are provided in Yi et al. (1998, 1999a,b) and Dyke, et al. (1999).

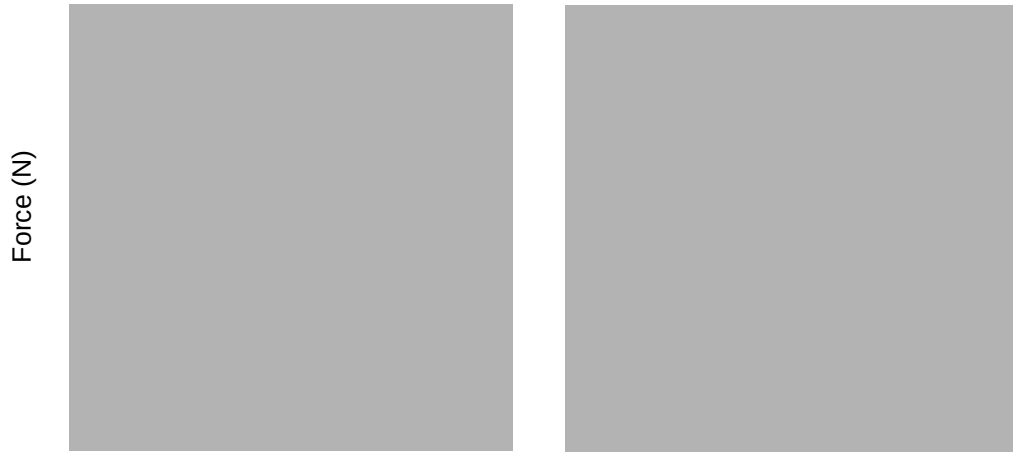

(a) Force–Displacement Hysteresis Loop **(b) Force–Velocity Hysteresis Loop**

FIGURE 3-2 Typical Responses of the Shear Mode MR Damper

Appropriate modeling of the control devices is essential for the accurate prediction of the behavior of the controlled system. The simple mechanical model shown in Fig. 3-3 was developed and shown to accurately predict the behavior of a shear-mode MR damper over a wide range of inputs (Yi, et al., 1998, 1999a,b; Dyke et a., 1999). This phenomenological model was developed based on a previous model used for the MR damper. (Spencer et al., 1997d).

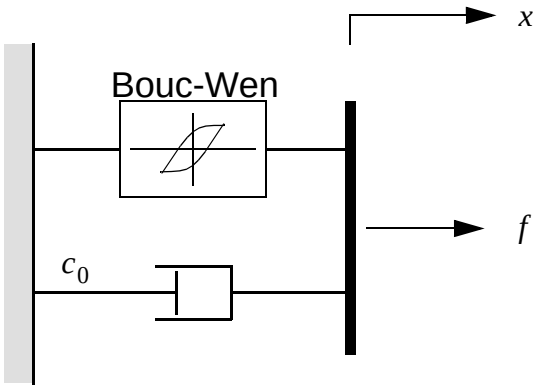

FIGURE 3-3 Mechanical Model of the Parallel Plate MR Damper

The equations governing the force *f* predicted by this model are

$$f = c_0\dot{x} + \alpha z \tag{3-1}$$

$$\dot{z} = -\gamma|\dot{x}|z|z|^{n-1} - \beta\dot{x}|z|^n + A\dot{x} \tag{3-2}$$

where *z* is an evolutionary variable that accounts for the history dependence of the response. The model parameters depend on the voltage *v* to the current driver as follows

$$\alpha = \alpha_a + \alpha_b u \qquad \text{and} \qquad c_0 = c_{0a} + c_{0b} u \tag{3-3}$$

where *u* is given as the output of the first-order filter

$$\dot{u} = -\eta(u - v)\,. \tag{3-4}$$

Eq. (3-4) is used to model the dynamics involved in reaching rheological equilibrium and in driving the electromagnet in the MR damper (Yi et al, 1998, 1999a,b; Dyke et al., 1999). This MR damper model is used to model the behavior of the MR damper herein.

3.2 Control Algorithms

Consider a seismically excited structure controlled with *n* MR dampers. Assuming that the forces provided by the control devices are adequate to keep the response of the primary structure from exiting the linear region, the equations of motion can be written as

$$\mathbf{M}_s\ddot{\mathbf{x}} + \mathbf{C}_s\dot{\mathbf{x}} + \mathbf{K}_s\mathbf{x} = \mathrm{L}\mathbf{f} - \mathbf{M}_s\mathrm{G}\ddot{x}_g \tag{3-5}$$

where **x** is a vector of the relative displacements of the floors of the structure, $\ddot{x}_g$ is a one-dimensional ground acceleration, $\mathbf{f} = [f_1, f_2, \ldots f_n]^T$ is the vector of measured control forces, defined by Eqs. (3-1) - (3-4), generated by the *n* MR dampers, Γ is a column vector of ones, and Λ is a vector determined by the placement of the MR dampers in the structure. This equation can be written in state-space form as

$$\dot{\mathbf{z}} = \mathbf{A}\mathbf{z} + \mathbf{B}\mathbf{f} + \mathbf{E}\ddot{x}_g \tag{3-6}$$

$$\mathbf{y} = \mathbf{C}\mathbf{z} + \mathbf{D}\mathbf{f} + \mathbf{v} \tag{3-7}$$

where **z** is the state vector, **y** is the vector of measured outputs, and **v** is the measurement noise vector. For these applications, the measurements typically available for control force determination include the absolute acceleration of selected points on the structure, the displacement of each control device, and a measurement of each control force.

A variety of approaches have been proposed in the literature for the control of semi-active devices. Subsequently, a selection of these approaches will be presented and evaluated in a numerical example. In developing the control laws, note that it is not possible to directly command the *i*th MR damper to generate a specified force, f_i, because the response of the MR damper is dependent on the local motion of the structure where the MR damper is attached. However, the forces produced by the MR damper may be increased or decreased by adjusting the value of the voltage applied to the current driver v_i. Based on this observation in the model, the following guidelines are used in developing the control laws: i) the control voltage to the *i*th device is restricted to the range $v_i = [0, V_{max}]$, and ii) for a

fixed set of states, the magnitude of the applied force $|f_i|$ increases when v_i increases, and decreases when v_i decreases. Furthermore, the first order lag in the device model (representing the dynamics involved in the current driver and electromagnet) limits the rate at which the MR effect is realized. Thus, in developing the control laws, one must consider the fact that the force varies continuously even when a step command signal is applied.

3.2.1 Control Based on Lyapunov Stability Theory

In some cases it is possible to employ Lyapunov's direct approach to stability analysis in the design of a feedback controller (Brogan, 1991). The approach requires the use of a Lyapunov function, denoted $V(\mathbf{z})$, which must be a positive definite function of the states of the system, **z**. Let us assume that the origin is a stable equilibrium point. According to Lyapunov stability theory, if the rate of change of the Lyapunov function, $\dot{V}(\mathbf{z})$, is negative semi-definite, the origin is stable i.s.L. (in the sense of Lyapunov). Thus, in developing the control law, the goal is to choose control inputs for each device that will result in making $\dot{V}$ as negative as possible. An infinite number of Lyapunov functions may be selected, that may result in a variety of control laws.

Leitmann (1994) applied Lyapunov's direct approach for the design of a semi-active controller. In this approach, a Lyapunov function is chosen of the form

$$V(\mathbf{z}) = \frac{1}{2}||\mathbf{z}||_P^2 \tag{3-8}$$

where $||\mathbf{z}||_P$ is the *P*-norm of the states defined by

$$||\mathbf{z}||_p = [\mathbf{z}^T\mathbf{P}\mathbf{z}]^{1/2} \tag{3-9}$$

and **P** is a real, symmetric, positive definite matrix. In the case of a linear system, to ensure $\dot{V}$ is negative definite, the matrix **P** is found using the Lyapunov equation

$$\mathbf{A}^T\mathbf{P} + \mathbf{P}\mathbf{A} = -\mathbf{Q}_P \tag{3-10}$$

for a positive definite matrix $\mathbf{Q}_P$. The derivative of the Lyapunov function for a solution of Eq. (3-6) is

$$\dot{V} = -\frac{1}{2}\mathbf{z}^T\mathbf{Q}_P\mathbf{z} + \mathbf{z}^T\mathbf{P}\mathbf{B}\mathbf{f} + \mathbf{z}^T\mathbf{P}\mathbf{E}\ddot{x}_g \tag{3-11}$$

The only term which can be directly effected by a change in the control voltage is the middle term which contains the force vector $\mathbf{f}$. Thus, the control law which will minimize $\dot{V}$ is

$$v_i = V_{max}H((-\mathbf{z})^T\mathbf{P}\mathbf{B}_i f_i) \tag{3-12}$$

where $H(\cdot)$ is the Heaviside step function, f_i is the measured force produced by the *i*th MR damper, and $\mathbf{B}_i$ is the *i*th column of the $\mathbf{B}$ matrix in Eq. (3-6). Notice that this algorithm is classified as a bang-bang controller, and is dependent on the sign of the measured control force and the states of the system. To implement this algorithm, a Kalman filter is used to estimate the states based on the available measurements (*i.e.*, device displacements, device forces, structural accelerations). Thus, in this algorithm, better performance is expected when measurements of the responses of the full structure are used. However, one challenge in the use of the Lyapunov algorithm is in the selection of an appropriate $\mathbf{Q}_P$ matrix.

3.2.2 Decentralized Bang-Bang Control

McClamroch and Gavin (1995) used a similar approach to develop the decentralized bang-bang control law for use with an electrorheological damper. In this approach, the Lyapunov function was chosen to represent the total vibratory energy in the structure (kinetic plus potential energy), as in

$$V = \frac{1}{2}\mathbf{x}^T\mathbf{K}_s\mathbf{x} + \frac{1}{2}(\dot{\mathbf{x}} + \Gamma\dot{x}_g)^T\mathbf{M}_s(\dot{\mathbf{x}} + \Gamma\dot{x}_g) \tag{3-13}$$

Using Eq. (3-5), the rate of change of the Lyapunov function is then

$$\dot{V} = \frac{1}{2}\mathbf{x}^T\mathbf{K}_s\dot{\mathbf{x}} + (\dot{\mathbf{x}} + \Gamma\dot{x}_g)^T(-\mathbf{C}_s\dot{\mathbf{x}} - \mathbf{K}_s\mathbf{x} + \Lambda\mathbf{f}) \tag{3-14}$$

In this expression, the only way to directly effect $\dot{V}$ is through the last term containing the force vector $\mathbf{f}$. To control this term and make $\dot{V}$ as large and negative as possible (maximizing the rate at which energy is dissipated), the following control law is chosen

$$v_i = V_{max}H(-(\dot{\mathbf{x}} + \Gamma\dot{x}_g)^T\mathrm{L}_i f_i) \tag{3-15}$$

where L_i is the *i*th column of the L matrix. Note that, because the only non-zero terms in the L matrix are those corresponding to the location of the MR dampers, this control law requires only measurements of the floor velocities and applied forces. Interestingly, when any of the semi-active devices are located between the ground and first floor, the absolute velocity of the first floor is required. When the control device is located in the upper floors, the interstory velocity is needed. Therefore, to implement this control algorithm, one would approximate the absolute velocity (obtain the pseudo velocity) by integrating the absolute acceleration (Spencer et al., 1997a) using

$$H(s) = \frac{39.5s}{39.5s^2 + 8.89s + 1}. \tag{3-16}$$

3.2.3 Maximum Energy Dissipation

This control algorithm is presented as a variation of the decentralized bang-bang approach proposed by McClamroch and Gavin. In the decentralized bang-bang approach, the Lyapunov function was chosen to represent the total vibratory energy in the system. Let us instead consider a Lyapunov function which represents the relative vibratory energy in the structure (*i.e.*, without including the velocity of the ground in the kinetic energy term), as in

$$V = \frac{1}{2}\mathbf{x}^T\mathbf{K}_s\mathbf{x} + \frac{1}{2}\mathbf{x}^T\mathbf{M}_s\dot{\mathbf{x}}. \tag{3-17}$$

Using the same procedure applied to develop the decentralized bang-bang approach, the term which can be directly effected by changes in the control voltage is identified and the following control law is obtained

$$v_i = V_{max} H(-\dot{\mathbf{x}}^T \Lambda_i f_i) \tag{3-18}$$

where L_i is the *i*th column of the L matrix. Note that this equation is also a bang-bang control law. As in the decentralized bang-bang approach, only local measurements (*i.e.*, the velocity and control force) are required to implement this control law. Note that if the semi-active device is not located on the first floor of the structure, the resulting control law will be the same as in the decentralized bang-bang approach. However, if the control device is on the first floor, notice that the control action depends on the relative velocity measurement rather than the absolute velocity which was used in the decentralized bang-bang approach. Both a numerical differentiation of the measured device displacements, and a subtraction of the absolute velocities using Eq. (3-16) were considered to determine the relative velocities. Numerical differentiation of the measurements of the relative displacement of the first floor was found to yield better results for this control algorithm and was used in this study.

Notice that the resulting control law will command the maximum voltage when the measured force and relative velocity are dissipating energy (producing large dissipative forces), and command the minimum voltage when energy is not being dissipated (producing small forces when the force is not dissipative). Thus, here it has been called the maximum energy dissipation algorithm.

3.2.4 Clipped-Optimal Control

One algorithm that has been shown to be effective for use with the MR damper is a clipped-optimal control approach, proposed by Dyke, *et al*. (1996c-e). The clipped-optimal control approach is to design a linear optimal controller $\mathbf{K}_C(s)$ that calculates a vector

of desired control forces $\mathbf{f}_c = [f_{c1}, f_{c2}, \ldots f_{cn}]^T$ based on the measured structural responses **y** and the measured control force vector **f** applied to the structure, *i.e.*,

$$\mathbf{f}_c = L^{-1}\left\{-\mathbf{K}_c(s)L\left\{\begin{matrix}\mathbf{y}\\ \mathbf{f}\end{matrix}\right\}\right\} \tag{3-19}$$

where $L\{\cdot\}$ is the Laplace transform.

Because the force generated in the MR damper is dependent on the local responses of the structural system, the desired optimal control force f_{ci} cannot always be produced by the MR damper. Only the control voltage v_i can be directly controlled to increase or decrease the force produced by the device. Thus, a force feedback loop is incorporated to induce the MR damper to generate approximately the desired optimal control force f_{ci}.

To induce the MR damper to generate approximately the corresponding desired optimal control force f_{ci}, the command signal v_i is selected as follows. When the *i*th MR damper is providing the desired optimal force (*i.e.*, $f_i = f_{ci}$), the voltage applied to the damper should remain at the present level. If the magnitude of the force produced by the damper is smaller than the magnitude of the desired optimal force and the two forces have the same sign, the voltage applied to the current driver is increased to the maximum level so as to increase the force produced by the damper to match the desired control force. Otherwise, the commanded voltage is set to zero. The algorithm for selecting the command signal for the *i*th MR damper is graphically represented in Fig. 3-4 and can be stated as

$$v_i = V_{\max} H(\{f_{ci} - f_i\} f_i) \tag{3-20}$$

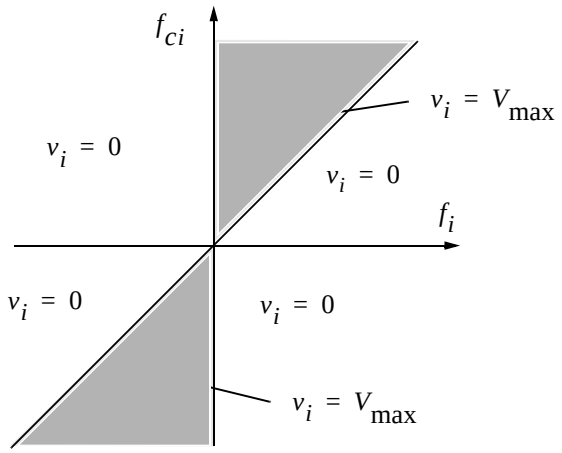

FIGURE 3-4 Graphical Representation of Algorithm for Selecting the Command Signal

Although a variety of approaches may be used to design the optimal controller, H_2 /LQG methods are advocated because of their successful application in previous studies. The approach to optimal control design is discussed in detail in (Dyke et al., 1996a-e).

3.2.5 Modulated Homogeneous Friction

Another semi-active control algorithm considered herein was originally proposed for use with a variable friction damper (Inaudi, 1997). This algorithm is considered herein because there are strong similarities between the behavior of a variable friction device and of the MR damper. In this approach, at every occurrence of a local extrema in the deformation of the device (*i.e.*, when the relative velocity between the ends of the semi-active device is zero), the normal force applied at the frictional interface is updated to a new value. The normal force, $N_i(t)$, is chosen to be proportional to the absolute value of the deformation of the semi-active device. The control law is written

$$N_i(t) = g_i \left| P[\Delta_i(t)] \right| \tag{3-21}$$

where g_i is a positive gain, and the operator $P[\cdot]$ (referred to as the prior-local-peak operator) is defined as

$$P[\Delta_i(t)] = \Delta_i(t-s), \text{ where } s = \{\min x \geq 0 : \dot{\Delta}_i(t-x)=0\}, \tag{3-22}$$

defining $\Delta_i(t-s)$ as the most recent local extrema in the deformation of the *i*th device.

Because this algorithm was developed for use with a variable friction device, the following modifications were necessary to apply it to the MR damper: i) there is no need to check if the force is greater than $\mu N_i(t)$, where μ is the coefficient of friction, because the MR damper is not subject to static friction, and ii) a force feedback loop was implemented to induce the MR damper to produce approximately the frictional force corresponding to the desired normal force. Thus, the goal is to generate a desired control force with a magnitude

$$f_{ni} = \mu g_i \left| P[\Delta_i(t)] \right| = g_{ni} \left| P[\Delta_i(t)] \right| \tag{3-23}$$

where the proportionality constant g_{ni} has units of stiffness (N/cm). For further clarification, Fig. 3-5 shows a plot of the typical desired control force produced by this algorithm as a function of the device displacement. $f_{ni} = g_{ni}\Delta_i$ is shown here as a dashed line because at each peak in the displacement, the magnitude of the desired control force is selected according to this relationship.

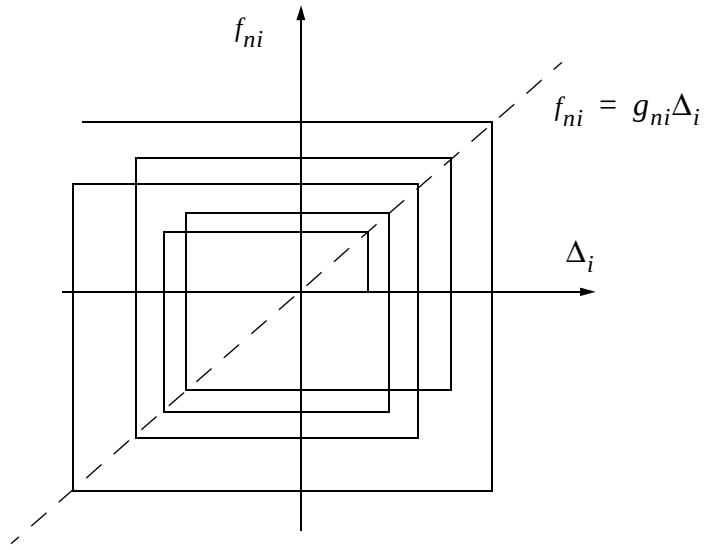

FIGURE 3-5 Typical Desired Control Force Produced with the Maximum Energy Dissipation Algorithm.

As in the clipped-optimal control law, because the force produced by the MR damper cannot be directly commanded, a force feedback loop is used. The measured force is compared to the desired force determined by Eq. (3-23), and the resulting control law is

$$v_i = V_{\max} H(f_{ni} - |f_i|) . \tag{3-24}$$

An appropriate choice of g_{ni} will keep the force f_{ni} within the operating envelope of each MR damper a majority of the time, allowing the MR damper forces to closely approximate the desired force of each device. However, the optimal value of g_{ni} is dependent on the amplitude of the ground excitation. Additionally, notice that this control law is quite straightforward to implement because it requires only measurements of applied force and the relative displacements of the control device.

3.3 Numerical Example

To evaluate these algorithms for use with the MR damper a numerical example is considered in which a model of a six-story building is controlled with four MR dampers. Two devices are rigidly connected between the ground and the first floor, and two devices are rigidly connected between the first and second floors, as shown in Fig. 3-6.

Each MR damper is capable of producing a force equal to 1.8% the weight of the entire structure, and the maximum voltage input to the MR devices is V_{max} = 5V. The governing equations can be written in the form of Eq. (3-5) by defining the mass of each floor, m_i, as 0.227 N/(cm/sec^2) (0.129 1b/(in/sec^2)), the stiffness of each floor, k_i, as 297 N/cm (169 lb/in), and a damping ratio for each mode of 0.5%. This system is a simple representation of the scaled, six-story, test structure that is being used for experimental control studies at the Washington University Structural Control and Earthquake Engineering Laboratory.

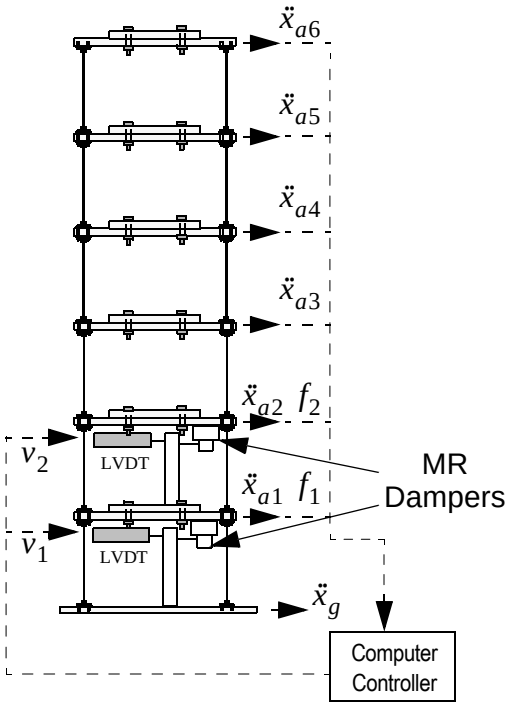

FIGURE 3-6 Schematic Diagram of the MR Damper Implementation.

In this example, the structural measurements available for calculating the control action include the absolute accelerations of the structure and the forces produced by the MR devices (*i.e.*, $\mathbf{y} = [\ddot{x}_{a1}, \ddot{x}_{a2}, \ddot{x}_{a3}, \ddot{x}_{a4}, \ddot{x}_{a5}, \ddot{x}_{a6}, f_1, f_2]^T$). Thus, the governing equations can be written in the form of Eqs. (3-6) - (3-7) by defining

$$\mathbf{A} = \begin{bmatrix} \mathbf{0} & \mathbf{I} \\ -\mathbf{M}_s^{-1}\mathbf{K}_s & -\mathbf{M}_s^{-1}\mathbf{C}_s \end{bmatrix}, \mathbf{B} = \begin{bmatrix} \mathbf{0} \\ \mathbf{M}_s^{-1}\Lambda \end{bmatrix}, \mathbf{E} = -\begin{bmatrix} \mathbf{0} \\ \Gamma \end{bmatrix},$$

$$\mathbf{C} = \begin{bmatrix} -\mathbf{M}_s^{-1}\mathbf{K}_s & -\mathbf{M}_s^{-1}\mathbf{C}_s \end{bmatrix}, \mathbf{D} = \begin{bmatrix} -\mathbf{M}_s^{-1}\Lambda \end{bmatrix}.$$

The MR damper parameters used in this study are c_{0a} = 0.0064 Nsec/cm, c_{0b} = 0.0052 Nsec/cmV, α_a = 8.66 N/cm, α_b = 8.86 N/cmV, γ = 300 cm^{-2}, β = 300 cm^{-2}, A = 120, and n = 2. These parameters were selected based on the identified model of the shear-mode prototype MR damper tested at Washington University (Yi, *et al.*, 1999a,b).

In simulation, the model of the structure is subjected to the NS component of the 1940 El Centro earthquake. The simulations were performed in MATLAB (1999). Because the building system considered is a scaled model, the amplitude of the earthquake was scaled to ten percent of the full-scale earthquake to represent the magnitude of displacements that would be observed in laboratory experiments with this structure.

The various control algorithms were evaluated using a set of evaluation criteria based on those used in the second generation linear control problem for buildings (Spencer et al., 1997a). The first evaluation criterion is a measure of the normalized maximum floor displacement relative to the ground, given as

$$J_1 = \max_{t,\,i}\left(\frac{|x_i(t)|}{x^{\max}}\right) \tag{3-25}$$

where $x_i(t)$ is the relative displacement of the *i*th floor over the entire response, and $x^{\max}$ denotes the uncontrolled maximum displacement. The second evaluation criterion is a measure of the reduction in the interstory drift. The maximum of the normalized interstory drift is

$$J_2 = \max_{t,\,i}\left(\frac{|d_i(t)/h_i|}{d_{\mathrm{n}}^{\max}}\right) \tag{3-26}$$

where h_i is the height of each floor (30 cm), $d_i(t)$ is the interstory drift of the above ground floors over the response history, and $d_{\mathrm{n}}^{\max}$ denotes the normalized peak interstory drift in the uncontrolled response. The third evaluation criterion is a measure of the normalized peak floor accelerations, given by

$$J_3 = \max_{t,\,i}\left(\frac{|\ddot{x}_{\mathrm{a}i}(t)|}{\ddot{x}_{\mathrm{a}}^{\max}}\right) \tag{3-27}$$

where the absolute accelerations of the *i*th floor, $\ddot{x}_{ai}(t)$, are normalized by the peak uncontrolled floor acceleration, denoted $\ddot{x}_{a}^{max}$.

The final evaluation criteria considered in this study is a measure of the maximum control force per device, normalized by the weight of the structure, given by

$$J_4 = \max_{t,\, i}\left(\frac{|f_i(t)|}{W}\right) \tag{3-28}$$

where W is the total weight of the structure (1335 N).

The corresponding uncontrolled responses are as follows: x^{max} = 1.313 cm, d_{n}^{max} = 0.00981 cm, $\ddot{x}_{a}^{max}$ = 146.95 cm/sec^2. The resulting evaluation criteria are presented in Table 3-1 for the control algorithms considered. As indicated in the table, the numbers in parentheses indicate the percent reduction as compared to the best passive case. Additionally, to compare the performance of the various control algorithms, the peak of the interstory drift and absolute acceleration responses for all floors were examined. Fig. 3-7 shows the peak response profile of the entire structure for a variety of cases.

TABLE 3-1. Normalized Controlled Maximum Responses due to Scaled El Centro Earthquake.

Control Strategy	J_1	J_2	J_3	J_4
Passive-Off	0.862	0.801	0.904	0.00292
Passive-On	0.506	0.696	1.41	0.0178
Lyapunov Controller A	0.686 (+35%)[a]	0.788 (+13%)	0.756 (-16%)	0.0178
Lyapunov Controller B	0.326 (-35%)	0.548 (-21%)	1.39 (+53%)	0.0178
Decentralized Bang-Bang	0.449 (-11%)	0.791 (+13%)	1.00 (+11%)	0.0178
Maximum Energy Dissipation	0.548 (+8%)	0.620 (-11%)	1.06 (+17%)	0.0121
Clipped-Optimal A	0.631 (+24%)	0.640 (-8%)	0.636 (-29%)	0.01095
Clipped-Optimal B	0.405 (-20%)	0.547 (-21%)	1.25 (+38%)	0.0178
Modulated Homogeneous Friction	0.421 (-17%)	0.559 (-20%)	1.06 (+17%)	0.0178

a. Numbers in parentheses indicate percent reduction as compared to the best passive case. Negative numbers correspond to a response reduction.

To compare the performance of the semi-active system to that of comparable passive systems, two cases are considered in which the MR dampers are used in a passive mode by maintaining a constant voltage to the devices. The results of both a *passive-off* (0V) and *passive-on* (5V) configuration are included. The passive-off system reduces the maximum floor displacement, maximum interstory displacement, and maximum absolute acceleration by 14%, 20%, and 10%, respectively, over the uncontrolled case. The passive-on system is able to further reduce the maximum floor displacement and maximum interstory displacement. However, notice that the passive-on system results in a larger acceleration than the passive-off system. Figure 3-7 shows that this occurs because the passive-on sys-

tem attempts to lock up the first two floors, increasing the drift of the upper floors, and increasing the absolute acceleration of the lower floors of the structure.

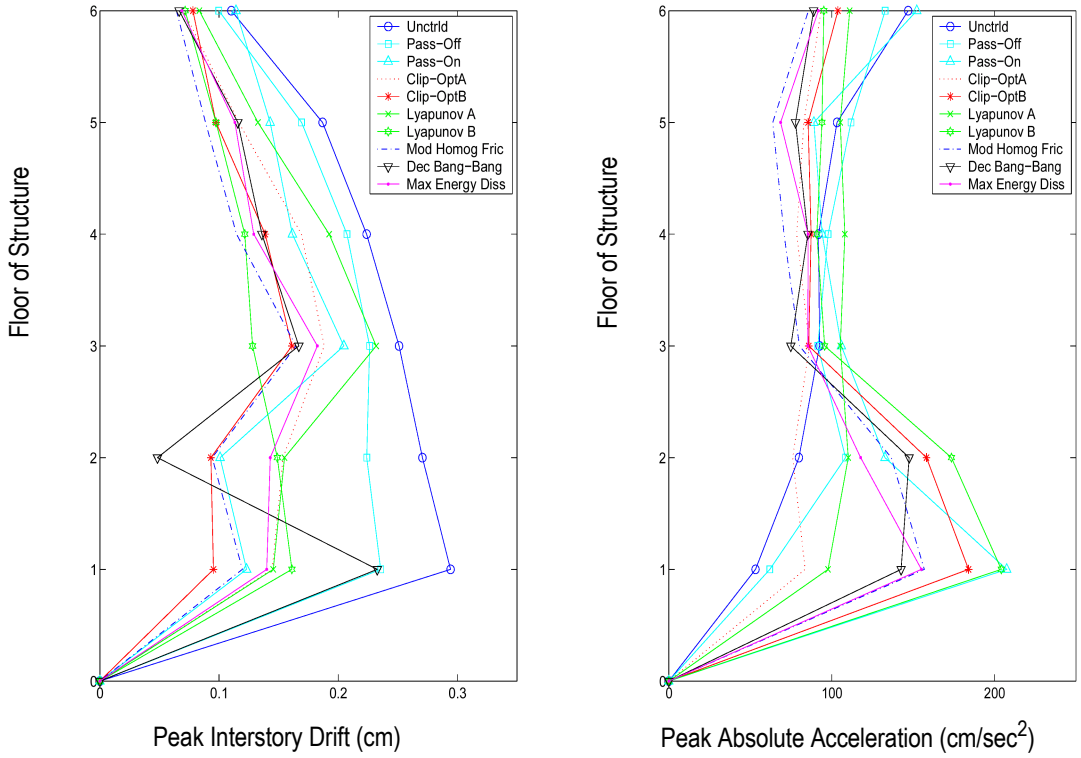

FIGURE 3-7 Peak Responses of Each Floor of the Structure to the Scaled El Centro Earthquake

For the Lyapunov controller there is no standard method of selecting the $\mathbf{Q}_P$ matrix, therefore, several 12×12 $\mathbf{Q}_P$ matrices were arbitrarily chosen and tested. As mentioned previously, the challenge in Lyapunov controller design is in the selection of $\mathbf{Q}_P$. Thus, a variety of combinations were tried, and two control designs that achieved good performance are discussed herein. Lyapunov controller A uses a $\mathbf{Q}_P$ matrix with nonzero values in the first row of the matrix and reduces the absolute acceleration by 16.4% over the best passive case. Figure 3-7 demonstrates that this algorithm reduces the peak absolute accelerations of all floors to about the same level. Lyapunov controller B uses a $\mathbf{Q}_P$ matrix with ones in the (7,1), (8,2), (9,3), (10,4), (11,5), and (12,6) positions. This design resulted in a reduction of the maximum floor displacement and maximum interstory displacement by 35.6% and 21.3% respectively over the best passive case. Figure 3-7 shows that the peak drift at the lower floors is reduced significantly, without locking up these floors.

Thus this control algorithm is able to achieve significant reductions in the drift throughout the structure.

The results obtained with the decentralized bang-bang controller show that this algorithm is capable of reducing the maximum floor displacement by 11.3% over the passive results, but is not very effective in reducing the maximum interstory displacement and absolute accelerations of this structure. Notice from Figure 3-7 that this control algorithm allows the first floor to displace significantly as in a base isolation system, but it locks up the second floor of the structure, resulting in increased absolute accelerations in the lower floors. Thus, the performance achieved with this device could be realized by removing the controllable MR damper between the first and second floors and replacing it with a passive device.

Similarly, the maximum energy dissipation algorithm achieves results that are quite similar to that of the passive-on system. The maximum relative displacement achieved is slightly larger than that of the passive-on system, although the maximum interstory drift is marginally less than that of the passive-on system. The maximum acceleration is not lower than that of the passive-off system. Therefore this control algorithm does not achieve significantly better results than the passive systems. To achieve this performance level, a passive energy dissipation device could be used. Thus, this control algorithm is not recommended.

Two clipped-optimal control designs with different capabilities were considered. Clipped-optimal controller A was designed by placing a moderate weighting (840 cm^{-2}) on the relative displacements of all floors. Clipped-optimal controller B was designed by placing a higher weighting (9000 cm^{-2}) on the relative displacements of all floors. The results show that clipped-optimal controller A appears to be quite effective in achieving significant reductions in both the maximum absolute acceleration and interstory displacement over the passive case. In fact, this controller achieves a 29.6% reduction in acceleration as compared to the better passive case, resulting in the lowest acceleration of all cases considered

here. Furthermore, Figure 3-7 indicates that the accelerations are reduced throughout the structure. If further reductions in displacement are desired in the controller, clipped-optimal control B achieves a reduction in the maximum floor displacement and maximum interstory drift of 20% and 21.4% over the best passive cases, although the absolute accelerations increased. Figure 3-7 shows that the drifts are quite small at the lower floors and the maximum drift occurs at the third floor of the structure, although the drifts are consistently lower than almost all of the other algorithms. Notice that the clipped-optimal control algorithm allows the designer some versatility depending on the control objectives for the particular structure under consideration.

The modulated homogeneous friction algorithm was designed by choosing a value of g_{ni} of 470 N/cm for this example. This value was selected because it utilizes the full range of forces for the MR device without saturating the range of the MR device. Thus, the desired force is always proportional to the previous local extrema in the device displacement. The results show that in this example the control algorithm achieves high levels of performance. The relative displacement and interstory drifts are reduced by 16.8% and 19.7% over the better passive case, although a small increase in the acceleration is observed.

From Figure 3-7 observe that, in terms of absolute acceleration, most of the semi-active controllers have qualitatively similar behavior in the upper floors. The smallest acceleration response is achieved with clipped-optimal controller A, and the lowest interstory displacement response is achieved with Lyapunov controller B and clipped-optimal controller B, while the modulated homogeneous friction algorithm achieves quite similar performance.

3.4 Summary

A selection of recently proposed semi-active control algorithms have been evaluated for application in a structural control system using multiple MR dampers. In a numerical example a six-story structure was controlled using MR dampers on the lower two floors. The

responses of the system to a scaled El Centro earthquake excitation were found for each controller through a simulation of the system. Each algorithm was implemented using available measurements of the structural system, including device forces and absolute structural accelerations. Each semi-active algorithm resulted in an improvement in performance over the best passive controller in some way, although the resulting responses varied greatly depending on the choice of control algorithm. Based on these results, three of these control algorithms were found to be most suited for use with MR dampers in a multi-input control system. The Lyapunov controller algorithm, the clipped-optimal algorithm, and the modulated homogeneous friction algorithm all achieved significant reductions in the responses. Lyapunov controller B and clipped-optimal controller B achieved virtually identical reductions in maximum interstory displacement (21.4%). The reduction in absolute acceleration was superior with clipped-optimal controller A (29.6%), and the reduction in relative displacement was superior with the Lyapunov controller B (35.6%). Furthermore, both of these algorithms possess the flexibility to allow the control designer to design for a range of control objectives. The modulated homogeneous friction algorithm achieved significant reduction in the displacements and drifts, although an increase in the accelerations was observed.

Chapter 4

Bridge and Bearing Models

In the same sense that it is desirable to control structural responses of building during earthquakes, it also of interest to protect bridges. The bridge used for the control study was modeled after a typical multi-span simply supported (MSSS) bridge. MSSS bridges are common in the central and southwestern United States and few studies have looked at the effects of retrofitting these bridges against the effects of earthquakes (DesRoches et al., 2000). A two dimensional (2D) model of a typical MSSS bridge was developed by Georgia Institute of Technology using DRAIN-2DX in order to study the seismic response modification of the bridge model with several retrofit measures (DesRoches et al., 2000). For this study, a 2D, five degree of freedom (5DOF) lumped mass bridge model based on the DRAIN-2DX model, with elastomeric bearings, was developed using MATLAB. Two basic bridge models, linear and nonlinear, were developed. The nonlinear bridge model contained nonlinear models for the elastomeric bearings. The nonlinear bearing models considered were a bilinear model and a Bouc-Wen model (Wen, 1976). This chapter describes the bridge and bearing models and provides a comparison of the bilinear and Bouc-Wen bearing models.

4.1 Modeling of the Bridge

4.1.1 Linear Bridge Model

The 2D-5DOF lumped mass bridge model developed in MATLAB consists of three decks, two columns, and six bearings. The bridge model shown in Fig. 4-1 is a linear model with springs in the locations of the bearings. The stiffnesses of the springs, k_1, k_2, k_3, k_4, k_5, and k_6, are that of the initial stiffness of the elastomeric bearing, 83.52 kip/in. The stiffness of each column, k_c, is 38.357 kip/in. The mass of the center bridge deck (m_2) is 2.49354 kip$\cdot$sec^2/in., and the mass of the outer bridge decks (m_1 and m_3) is 1.24626 kip$\cdot$sec^2/in. Furthermore, the mass of the columns (m_4 and m_5) is 0.26929 kip$\cdot$sec^2/in. The gap between the bridge decks and between the decks and abutments is 4 in. Damping for the bridge model is 0.3% of the stiffness.

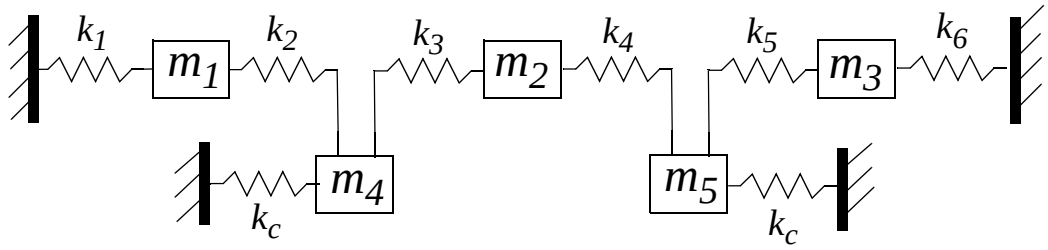

FIGURE 4-1 Schematic of Linear Bridge Model

The equations of motion of the linear bridge from a ground excitation can be written as

$$\mathbf{M}\ddot{\mathbf{x}} + \mathbf{C}\dot{\mathbf{x}} + \mathbf{K}\mathbf{x} = -\mathbf{M}G\ddot{x}_g \tag{4-1}$$

where **x** is a vector of the displacements of the masses of the bridge relative to the ground, $\ddot{x}_g$ is a one-dimensional ground acceleration, G is a column vector of ones, and

$$\mathbf{M} = \begin{bmatrix} 1.25 & 0 & 0 & 0 & 0 \\ 0 & 2.49 & 0 & 0 & 0 \\ 0 & 0 & 1.25 & 0 & 0 \\ 0 & 0 & 0 & 0.27 & 0 \\ 0 & 0 & 0 & 0 & 0.27 \end{bmatrix}, \mathbf{K} = \begin{bmatrix} 167 & 0 & 0 & -83.5 & 0 \\ 0 & 167 & 0 & -83.5 & -83.5 \\ 0 & 0 & 167 & 0 & -83.5 \\ -83.5 & -83.5 & 0 & 205.4 & 0 \\ 0 & -83.5 & -83.5 & 0 & 205.4 \end{bmatrix} \text{ and}$$

$$\mathbf{C} = \begin{bmatrix} 0.501 & 0 & 0 & -0.251 & 0 \\ 0 & 0.501 & 0 & -0.251 & -0.251 \\ 0 & 0 & 0.501 & 0 & -0.251 \\ -0.251 & -0.251 & 0 & 0.616 & 0 \\ 0 & -0.251 & -0.251 & 0 & 0.616 \end{bmatrix}.$$

This equation can be written in state space form as

$$\dot{\mathbf{z}} = \mathbf{A}\mathbf{z} + \mathbf{B}\ddot{x}_g \tag{4-2}$$

$$\mathbf{y} = \mathbf{C}\mathbf{z} + \mathbf{D}\ddot{x}_g \tag{4-3}$$

where **z** is the state vector and **y** is the vector of measured outputs. For this model, the states are the displacement and velocity of each mass relative to the ground, and the measured outputs are the relative displacement, relative velocity, and absolute acceleration of each mass. Then the **A, B, C,** and **D** matrices can be defined by

$$\mathbf{A} = \begin{bmatrix} \mathbf{0} & \mathbf{I} \\ -\mathbf{M}^{-1}\mathbf{K} & -\mathbf{M}^{-1}\mathbf{C} \end{bmatrix}, \mathbf{B} = -\begin{bmatrix} \mathbf{0} \\ \mathrm{G} \end{bmatrix}$$

$$\mathbf{C} = \begin{bmatrix} & \mathbf{I} & \\ -\mathbf{M}^{-1}\mathbf{K} & & -\mathbf{M}^{-1}\mathbf{C} \end{bmatrix}, \text{ and } \mathbf{D} = [\mathbf{0}]$$

For the analytical study of the bridge model, a simulation was developed in SIMULINK (1999). The simulation is shown in Figure 4-2.

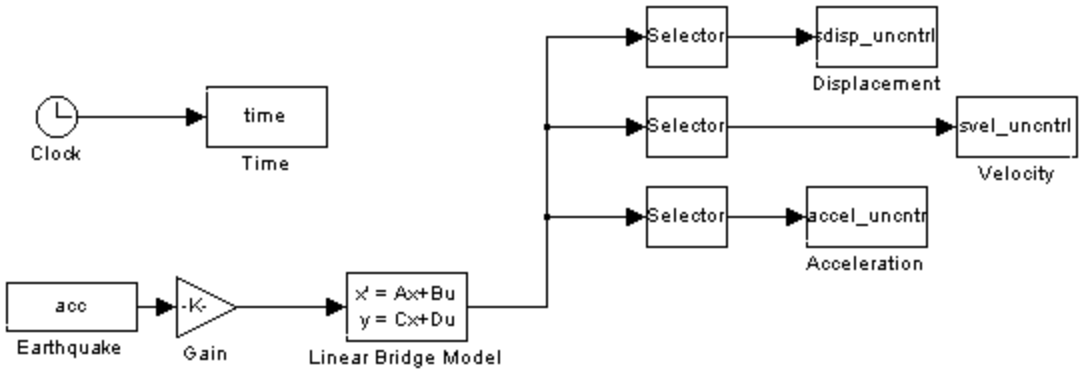

FIGURE 4-2 Linear Bridge Model Simulation in SIMULINK

Using this simulation, the linear bridge model was excited with a number of time histories in order to obtain the bridge responses of relative displacement, velocity, and absolute acceleration of each mass.

4.1.2 Nonlinear Bridge Model

To form a model of the bridge including the nonlinear bearing models, each spring element is replaced with a bearing model, bilinear or Bouc-Wen. Fig. 4-3 shows a schematic of the bridge model with the bearing elements, where B_1, B_2, B_3, B_4, B_5, and B_6 represent bearing forces.

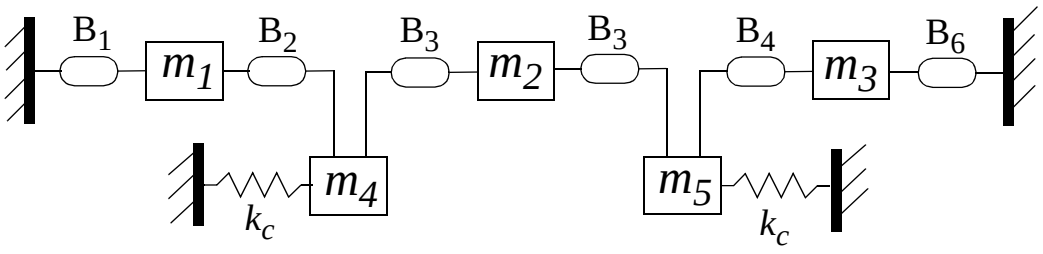

FIGURE 4-3 Schematic of Nonlinear Bridge Model

The equation of motion of the bridge with the bearing elements will change to

$$\mathbf{M}\ddot{\mathbf{x}} + \mathbf{C}\dot{\mathbf{x}} + \mathbf{K}\mathbf{x} = L_b\mathbf{f}_b - \mathbf{M}G\ddot{x}_g \qquad (4\text{-}4)$$

where **x** is a vector of bridge mass displacements relative to the ground, $\mathbf{f}_b$ is a vector of bearing forces ($[f_{b1}, f_{b2}, f_{b3}, f_{b4}, f_{b5}, f_{b6}]^T$), L_b is defined from the contribution of each bearing force as

$$\mathrm{L}_b = \begin{bmatrix} 1 & -1 & 0 & 0 & 0 & 0 \\ 0 & 0 & 1 & -1 & 0 & 0 \\ 0 & 0 & 0 & 0 & 1 & 1 \\ 0 & 1 & -1 & 0 & 0 & 0 \\ 0 & 0 & 0 & 1 & -1 & 0 \end{bmatrix},$$

M and **C** are the same as defined in the linear bridge model and the new stiffness matrix is

$$\mathbf{K} = \begin{bmatrix} 0 & 0 & 0 & 0 & 0 \\ 0 & 0 & 0 & 0 & 0 \\ 0 & 0 & 0 & 0 & 0 \\ 0 & 0 & 0 & 38.4 & 0 \\ 0 & 0 & 0 & 0 & 38.4 \end{bmatrix}$$

The equations governing the state space representation of the bridge with the nonlinear bearing elements will change to

$$\dot{\mathbf{z}} = \mathbf{A}\mathbf{z} + \mathbf{B}\begin{bmatrix} \ddot{x}_g \\ \mathbf{u}_b \end{bmatrix} \tag{4-5}$$

$$\mathbf{y} = \mathbf{C}\mathbf{z} + \mathbf{D}\begin{bmatrix} \ddot{x}_g \\ \mathbf{u}_b \end{bmatrix} \tag{4-6}$$

where **z** is as defined in Eqs. (4-2) and (4-3), **y** is a vector of the measured outputs of relative displacement, relative velocity, absolute acceleration, and bearing forces, and $\mathbf{u}_b$ is a vector of bearing forces. The **A, B, C,** and **D** matrices can then be defined as

$$\mathbf{A} = \begin{bmatrix} \mathbf{0} & \mathbf{I} \\ -\mathbf{M}^{-1}\mathbf{K} & -\mathbf{M}^{-1}\mathbf{C} \end{bmatrix}, \mathbf{B} = \begin{bmatrix} \mathbf{0} \\ -\mathrm{G} \quad -\mathbf{M}^{-1}\mathrm{L}_b \end{bmatrix}$$

$$\mathbf{C} = \begin{bmatrix} \mathbf{I} \\ -\mathbf{M}^{-1}\mathbf{K} \quad -\mathbf{M}^{-1}\mathbf{C} \end{bmatrix}, \text{ and } \mathbf{D} = \begin{bmatrix} \mathbf{0} \\ \mathbf{0} \quad -\mathbf{M}^{-1}\mathrm{L}_b \end{bmatrix}$$

As with the linear bridge model, a simulation for the nonlinear bridge model was also developed in SIMULINK. A schematic of the nonlinear bridge model simulation is shown in Figure 4-4.

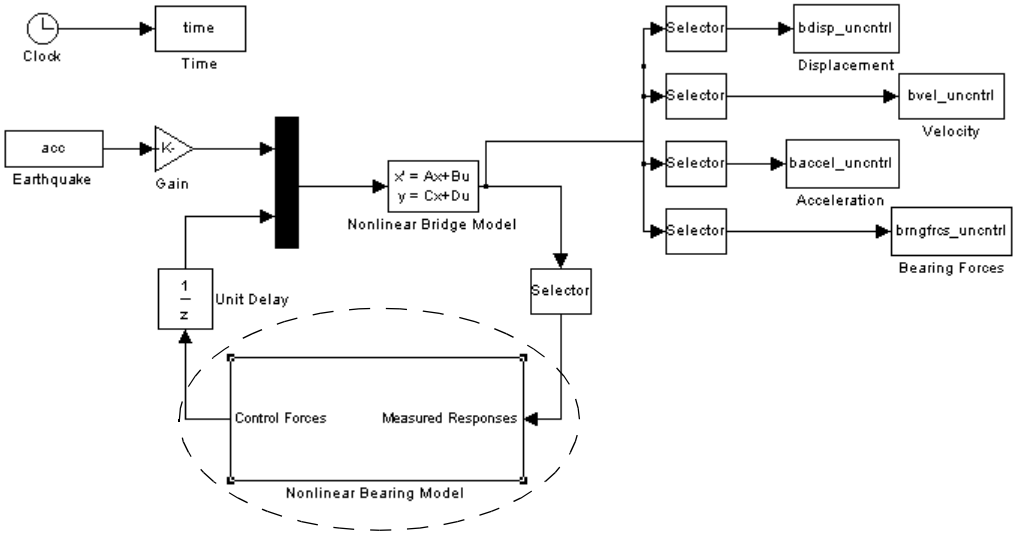

FIGURE 4-4 Nonlinear Bridge Model Simulation in SIMULINK

When comparing the simulations for the linear and nonlinear bridge models, one difference is observed. The difference is the addition of the bearing models in the nonlinear bridge model simulation. In Figure 4-4, the bearing models are contained within the dotted oval. Here, the measured responses are the bridge mass relative displacements. Through a feedback loop, the relative displacements of the bridge masses are fed into the bearing models in order to generate the appropriate bearing forces. The bearing forces are then fed back into the structural model of the nonlinear bridge. The nonlinear bearing models considered are the bilinear and the Bouc-Wen models. These bearing models will be described in the next section.

4.2 Modeling of the Bearings

4.2.1 Bilinear Bearing Model

A bilinear model can be used to represent the behavior of an elastomeric bearing. The bilinear model (Fig. 4-5) is based on three parameters, K_1, K_2, and Q (Kelly 1997). These parameters are governed by the type and size of the bearing (DesRoches et al., 2000). For the bearings in this study, K_1 = 83.6 kip/in. and K_2 = 0.333*K_1 = 27.84 kip/in.

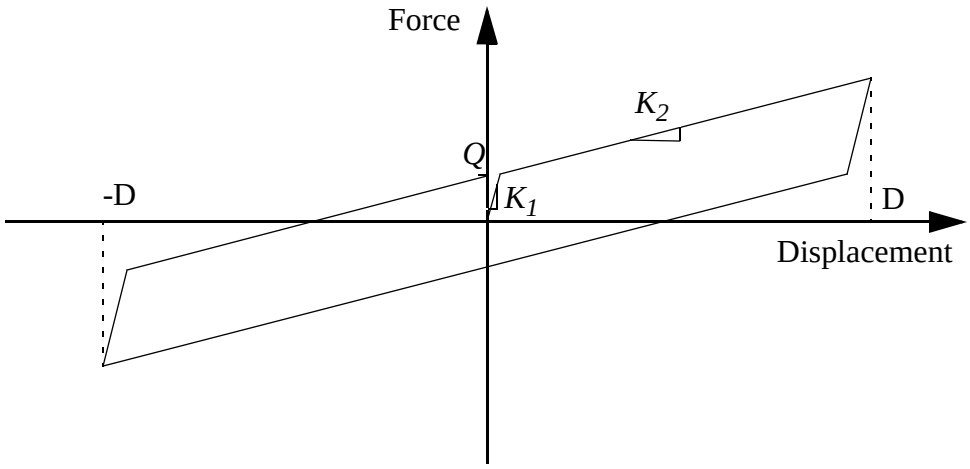

FIGURE 4-5 Bilinear Behavior

To model the bilinear behavior in MATLAB, a spring in parallel with the combination of a spring in series with the backlash block from SIMULINK is used. Figure 4-6 shows a schematic depicting the modeling of the bilinear bearing as well as the simulation developed in SIMULINK. The spring stiffnesses are the same as those defined above for the elastomeric bearing. The spring stiffness, K_1**,** represents the initial slope of the force displacement behavior of the elastomeric bearing. Furthermore, the spring stiffness, K_2-K_1**,** represents the change in slope when the elastomeric bearing begins yielding.

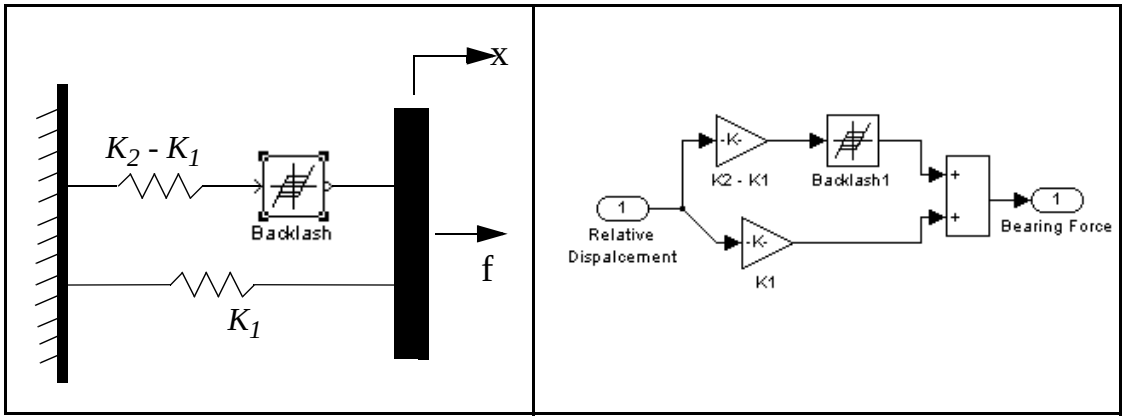

(a) Schematic of Bilinear Bearing Model

(b) Bilinear Bearing Simulation in SIMULINK

FIGURE 4-6 Modeling of Bilinear Bearing Model

The backlash element in SIMULINK is used to simplify a system in which there is a band in which an input results in a zero output. Beyond this range of inputs, the output varies linearly with additional inputs. Taking the initial input as 0, the only parameter that needs to be defined when using the backlash block is the deadband (*DBwidth*), which refers to the amount of side-to-side play in the system and is centered around the output (MATLAB 1999).

In order to determined an appropriate value for the deadband parameter and verify the MATLAB model, a comparison was made between a bilinear bearing modeled in MATLAB and one modeled in DRAIN-2DX using a bilinear element. A value of 44.8 was found for *DBwidth* to achieve the desired behavior.

4.2.2 Bouc-Wen Bearing Model

A schematic of a bearing model based on the Bouc-Wen model (Wen, 1976) developed in MATLAB is shown in Fig. 4-7.

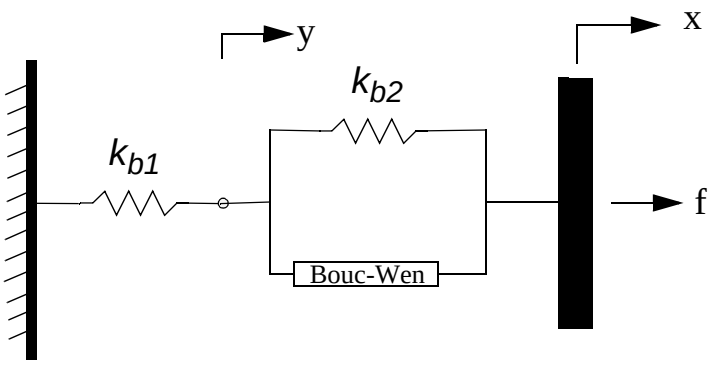

FIGURE 4-7 Bouc-Wen Bearing Model in MATLAB

The equations governing this model are the following

$$f = k_{b1}y = \alpha z + k_{b2}(x - y) \tag{4-7}$$

$$\dot{z} = -\gamma|\dot{x} - \dot{y}|z|z|^{n-1} - \beta(\dot{x} - \dot{y})|z|^{n} + A(\dot{x} - \dot{y}) \tag{4-8}$$

Where z is an evolutionary variable that accounts for the history dependence of the response, k_{b1} and k_{b2} are stiffness parameters relating to the elastomeric bearing stiffness, and a, b, n, A, and g are model parameters corresponding to the bearing behavior.

Determination of Bouc-Wen Model Parameters

Initially, in order to determine equivalent values for the parameters k_{b1}, k_{b2}, a, b, and g, the MATLAB Bouc-Wen model was compared to the DRAIN-2DX bilinear bearing model. The comparison was made by examining force-displacement curves for each model generated using a sine wave signal. The first sine wave signal was chosen to have an amplitude of 5.5, which corresponds to the maximum amplitude achieved by the elastomeric bearings in the DRAIN-2DX bridge model when the HT7545 earthquake is applied, and a frequency of 0.8475 Hz, which is the first frequency of the DRAIN-2DX bridge model with elastomeric bearings. The stiffness parameters along with the Bouc-Wen model parameters of a, b, and g were varied in the MATLAB model until a good correspondence between the force-displacement curves generated by the DRAIN-2DX bilinear model and

MATLAB Bouc-Wen model was achieved. This procedure resulted in the following set of parameters: k_{b1} = 112.3 kips/in., k_{b2} = 0.33*k_{b1}= 37.1 kips/in., a = 740, b = 0.5, g = 125, A = 0.2, and N = 2. This set of parameters was then used with several different sine wave signals of varying amplitude and frequency to again compare the force-displacement curves produced by the two models of the elastomeric bearing. Figure 4-8 shows a comparison of the two bearing models.

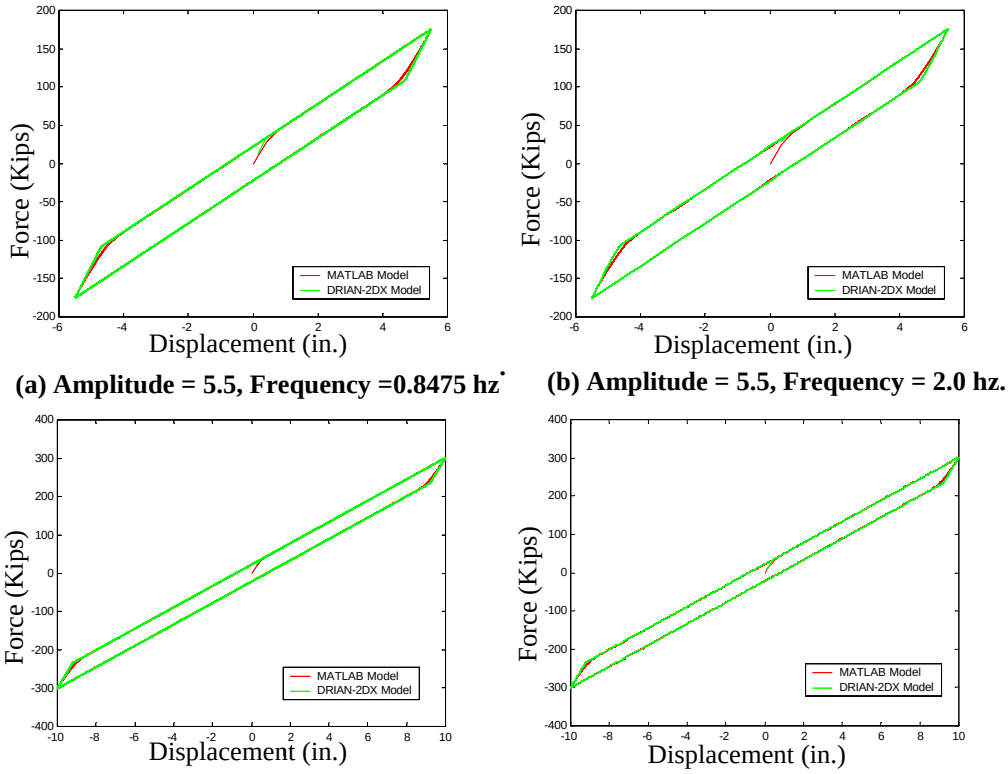

(a) Amplitude = 5.5, Frequency =0.8475 hz. **(b) Amplitude = 5.5, Frequency = 2.0 hz.**

(c) Amplitude = 10, Frequency = 0.8475 hz. **(d) Amplitude = 10, Frequency = 2.0 hz**

FIGURE 4-8 Comparison of MATLAB Bouc-Wen Model and DRAIN-2DX Bilinear Model with Different Sine Wave Inputs

As the figures show, the final set of parameters produces force-displacement curves for the DRAIN-2DX bilinear model and MATLAB Bouc-Wen model of an elastomeric bearing that correspond well when sine waves of differing amplitudes and frequencies are applied as the input signal. However, it will be shown later that when the MATLAB Bouc-Wen bearing model is implemented in the bridge model, there is a dependency on frequency.

4.3 Comparison of Bilinear and Bouc-Wen Models

With both the MATLAB bilinear and Bouc-Wen bearing models designed, these models can be implemented into the bridge model for a comparison. The bilinear model is typically used to model the behavior of an elastomeric bearing. However, the Bouc-Wen model can also model the nonlinear bearing behavior. The purpose of the comparison is to determine if the Bouc-Wen model is a better representation of the behavior of an elastomeric bearing than the traditional bilinear model.

4.3.1 Ground Motion Records

The ground motion records used in this study were generated based on a modified approach to the spectrum compatible ground acceleration approach (Clough and Penzien, 1993) as described in Chapter 2. In order to analyze the responses of the nonlinear bridge models, a set of three earthquakes was generated and each of the three earthquakes in the set was scaled to produce new sets of earthquakes, each set with a different magnitude. Three earthquakes were chosen for each set because that number of earthquakes would give a representative sample of earthquakes. The first set of earthquakes, the linear case, had an average peak acceleration of 2.34 in/sec^2 and excited the bridge within the linear region. The second set of earthquakes, the moderate case, had an average peak acceleration of 9.38 in/sec^2 and excited the bridge in the linear region much of the time with some nonlinearity. The third set of earthquakes, the nonlinear case, had an average peak acceleration of 37.92 in/sec^2 and excited the bridge in the highly nonlinear region. Table 4-1 summarizes the different test cases used for this study and Figure 4-9 shows the synthetic time history for the moderate case.

TABLE 4-1. Test Cases

Case	***Behavior***	***Avg. Peak Acceleration (in/sec^2)***
Linear	Linear	2.34
Moderate	Linear with some non-linearity	9.38
Nonlinear	High nonlinearity	37.92

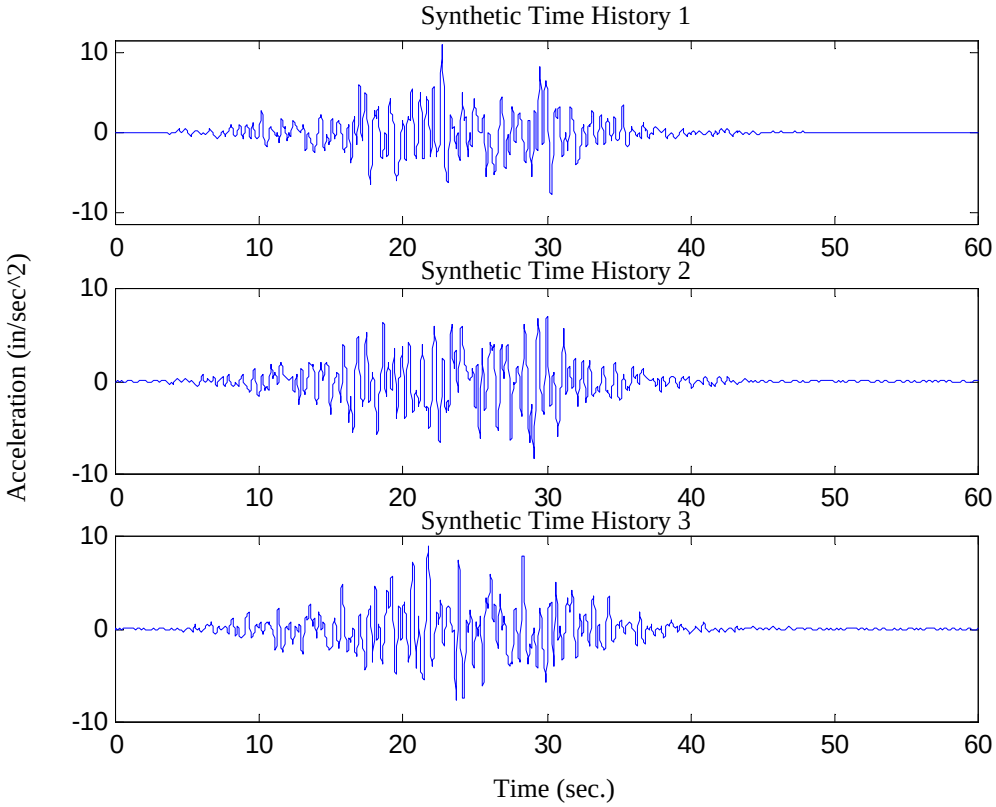

FIGURE 4-9 Synthetic Time Histories for Moderate Case

4.3.2 Evaluation Criteria

Nonlinear Bridge Model 1 will refer to the bridge model with the bearings represented by the bilinear model; and Nonlinear Bridge Model 2 will refer to the bridge model with the

bearings represented by the Bouc-Wen model. Also, the Linear Bridge Model will refer to the bridge model with springs to represent the bearings.

To evaluate the performance of each bearing model, peak and RMS relative displacement, relative velocity, and absolute acceleration responses were calculated for each bearing model with each case of earthquake. The peak displacement D_{pi} (in.), velocity V_{pi} (in/sec), and acceleration A_{pi} (in/sec^2) responses for the ith mass are defined by

$$D_{pi} = \max_t |x_i(t)| \tag{4-9}$$

$$V_{pi} = \max_t |\dot{x}_i(t)| \tag{4-10}$$

$$A_{pi} = \max_t |\ddot{x}_i(t)| \tag{4-11}$$

Furthermore, the RMS displacement, velocity, and acceleration responses are defined by

$$D_{ri} = \sqrt{\sum_{t=1}^{T} x_i^2(t)} \tag{4-12}$$

$$V_{ri} = \sqrt{\sum_{t=1}^{T} \dot{x}_i^2(t)} \tag{4-13}$$

$$A_{ri} = \sqrt{\sum_{t=1}^{T} \ddot{x}_i^2(t)} \tag{4-14}$$

where $x_i(t)$, $\dot{x}_i(t)$, and $\ddot{x}_i(t)$ are the ith mass displacement, velocity, and acceleration, respectively, and T is the length of the simulation. In addition, the bilinear and Bouc-Wen models were evaluated for each mass by comparing the difference between peak and RMS responses as defined by the criteria given in Eqs. (4-15) through (4-20).

$$J_1 = \frac{[(D_{pi})_{bilinear} - (D_{pi})_{bouc}]}{(D_{pi})_{bilinear}} \times 100 \quad (4\text{-}15)$$

$$J_2 = \frac{[(V_{pi})_{bilinear} - (V_{pi})_{bouc}]}{(V_{pi})_{bilinear}} \times 100 \quad (4\text{-}16)$$

$$J_3 = \frac{[(A_{pi})_{bilinear} - (A_{pi})_{bouc}]}{(A_{pi})_{bilinear}} \times 100 \quad (4\text{-}17)$$

$$J_4 = \frac{[(D_{ri})_{bilinear} - (D_{ri})_{bouc}]}{(D_{ri})_{bilinear}} \times 100 \quad (4\text{-}18)$$

$$J_5 = \frac{[(V_{ri})_{bilinear} - (V_{ri})_{bouc}]}{(V_{ri})_{bilinear}} \times 100 \quad (4\text{-}19)$$

$$J_6 = \frac{[(A_{ri})_{bilinear} - (A_{ri})_{bouc}]}{(A_{ri})_{bilinear}} \times 100 \quad (4\text{-}20)$$

Before comparing the nonlinear bridge models, the Linear Bridge Model and Nonlinear Bridge Model 1 were compared for a linear case earthquake to verify the models. The result was that for a linear case earthquake the linear model and Nonlinear Bridge Model 1 responses were identical, indicating that the nonlinear model was correct.

4.3.3 Results of Comparison

To again look at the dependence of the Bouc-Wen model on frequency and amplitude, force-displacement curves for Nonlinear Bridge Models 1 and 2 were compared for varying amplitude and frequency sine waves. The amplitude was varied from 10 to 40 and the frequency was varied from 0.8475 Hz, the first mode of the bridge, to 2 hz. Figure 4-10 shows the results of this analysis.

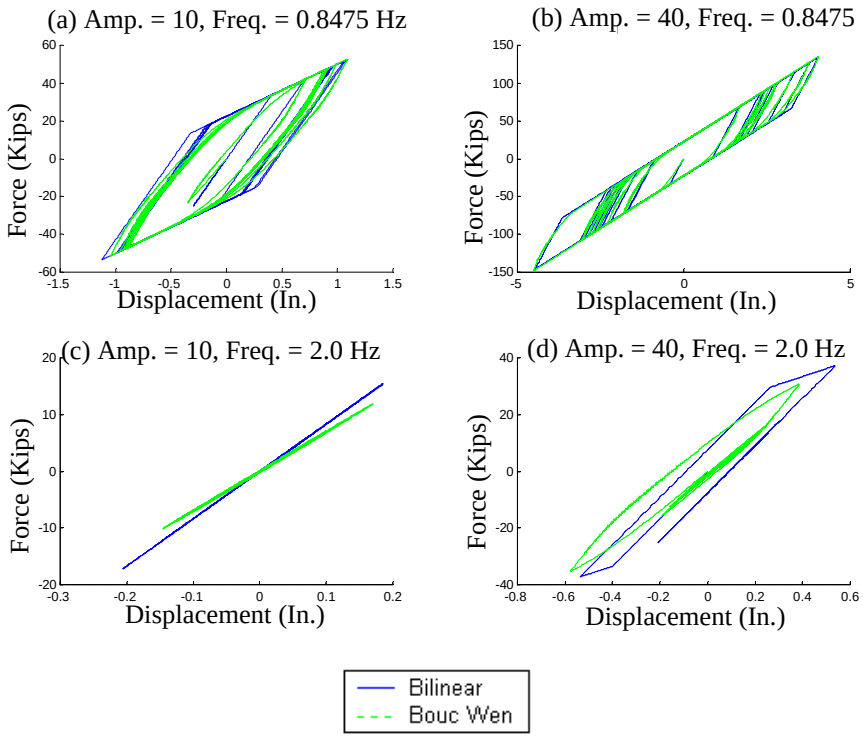

FIGURE 4-10 Comparison of MATLAB Bilinear and Bouc-Wen Models with Different Sine Wave Inputs

As demonstrated in the graphs, the slope of the Bouc-Wen model changes with a change in frequency. This same effect was also evident when using the synthetic ground motion records. As a result, the stiffness parameter k_{b1} for the was modified to a value of 145.5 kips/in for the Bouc-Wen bearing model so that the force-displacement curves for the bi-linear and Bouc-Wen bearing models had the same slope for the linear case of earth-quakes.

Nonlinear Bridge Models 1 and 2 were evaluated using the linear, moderate, and nonlinear cases of earthquakes. Tables 4-2 through 4-7 show the comparison of the peak and RMS responses using the evaluation criteria defined in the previous section; and Tables 4-8 through 4-19 give the peak and RMS responses for each case of earthquakes.

TABLE 4-2. Percent Difference of Peak Responses: Linear Case

		Mass 1	*Mass 2*	*Mass 3*	*Mass 4*	*Mass 5*
Record 1	J_1	1.94	3.39	1.94	3.13	3.13
	J_2	-0.17	0.75	-0.17	1.93	1.93
	J_3	-1.37	0.78	-1.37	0.16	0.16
Record 2	J_1	-1.04	3.23	-1.04	1.93	1.93
	J_2	-3.58	0.93	-3.58	3.81	3.81
	J_3	-5.20	0.00	-5.20	-0.54	-0.54
Record 3	J_1	-3.35	0.05	-3.35	0.63	0.63
	J_2	-1.74	-0.48	-1.74	0.41	0.41
	J_3	-2.59	-0.39	-2.59	0.29	0.29

TABLE 4-3. Percent Difference of Peak Responses: Moderate Case

		Mass 1	*Mass 2*	*Mass 3*	*Mass 4*	*Mass 5*
Record 1	J_1	14.18	16.36	14.18	15.72	15.72
	J_2	15.47	11.49	15.47	14.19	14.19
	J_3	12.69	4.61	12.69	48.86	48.86
Record 2	J_1	18.88	11.18	18.88	9.80	9.80
	J_2	13.82	4.02	13.82	19.63	19.63
	J_3	13.74	1.93	13.74	30.37	30.37
Record 3	J_1	6.55	11.44	6.55	11.90	11.90
	J_2	8.68	8.61	8.68	20.76	20.76
	J_3	4.19	5.29	4.19	38.20	38.20

TABLE 4-4. Percent Difference of Peak Responses: Nonlinear Case

		Mass 1	*Mass 2*	*Mass 3*	*Mass 4*	*Mass 5*
Record 1	J_1	17.43	-5.24	17.43	12.04	12.04
	J_2	12.71	1.76	12.71	-3.99	-3.99
	J_3	-6.88	-11.20	-6.88	38.82	38.82
Record 2	J_1	1.48	-5.19	1.48	-15.75	-15.75
	J_2	-9.77	-15.85	-9.77	-16.05	-16.05
	J_3	-9.58	-18.60	-9.58	17.22	17.22
Record 3	J_1	-3.63	-3.49	-3.63	-9.91	-9.91
	J_2	3.28	0.20	3.28	5.94	5.94
	J_3	-1.37	-13.84	-1.37	25.47	25.47

TABLE 4-5. Percent Difference of RMS Responses: Linear Case

		Mass 1	*Mass 2*	*Mass 3*	*Mass 4*	*Mass 5*
Record 1	J_4	1.46	2.45	1.46	2.46	2.46
	J_5	-0.30	2.33	-0.30	2.35	2.35
	J_6	-2.53	2.05	-2.53	1.89	1.89
Record 2	J_4	1.80	3.26	1.80	3.28	3.28
	J_5	-0.90	3.10	-0.90	3.09	3.09
	J_6	-4.34	2.68	-4.34	2.45	2.45
Record 3	J_4	-1.37	-0.15	-1.37	-0.14	-0.14
	J_5	-2.68	-0.16	-2.68	-0.19	-0.19
	J_6	-4.48	-0.48	-4.48	-0.71	-0.71

TABLE 4-6. Percent Difference of RMS Responses: Moderate Case

		Mass 1	*Mass 2*	*Mass 3*	*Mass 4*	*Mass 5*
Record 1	J_4	12.85	14.36	12.85	14.48	14.48
	J_5	12.47	14.29	12.47	14.90	14.90
	J_6	10.50	14.02	10.50	21.15	21.15
Record 2	J_4	11.05	14.53	11.05	9.20	9.20
	J_5	13.48	9.27	13.48	9.92	9.92
	J_6	14.07	9.59	14.07	16.69	16.69
Record 3	J_4	18.47	18.76	18.47	19.05	19.05
	J_5	14.36	17.72	14.36	18.08	18.08
	J_6	11.40	17.40	11.40	20.67	20.67

TABLE 4-7. Percent Difference of RMS Responses: Nonlinear Case

		Mass 1	*Mass 2*	*Mass 3*	*Mass 4*	*Mass 5*
Record 1	J_4	3.84	2.09	3.84	1.77	1.77
	J_5	2.88	-0.48	2.88	2.65	2.65
	J_6	2.56	-1.45	2.56	26.54	26.54
Record 2	J_4	9.51	3.53	9.51	-0.58	-0.58
	J_5	-1.60	0.76	-1.60	1.85	1.85
	J_6	-2.05	-0.14	-2.05	23.90	23.90
Record 3	J_4	6.93	-0.21	6.93	-3.78	-3.78
	J_5	0.90	-4.64	0.90	-0.30	-0.30
	J_6	2.16	-5.84	2.16	35.60	35.60

TABLE 4-8. Peak Responses for Bilinear Model: Linear Case

		Mass 1	*Mass 2*	*Mass 3*	*Mass 4*	*Mass 5*
Record 1	D_{pi}	0.15	0.31	0.15	0.19	0.19
	V_{pi}	1.10	1.68	1.10	1.01	1.01
	A_{pi}	8.89	9.49	8.89	6.21	6.21
Record 2	D_{pi}	0.16	0.38	0.16	0.23	0.23
	V_{pi}	1.08	2.26	1.08	1.18	1.18
	A_{pi}	8.03	11.93	8.03	6.67	6.67
Record 3	D_{pi}	0.14	0.26	0.14	0.16	0.16
	V_{pi}	0.95	1.48	0.95	0.97	0.97
	A_{pi}	7.79	9.15	7.79	5.51	5.51

TABLE 4-9. Peak Responses for Bouc-Wen Model: Linear Case

		Mass 1	*Mass 2*	*Mass 3*	*Mass 4*	*Mass 5*
Record 1	D_{pi}	0.14	0.30	0.14	0.18	0.18
	V_{pi}	1.10	1.67	1.10	0.99	0.99
	A_{pi}	9.01	9.42	9.01	6.20	6.20
Record 2	D_{pi}	0.16	0.37	0.16	0.22	0.22
	V_{pi}	1.12	2.24	1.12	1.13	1.13
	A_{pi}	8.45	11.93	8.45	6.70	6.70
Record 3	D_{pi}	0.14	0.26	0.14	0.16	0.16
	V_{pi}	0.97	1.49	0.97	0.97	0.97
	A_{pi}	7.99	9.18	7.99	5.50	5.50

TABLE 4-10. Peak Responses for Bilinear Model: Moderate Case

		Mass 1	*Mass 2*	*Mass 3*	*Mass 4*	*Mass 5*
Record 1	D_{pi}	0.51	1.04	0.51	0.61	0.61
	V_{pi}	4.10	5.95	4.10	3.86	3.86
	A_{pi}	28.59	29.82	28.59	37.12	37.12
Record 2	D_{pi}	0.54	1.39	0.54	0.68	0.68
	V_{pi}	3.78	7.28	3.78	4.47	4.47
	A_{pi}	29.72	35.76	29.72	37.05	37.05
Record 3	D_{pi}	0.51	0.95	0.51	0.58	0.58
	V_{pi}	2.96	5.59	2.96	3.58	3.58
	A_{pi}	27.39	30.65	27.39	29.29	29.29

TABLE 4-11. Peak Responses for Bouc-Wen Model: Moderate Case

		Mass 1	*Mass 2*	*Mass 3*	*Mass 4*	*Mass 5*
Record 1	D_{pi}	0.44	0.87	0.44	0.52	0.52
	V_{pi}	3.46	5.26	3.46	3.32	3.32
	A_{pi}	24.96	28.44	24.96	18.99	18.99
Record 2	D_{pi}	0.44	1.24	0.44	0.61	0.61
	V_{pi}	3.26	6.99	3.26	3.59	3.59
	A_{pi}	25.64	35.07	25.64	25.80	25.80
Record 3	D_{pi}	0.47	0.84	0.47	0.51	0.51
	V_{pi}	2.70	5.11	2.70	2.83	2.83
	A_{pi}	26.24	29.03	26.24	18.10	18.10

TABLE 4-12. Peak Responses for Bilinear Model: Nonlinear Case

		Mass 1	*Mass 2*	*Mass 3*	*Mass 4*	*Mass 5*
Record 1	D_{pi}	1.33	1.97	1.33	1.27	1.27
	V_{pi}	7.78	10.45	7.78	6.67	6.67
	A_{pi}	53.43	45.59	53.43	78.85	78.85
Record 2	D_{pi}	1.13	3.25	1.13	1.34	1.34
	V_{pi}	7.09	13.81	7.09	6.67	6.67
	A_{pi}	53.45	60.92	53.45	77.40	77.40
Record 3	D_{pi}	1.28	2.96	1.28	1.34	1.34
	V_{pi}	8.25	14.66	8.25	9.75	9.75
	A_{pi}	53.13	58.69	53.13	77.84	77.84

TABLE 4-13. Peak Responses for Bouc-Wen Model: Nonlinear Case

		Mass 1	*Mass 2*	*Mass 3*	*Mass 4*	*Mass 5*
Record 1	D_{pi}	1.10	2.08	1.10	1.12	1.12
	V_{pi}	6.80	10.27	6.80	6.94	6.94
	A_{pi}	57.11	50.70	57.11	48.24	48.24
Record 2	D_{pi}	1.12	3.42	1.12	1.55	1.55
	V_{pi}	7.78	16.00	7.78	7.74	7.74
	A_{pi}	58.57	72.25	58.57	64.07	64.07
Record 3	D_{pi}	1.33	3.06	1.33	1.47	1.47
	V_{pi}	7.98	14.63	7.98	9.17	9.17
	A_{pi}	53.86	66.81	53.86	58.02	58.02

TABLE 4-14. RMS Responses for Bilinear Model: Linear Case

		Mass 1	*Mass 2*	*Mass 3*	*Mass 4*	*Mass 5*
Record 1	D_{ri}	8.75	22.30	8.75	12.82	12.82
	V_{ri}	56.36	120.83	56.36	69.35	69.35
	A_{ri}	457.17	654.85	457.17	377.64	377.64
Record 2	D_{ri}	9.13	23.37	9.13	13.45	13.45
	V_{ri}	58.04	126.18	58.04	72.52	72.52
	A_{ri}	463.29	683.74	463.29	395.10	395.10
Record 3	D_{ri}	8.16	20.53	8.16	11.80	11.80
	V_{ri}	53.80	111.45	53.80	63.96	63.96
	A_{ri}	448.33	606.35	448.33	350.07	350.07

TABLE 4-15. RMS Responses for Bouc-Wen Model: Linear Case

		Mass 1	*Mass 2*	*Mass 3*	*Mass 4*	*Mass 5*
Record 1	D_{ri}	8.63	21.75	8.63	12.51	12.51
	V_{ri}	56.53	118.01	56.53	67.72	67.72
	A_{ri}	468.74	641.44	468.74	370.49	370.49
Record 2	D_{ri}	8.97	22.61	8.97	13.01	13.01
	V_{ri}	58.57	122.27	58.57	70.27	70.27
	A_{ri}	483.40	665.38	483.40	385.42	385.42
Record 3	D_{ri}	8.27	20.56	8.27	11.82	11.82
	V_{ri}	55.25	111.64	55.25	64.08	64.08
	A_{ri}	468.44	609.26	468.44	352.54	352.54

TABLE 4-16. RMS Responses for Bilinear Model: Moderate Case

		Mass 1	*Mass 2*	*Mass 3*	*Mass 4*	*Mass 5*
Record 1	D_{ri}	28.17	70.42	28.17	40.39	40.39
	V_{ri}	185.09	382.72	185.09	219.60	219.60
	A_{ri}	1559.70	2077.79	1559.70	1317.29	1317.29
Record 2	D_{ri}	26.74	64.52	26.74	34.38	34.38
	V_{ri}	202.93	330.01	202.93	189.00	189.00
	A_{ri}	1905.52	1839.07	1905.52	1208.36	1208.36
Record 3	D_{ri}	32.46	78.62	32.46	45.12	45.12
	V_{ri}	200.82	420.46	200.82	241.39	241.39
	A_{ri}	1665.80	2284.69	1665.80	1382.45	1382.45

TABLE 4-17. RMS Responses for Bouc-Wen Model: Moderate Case

		Mass 1	*Mass 2*	*Mass 3*	*Mass 4*	*Mass 5*
Record 1	D_{ri}	24.55	60.31	24.55	34.54	34.54
	V_{ri}	162.00	328.05	162.00	186.87	186.87
	A_{ri}	1395.87	1786.54	1395.87	1038.70	1038.70
Record 2	D_{ri}	23.79	55.14	23.79	31.22	31.22
	V_{ri}	175.56	299.42	175.56	170.25	170.25
	A_{ri}	1637.47	1662.79	1637.47	1006.64	1006.64
Record 3	D_{ri}	26.47	63.87	26.47	36.52	36.52
	V_{ri}	171.98	345.95	171.98	197.74	197.74
	A_{ri}	1475.82	1887.19	1475.82	1096.73	1096.73

TABLE 4-18. RMS Responses for Bilinear Model: Nonlinear Case

		Mass 1	***Mass 2***	***Mass 3***	***Mass 4***	***Mass 5***
Record 1	D_{ri}	*62.49*	*141.13*	*62.49*	*78.16*	*78.16*
	V_{ri}	*380.94*	712.34	380.94	410.03	410.03
	A_{ri}	*3267.25*	3686.53	3267.25	3573.23	3573.23
Record 2	D_{ri}	*75.67*	174.21	75.67	88.41	88.41
	V_{ri}	*416.57*	838.13	416.57	463.94	463.94
	A_{ri}	*3375.52*	4213.57	3375.52	3703.07	3703.07
Record 3	D_{ri}	*63.40*	147.42	63.40	74.58	74.58
	V_{ri}	*380.72*	721.29	380.72	404.55	404.55
	A_{ri}	*3340.46*	3647.78	3340.46	4084.32	4084.32

TABLE 4-19. RMS Responses for Bouc-Wen Model: Nonlinear Case

		Mass 1	***Mass 2***	***Mass 3***	***Mass 4***	***Mass 5***
Record 1	D_{ri}	*60.09*	138.19	60.09	76.77	76.77
	V_{ri}	*369.95*	715.79	369.95	399.15	399.15
	A_{ri}	*3183.61*	3739.95	3183.61	2625.03	2625.03
Record 2	D_{ri}	*68.48*	168.05	68.48	88.92	88.92
	V_{ri}	*423.22*	831.76	423.22	455.35	455.35
	A_{ri}	*3444.75*	4219.65	3444.75	2817.93	2817.93
Record 3	D_{ri}	*59.00*	147.72	59.00	77.40	77.40
	V_{ri}	*377.30*	754.72	377.30	405.75	405.75
	A_{ri}	*3268.34*	3860.80	3268.34	2630.31	2630.31

For the linear and nonlinear case of earthquakes, some Bouc-Wen model peak and RMS bridge responses increased over the same bilinear model responses. However, for the moderate earthquake case, all peak and RMS bridge responses from the Bouc-Wen model decreased when compared with the bilinear model responses. Moreover, for the moderate case the largest decrease in peak responses from the Bouc-Wen model over the bilinear model was 48.9% for the acceleration of mass 4 and of mass 5. For the linear case, the deviation between the bilinear and Bouc-Wen peak responses was small, with the largest deviation being -5.2% for acceleration of mass 1 and of mass 3.

4.4 Summary

In this chapter, both linear and nonlinear bridge models have been developed for a multi span simply supported bridge. For the nonlinear bridge model, the nonlinear bearing models considered were a bilinear model and a Bouc-Wen model (Wen, 1976). The modeling of these nonlinear bearing models was also discussed in this chapter. Varying amplitudes of earthquakes were used to evaluate and compare the bridge responses when using the bilinear and Bouc-Wen bearing models. However, when comparing the bridge responses from the two bearing models, at this time, it cannot be determined which model, bilinear or Bouc-Wen, is a better representation of the behavior of an elastomeric bearing. In order to determine which model is a more accurate representation of the bearing behavior, experimental results from actual elastomeric bearings are needed. Experimental testing is scheduled to be performed at Georgia Institute of Technology. In the next chapter, the Linear Bridge Model and Nonlinear Bridge Model 1 will be used to compare the effectiveness of passive, active, and semi-active control strategies.

Chapter 5

Bridge Control Study

The linear and nonlinear bridge models developed in Chapter 4 of a multi-span simply supported bridge are used here to evaluate different control strategies for the bridge. The control strategies investigated are ideal passive, active, and semi-active control and were designed as described in Chapter 2. The effectiveness of the addition of control devices is evaluated by comparing bridge deck displacements for each control strategy. Furthermore, several different device locations are considered. This chapter will modify the linear and nonlinear bridge models presented in Chapter 4 for the addition of control. In addition, through simulation, the effectiveness of control strategies for both the linear and nonlinear bridge models will be compared.

5.1 Control Study for Linear Bridge Model

With the addition of *n* control devices to the linear bridge model, the equations of motion will change to

$$\mathbf{M}\ddot{\mathbf{x}} + \mathbf{C}\dot{\mathbf{x}} + \mathbf{K}\mathbf{x} = \mathrm{L}_c\mathbf{f}_c - \mathbf{M}\mathrm{G}\ddot{x}_g \tag{5-1}$$

where $\mathbf{x}$ is a vector of the displacements of the bridge masses relative to the ground, $\mathbf{f}_c = [f_{1c}, f_{2c}, \ldots f_{nc}]^T$ is a vector of the control forces generated by the *n* control devices,

G is a column vector of ones, and L_c is a matrix determined by the placement of the *n* control devices. Furthermore, the **M, C,** and **K** matrices are the same as defined for the linear bridge model in Chapter 4. Using this equation, the state space form can be written

$$\dot{\mathbf{z}} = \mathbf{A}\mathbf{z} + \mathbf{B}\begin{bmatrix} \ddot{x}_g \\ \mathbf{u}_c \end{bmatrix} \tag{5-2}$$

$$\mathbf{y} = \mathbf{C}\mathbf{z} + \mathbf{D}\begin{bmatrix} \ddot{x}_g \\ \mathbf{u}_c \end{bmatrix} \tag{5-3}$$

where **z** is the state vector, **y** is the vector of measured outputs for determining the control action and $\mathbf{u}_c$ is a vector of control forces. For this model, the state vector consists of the displacement and velocity of each mass relative to the ground and the measured outputs for determining the control action are the absolute acceleration and control forces. The **A**, **B**, **C,** and **D** matrices can be redefined as

$$\mathbf{A} = \begin{bmatrix} \mathbf{0} & \mathbf{I} \\ -\mathbf{M}^{-1}\mathbf{K} & -\mathbf{M}^{-1}\mathbf{C} \end{bmatrix}, \mathbf{B} = -\begin{bmatrix} \mathbf{0} \\ \mathrm{G} \qquad \mathbf{M}^{-1}\mathrm{L}_c \end{bmatrix},$$

$$\mathbf{C} = \begin{bmatrix} \mathbf{I} \\ -\mathbf{M}^{-1}\mathbf{K} \qquad -\mathbf{M}^{-1}\mathbf{C} \end{bmatrix} \text{ and } \mathbf{D} = \begin{bmatrix} \mathbf{0} \\ \mathbf{0} \qquad -\mathbf{M}^{-1}\mathrm{L}_c \end{bmatrix}$$

The mode shapes and natural frequencies of the uncontrolled bridge are given in Figure 5-1.

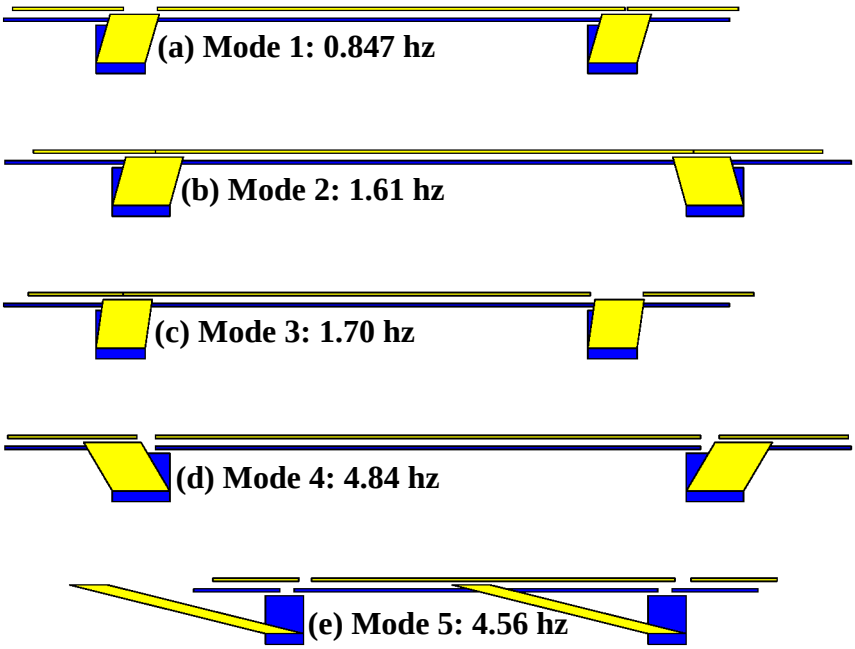

FIGURE 5-1 Mode Shapes of Uncontrolled Bridge

5.1.1 Ground Motion Records

The ground motion records used for simulation of the linear bridge were generated using the modified spectrum compatible approach defined in Chapter 2. Three different ground motion records of the same magnitude were utilized. Figure 5-2 shows the different time histories. The magnitude of the three time histories is 0.26, 0.19, and 0.21 g, respectively, and was determined such that the earthquakes excited the bridge model in the moderate region. Here the moderate region is defined as a region in which there is occasional impacting between the decks and/or the deck and abutment during the simulation, but not frequent impacting.

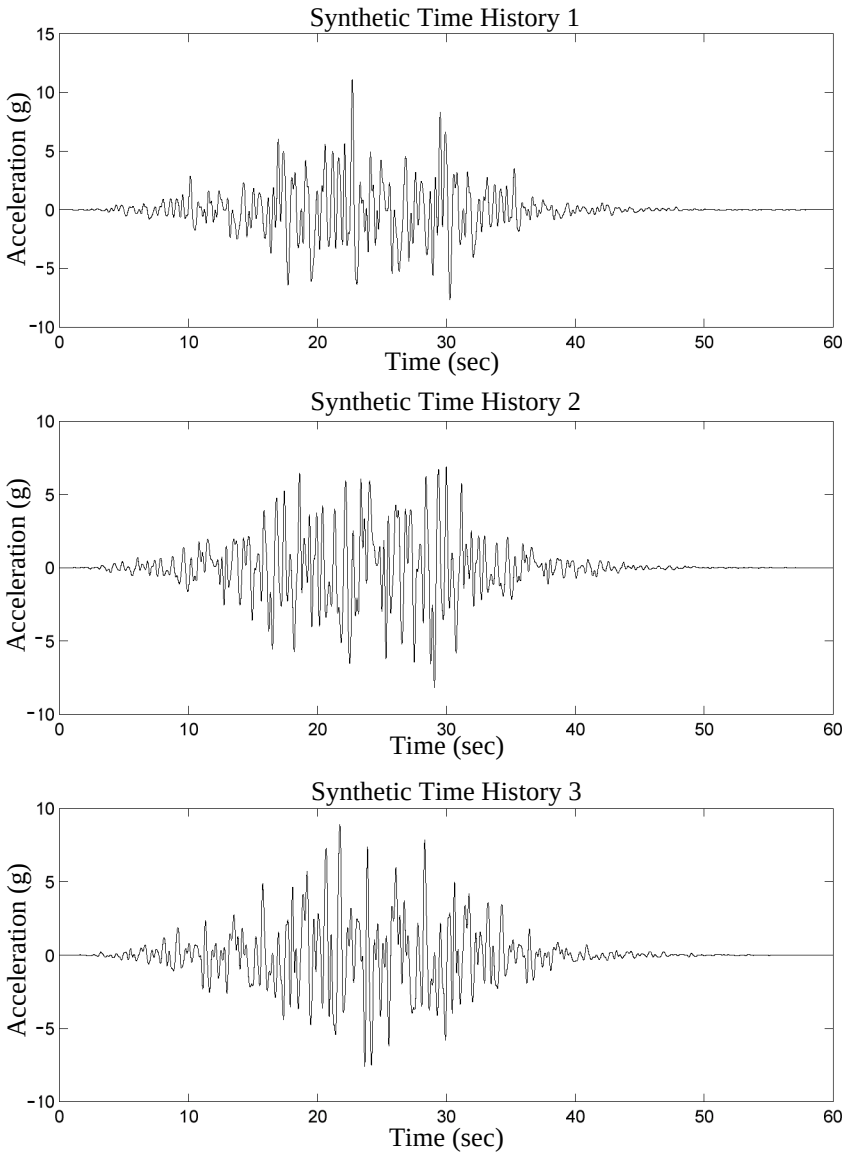

FIGURE 5-2 Synthetic Time Histories

The responses of the bridge for the best device placement case were also evaluated for the Kobe, Northridge, and El Centro Earthquakes in addition to the synthetic time histories. The magnitude of the Kobe, Northridge, and El Centro Earthquakes was scaled to 0.29 g, 0.29 g, and 0.28 g, respectively, to achieve an excitation of the bridge in the moderate region.

5.1.2 Simulation Test Cases

In order to evaluate the effectiveness of control on the linear bridge model, several different combinations of device placement were considered. Each device location case is summarized in Table 5-1 and depicted in Figure 5-3.

TABLE 5-1. Location Cases for Control Device Placement

Location Case (#)	Description
LOCEND (1)	One device each is placed between the left abutment and deck 1 and deck3 and the right abutment. (2 devices total)
LOCMID (2)	One device each is placed between deck 1 and deck 2 and between deck 2 and deck 3. (2 devices total)
LOC123 (3)	One device each is placed between the left abutment and deck1, deck 1 and deck2, and deck 2 and deck 3. (3 devices total)
LOCALL (4)	One device each is placed between the left abutment and deck1, deck 1 and deck2, deck 2 and deck 3, and deck 3 and the right abutment. (4 devices total)

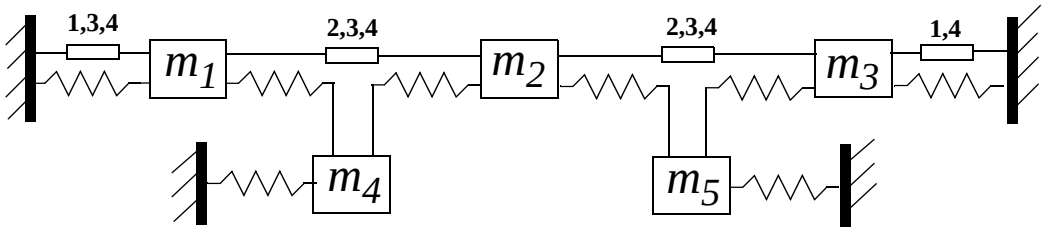

FIGURE 5-3 Placement of Control Devices for Each Location Case

All four location cases were evaluated for synthetic time history 1 from which the two most promising device location cases were chosen and evaluated for the three generated earthquakes. Furthermore, the best device location case chosen based on the three synthetic time histories were also evaluated for the Kobe, Northridge, and El Centro earthquakes.

The control strategies considered for the bridge were passive, active, and semi-active. These control strategies were designed as described in Chapter 2. In addition, for the active and semi-active control strategies, three weighting methods were tried. These weighting methods are defined in Table 5-2.

TABLE 5-2. Responses Weighted in Control Design

Type	Description
AA	All bridge mass accelerations
AD	All bridge mass displacement
EN	Total bridge energy

5.1.3 Evaluation Criteria

For ease in comparison, the peak controlled responses for the passive, active, and semi-active control strategies were normalized by the peak uncontrolled responses. Peak uncontrolled responses for synthetic time histories 1, 2, and 3 are given in Table 5-3 and for the Kobe, Northridge, and El Centro earthquakes in Table 5-4.

TABLE 5-3. Peak Uncontrolled Responses for Synthetic Time Histories

	Response	*Decks 1 & 3*	*Deck 2*
Time History 1	Displacement (in)	5.27	11.17
	Velocity (in/sec)	39.63	60.48
	Acceleration (in/sec^2)	320.0	341.7
Time History 2	Displacement (in)	5.65	13.81
	Velocity (in/sec)	38.96	81.31
	Acceleration (in/sec^2)	289.2	429.4
Time History 3	Displacement (in)	4.93	9.23
	Velocity (in/sec)	34.25	53.40
	Acceleration (in/sec^2)	280.5	329.3

TABLE 5-4. Peak Uncontrolled Responses for Recorded Earthquakes

	Response	*Decks 1 & 3*	*Deck 2*
Kobe	Displacement (in)	3.79	7.43
	Velocity (in/sec)	26.40	42.47
	Acceleration (in/sec^2)	213.2	241.7
Northridge	Displacement (in)	3.12	6.32
	Velocity (in/sec)	20.52	30.91
	Acceleration (in/sec^2)	170.0	205.3
EL Centro	Displacement (in)	3.70	7.93
	Velocity (in/sec)	26.32	43.63
	Acceleration (in/sec^2)	200.2	261.3

It should be noted that because the bridge model is symmetric, decks 1 and 3 have the same uncontrolled responses.

The normalized peak relative displacement for each time history, can be defined by

$$D_{pi} = \max_t \left(\frac{|x_i(t)|}{x_i^{\max}} \right) \tag{5-4}$$

where $x_i(t)$ is the relative displacement of the *i*th deck over the entire response, and $x_i^{\max}$ denotes the uncontrolled maximum displacement of the *i*th deck. The normalized peak relative velocity can be defined by

$$V_{pi} = \max_t \left(\frac{|\dot{x}_i(t)|}{\dot{x}_i^{\max}} \right) \tag{5-5}$$

where $\dot{x}_i(t)$ is the relative velocity of the *i*th deck over the entire response, and $\dot{x}_i^{\max}$ denotes the uncontrolled maximum velocity of the *i*th deck. Furthermore, the normalized peak absolute acceleration can be defined by

$$A_{pi} = \max_t \left(\frac{|\ddot{x}_{ai}(t)|}{\ddot{x}_{ai}^{\max}} \right) \tag{5-6}$$

where $\ddot{x}_{ai}(t)$ is the absolute acceleration of the *i*th deck over the entire response, and $\ddot{x}_{ai}^{\max}$ denotes the uncontrolled maximum absolute acceleration of the *i*th deck.

In order to achieve no impacting between decks and decks and abutments, the response of primary interest when comparing the effectiveness of the control strategies was relative deck displacement. Thus, the performance of the control strategies were compared by determining the minimum peak normalized relative deck displacement defined by

$$D_{min} = min(\mathbf{D_p}) \tag{5-7}$$

where $\mathbf{D_p} = \left[D_{p1}\ D_{p2}\ D_{p3} \right]$ with the subscript numbers referring to the appropriate deck section. The corresponding minimum peak normalized relative velocity and absolute acceleration defined by

$$V_{min} = min(\mathbf{V_p}) \tag{5-8}$$

$$A_{min} = min(\mathbf{A_p}) \tag{5-9}$$

where $\mathbf{V_p} = \left[V_{p1}\ V_{p2}\ V_{p3} \right]$ and $\mathbf{A_p} = \left[A_{p1}\ A_{p2}\ A_{p3} \right]$ were also calculated.

In addition to deck displacement, the control strategies were compared using peak control force $F_{c,\,max}$ and peak total force $F_{T,\,max}$ defined by

$$F_{c,\,max} = max\left[\mathbf{F_c} \right] \text{ and} \tag{5-10}$$

$$F_{T,\,max} = max\left[\mathbf{F_T} \right] \tag{5-11}$$

where $\mathbf{F_C}$ and $\mathbf{F_T}$ can be written as

$$\mathbf{F_C} = \max_t \left[f_{1c}(t)\ f_{2c}(t)\ \ldots f_{nc}(t) \right] \text{ and} \tag{5-12}$$

$$\mathbf{F_T}(\mathrm{t}) = \max_t \left[\left[f_{1c}(t)\ f_{2c}(t)\ \ldots f_{nc}(t) \right] + \left[f_{1b}(t)\ f_{2b}(t)\ \ldots f_{nb}(t) \right] \right] \tag{5-13}$$

Here, $f_{nc}(t)$ is the control force produced by the *n*th control device at time *t* of the simulation and $f_{nb}(t)$ is the bearing force at the location of the *n*th control device at time *t* of the simulation.

5.1.4 Results

Initially, all four location cases, *LocEND, LocMID, Loc123,* and *LocALL,* were simulated for synthetic time history 1 using all three weighting cases, *AA, AD,* and *EN*. The two location cases that produced the most promising results were *LocMID* and *LocALL*. Figure 5-4 shows plots of the peak normalized deck displacement versus peak total force for all location cases and the *EN* weighting subjected to synthetic time history 1. Here, the peak total force refers to the peak over all total forces, control plus bearing forces. Likewise, the peak deck displacement is the peak deck displacement over all of the three bridge decks. The graphs were generated by varying the amount of weighting for the passive, active, and semi-active control strategies. Furthermore, the passive control case was limited by stability of the controller. Thus, the line on the graphs corresponding to the passive case ends when the control weighting causes the passive control system to go unstable. The vertical and horizontal lines in the plots represent impact boundaries, with the location of no impacting for each control case being in the direction of the arrows.

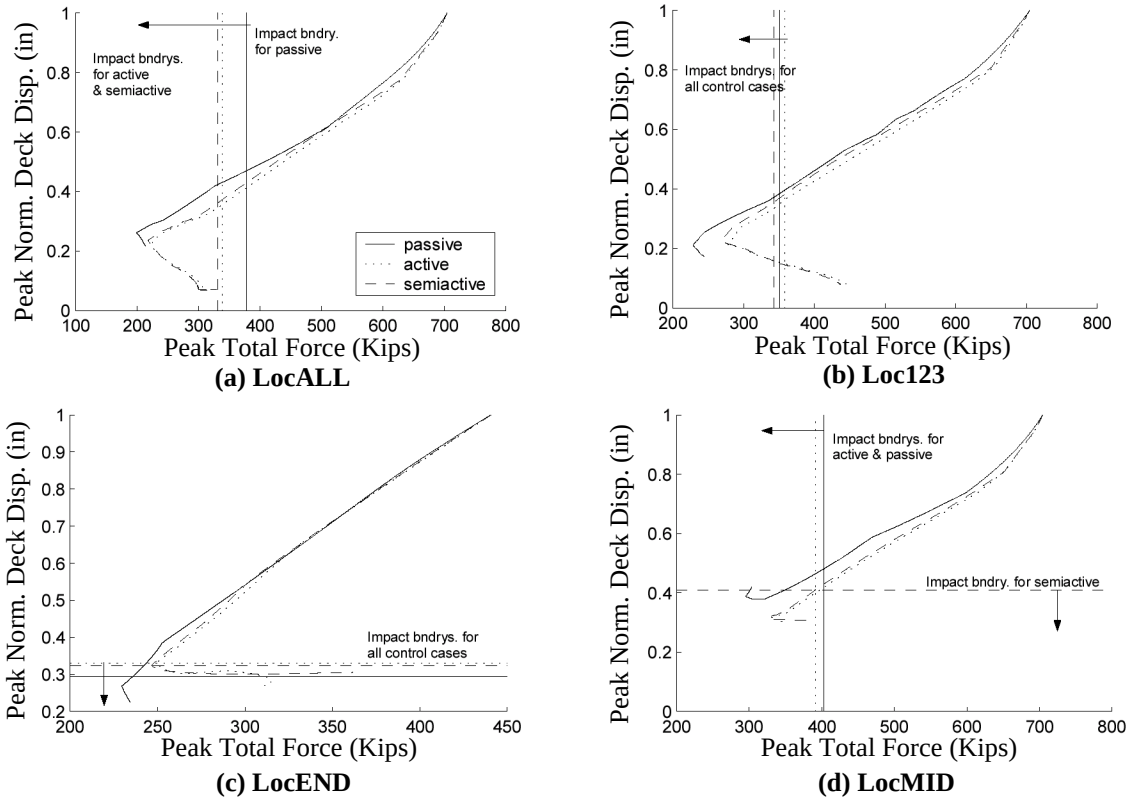

FIGURE 5-4 Peak Normalized Deck Displacement vs. Peak Total Force for All Location Cases with EN weighting

As the plots show for the *LOCALL* and *LocMID* cases, the active and semi-active control strategies are able to achieve or exceed the minimum peak normalized deck displacement achieved by the passive case at a comparable peak total force. On the other hand for the *Loc123* case, the active and semi-active control strategies require a larger total force to achieve the same minimum peak normalized deck displacement as the passive case. Moreover, *Loc123* requires an asymmetric placement of the control devices. The active and semi-active control strategies for the *LocEND* case cannot achieve as low of a minimum peak normalized deck displacement as the passive case. Therefore, since the location cases of *LocALL* and *LocMID* produce the best results for synthetic time history 1, these two location cases are also simulated for synthetic time histories 2 and 3. Again, all three weighting cases are used.

The most effective control strategy was found to be the case in which the total energy of the system is weighted (*EN* case). Figure 5-5 gives the plots of peak normalized deck displacement versus peak total force for *LocALL* and all weighting cases using synthetic time history 1. As can be seen from the plots, the *EN* weighting is able to achieve lower peak normalized deck displacements for both the active and semi-active control strategies. The same result is also evident with the *LocMID* case as well as synthetic time histories 2 and 3. Thus, the *EN* weighing case was chosen to be the best weighting method for the active and semi-active control strategies and will be the only weighing case discussed in subsequent analyses using the synthetic time histories.

In order to determine the best device placement case from those chosen, *LocMID* or *LocALL*, the bridge deck responses as defined in Eqs. (5-7) through (5-9) were compared for the passive, active, and semi-active control strategies. To compare the effectiveness of the use of four control devices (*LocALL)* versus two control devices (*LocMID)*, plots of peak normalized deck displacement versus peak control force and peak total force are presented in Figure 5-6. The results in Figure 5-6 are from synthetic time history 2. As the plots show, for both location cases a lower peak normalized deck displacement is achieved for the active and semi-active control strategies at a higher peak control force than for the passive case. However, the active and semi-active control strategies are able to achieve lower peak normalized deck displacements over the passive case at the same peak total force. Here, the peak total force, control force plus bearing force, would be more important because of its use in designing the bridge connections.

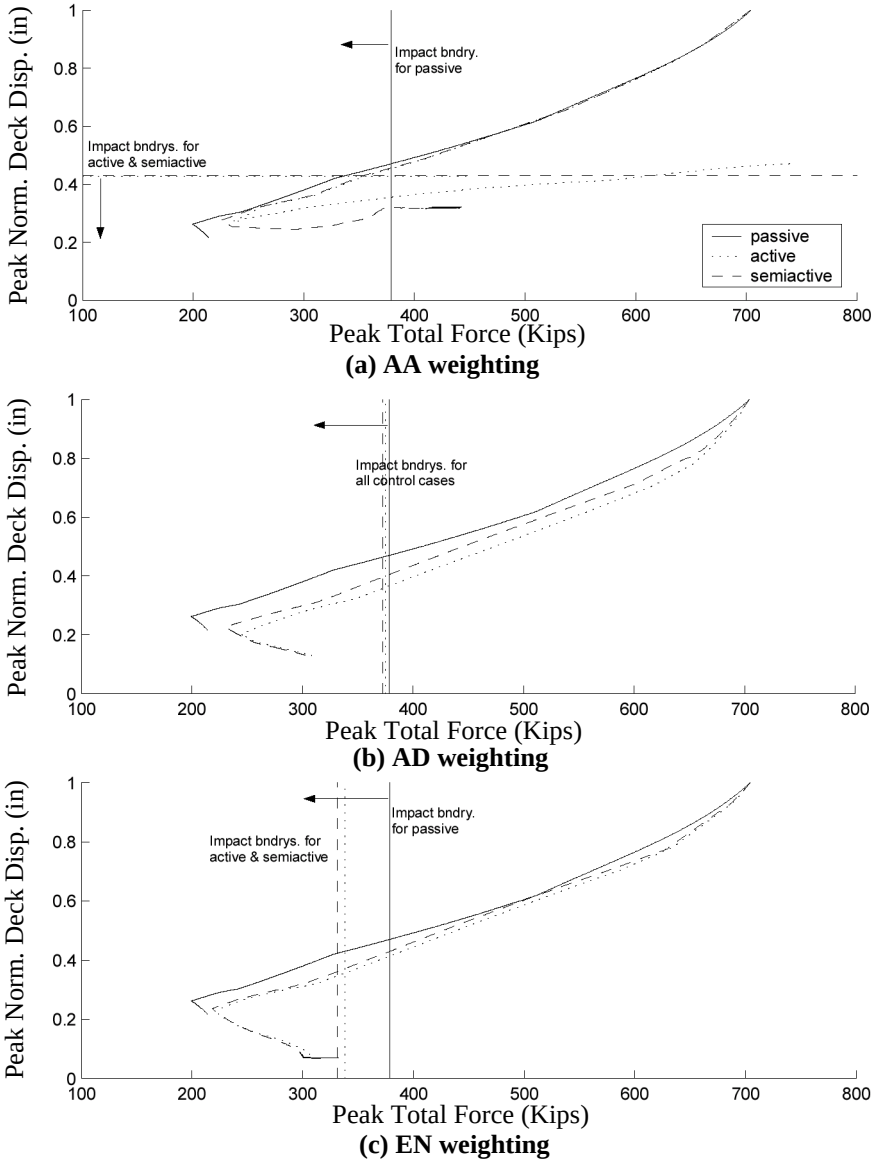

FIGURE 5-5 Peak Normalized Deck Displacement vs. Peak Total Force for *LocALL* and all weighting cases Due to Synthetic Time History 1

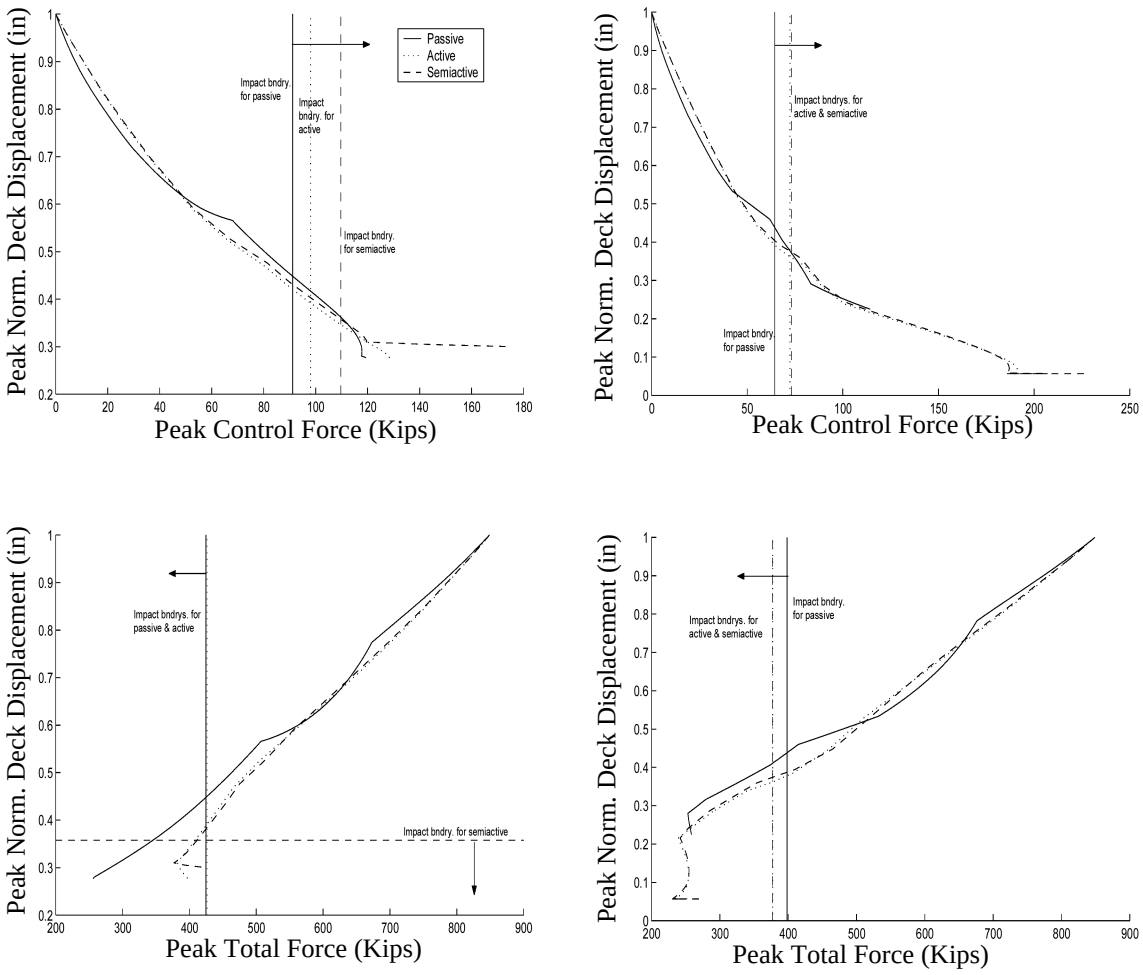

(a) LocMID **(b) LocALL**

FIGURE 5-6 Force vs. Displacement Plots Due to Synthetic Time History 2 for *LocMID* and *LocALL* with the *EN* Weighting Case

Moreover, with the use of four devices (*LocALL*) the active and semi-active control strategies are able to achieve a lower minimum peak normalized deck displacement and lower peak total force than the passive case. However, with the use of two devices (*LocMID*) the active and semi-active control strategies are not able to out perform the passive case.

Table 5-5 summarize the bridge deck responses obtained for the passive, active, and semi-active control strategies using synthetic time history 2. The responses presented in Table

5-5 are normalized by the uncontrolled responses reported earlier. For the passive case, the results in the table represent the best reduction in relative deck displacement that can be achieved. Furthermore, for the active and semi-active cases, the results in the table represent the best relative deck displacement that can be achieved with respect to a low total force when compared to the total force requirement for the passive case. As indicated in the table, the numbers in parenthesis represent the percent reduction over the passive case.

TABLE 5-5. Normalized Bridge Deck Responses for *Loc23* and *LocALL* Due To Synthetic Time History 2

		D_{min}	V_{min}	A_{min}	$F_{c,max}$	$F_{T,max}$
LocMID	Passive (c = 11.82)	0.277	0.300	0.341	119.3	255.8
	Active (*EN*) (wt = 30)	0.309 (+12%)[a]	0.318 (+6%)	0.302 (-11%)	120.3 (+0.84%)	382.4 (+49%)
	Semi-active (*EN*) (wt = 60)	0.310 (+12%)	0.308 (+2.7%)	0.306 (-11%)	119.4 (0%)	377.0 (+32%)
LocALL	Passive (c = 9.8201)	0.225	0.239	0.225	114.2	258.4
	Active (*EN*) (wt = 40,000)	0.049 (-78%)	0.057 (-76%)	0.175 (-29%)	187.8 (+64%)	227.7 (-12%)
	Semi-active (*EN*) (wt = 7300)	0.058 (-74%)	0.066 (-72%)	0.183 (-19%)	186.0 (+63%)	231.9 (-10%)

a. Numbers in parentheses indicate percent reduction as compared to the passive case. Negative numbers correspond to a response reduction.

As the numbers in the table indicate, the *LocALL* case is able to greatly reduce the deck responses of displacement, velocity, and acceleration with reductions over the passive case of 78%, 76%, and 29%, respectively, for active control and 74%, 72%, and 19%, respectively for semi-active control. In addition, peak total force is reduced over the passive case by 12% with active control and 10% with semi-active control. On the other hand, the *LocMID* case achieves an increase of all deck responses, except acceleration, over the passive case for both active and semi-active control. Furthermore, there is a significant increase in

peak total force over the passive case with active and semi-active control. From these observations, it appears that the use of four devices (*LocALL*) is the better choice.

Here, it should be noted that the active and semi-active control strategies achieve similar results, as demonstrated in Table 5-5. However, semi-active control systems have significant advantages over active control systems. For example, an active control system can add energy to the overall structural system, whereas a semiactive control system cannot. Thus, a semi-active control system is considered to be stable (in a bounded-input, bounded-output sense). Moreover, semi-active control systems only require a minimal amount of power, such as a battery. As a result, semi-active control devices appear to be a more reliable choice over active control devices.

Previously, it was shown that the minimum peak normalized deck displacement produced by synthetic time history 1 for the *LocMID* and *LocALL* cases was less for the active and semi-active control strategies than for the passive case at the same total force requirement. The same result is also evident for synthetic time histories 2 and 3. For example, if a total force requirement of 275 kips is chosen for the *LocALL* case and 450 kips for the *LocMID* case, a bar chart showing a comparison of the minimum peak normalized deck displacement for each control strategy due to each synthetic time history can be produced and is shown in Figure 5-7. As the figure shows, for the same total force requirement both active and semi-active control achieve reduced peak normalized deck displacements over passive control for both the *LocMID* and *LocALL* cases with all time histories. In addition, the bar chart comparison shows that the *LocALL* case achieves a lower reduction of the peak normalized deck displacement over the passive case than does the *LocMID* case.

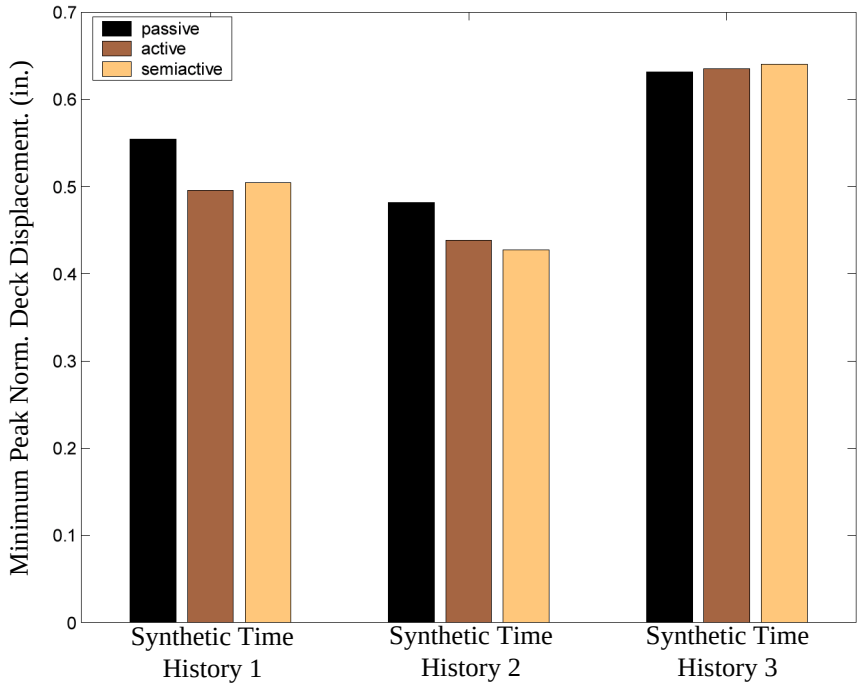

(a) LocMID

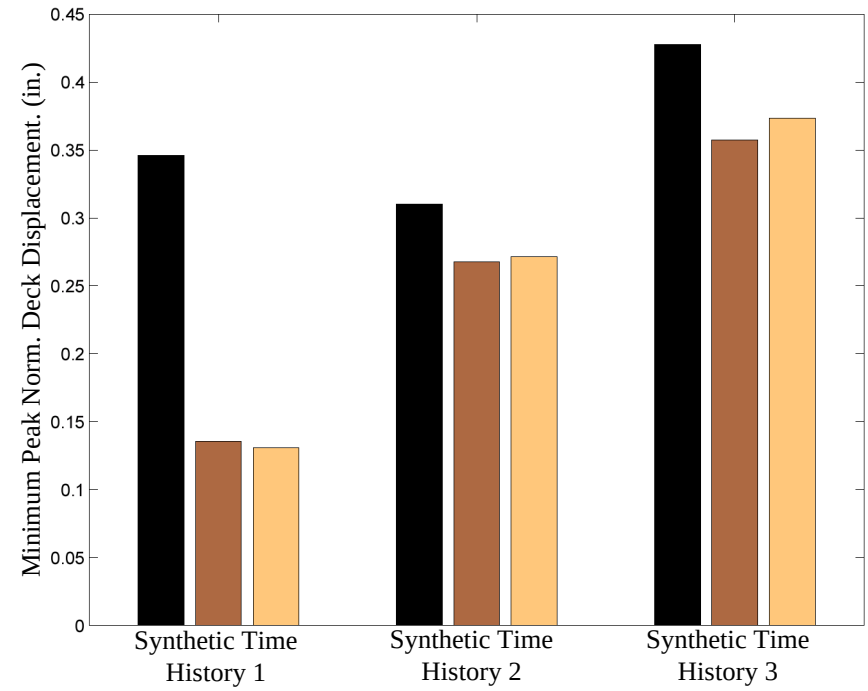

(b) LocALL

FIGURE 5-7 Bar Chart Comparison of Minimum Peak Normalized Deck Displacement for *LocMID* and *LocALL*.

To further investigate the best device placement case (*LocALL*) chosen based on simulations using the synthetic time histories, the Kobe, Northridge, and El Centro earthquakes were used in simulation to evaluate the bridge responses with the *LocALL* device placement case. The results are presented in Table 5-6. For the active and semi-active cases, the results in the table represent the best relative deck displacement that can be achieved with respect to a low total force when compared to the total force requirement for the passive case. Furthermore, as indicated in the table, the numbers in parenthesis represent the percent reduction over the passive case.

TABLE 5-6. Normalized Bridge Deck Responses for *LocALL* due to the Kobe, Northridge, and El Centro Earthquakes

		D_{min}	V_{min}	A_{min}	$F_{c,max}$	$F_{T,max}$
Kobe	Passive (c = 9.8201)	0.402	0.540	0.438	292.4	140.8
	Active (*AA*) (wt = 20)	0.290 (-28%)[a]	0.378 (-30%)	0.216 (-51%)	293.2 (0%)	146.1 (+3.8%)
	Semi-active (*AA*) (wt = 40)	0.296 (-26%)	0.379 (-30%)	0.227 (-48%)	289.5 (-1%)	153.9 (+9.3%)
Northridge	Passive (c = 9.8201)	0.461	0.585	0.445	254.4	117.9
	Active (*AD*) (wt = 4700)	0.355 (-23%)	0.573 (-2.1%)	0.410 (-7.9%)	248.6 (-2.3%)	144.0 (+22%)
	Semi-active (*AD*) (wt = 4800)	0.369 (-20%)	0.551 (-5.8%)	0.410 (-7.9%)	248.6 (-2.3%)	147.0 (+25%)
El Centro	Passive (c = 9.8201)	0.570	0.374	0.421	299.1	109.1
	Active (*AD*) (wt = 4900)	0.470 (-18%)	0.383 (+2.4%)	0.421 (0%)	290.7 (-2.8%)	145.1 (+33%)
	Semi-active (*AD*) (wt = 4100)	0.485 (-15%)	0.374 (0%)	0.421 (0%)	288.7 (-3.5%)	137.8 (+26%)

a. Numbers in parentheses indicate percent reduction as compared to the passive case. Negative numbers correspond to a response reduction.

As the results in the table indicate, significant reductions are achieved over the passive case by the active and semi-active control strategies for all three recorded earthquakes. The greatest reductions in relative displacement, velocity and absolute acceleration are obtained for the Kobe earthquake with reductions of 28%, 30%, and 51%, respectively, for the active case and 26%, 30%, and 48%, respectively for the semi-active case. Furthermore, the best control weighting method for the Kobe earthquake was the all mass acceleration weighting (*AA*). However, for the Northridge and EL Centro earthquakes, the best weighting method was the all mass displacement weighting (*AD*).

5.2 Control Study of Nonlinear Bridge Model

The model considered for this control study is Nonlinear Bridge Model 1, using the bilinear bearing model as described in Chapter 4. With the addition of *n* control devices to the nonlinear bridge model, the equations of motion will change to

$$\mathbf{M}\ddot{\mathbf{x}} + \mathbf{C}\dot{\mathbf{x}} + \mathbf{K}\mathbf{x} = \mathrm{L}_b\mathbf{f}_b + \mathrm{L}_c\mathbf{f}_c - \mathbf{M}\mathrm{G}\ddot{x}_g \tag{5-14}$$

where **x** is a vector of the displacements of the bridge masses relative to the ground, $\mathbf{f}_b$ is a vector of bearing forces ($[f_{b1}, f_{b2}, f_{b3}, f_{b4}, f_{b5}, f_{b6}]^T$), $\mathbf{f}_c = [f_{1c}, f_{2c}, \ldots f_{nc}]^T$ is a vector of the control forces generated by the *n* control devices, G is a column vector of ones, L_c is a matrix determined by the placement of the *n* control devices, and L_b is defined from the contribution of each bearing force as

$$\mathrm{L}_b = \begin{bmatrix} 1 & -1 & 0 & 0 & 0 & 0 \\ 0 & 0 & 1 & -1 & 0 & 0 \\ 0 & 0 & 0 & 0 & 1 & 1 \\ 0 & 1 & -1 & 0 & 0 & 0 \\ 0 & 0 & 0 & 1 & -1 & 0 \end{bmatrix}$$

Furthermore, the **M, C,** and **K** matrices are the same as defined for the nonlinear bridge model in Chapter 4. Using this equation, the state space form can be written

$$\dot{\mathbf{z}} = \mathbf{A}\mathbf{z} + \mathbf{B}\begin{bmatrix} \ddot{x}_g \\ \mathbf{u}_b \\ \mathbf{u}_c \end{bmatrix} \tag{5-15}$$

$$\mathbf{y} = \mathbf{C}\mathbf{z} + \mathbf{D}\begin{bmatrix} \ddot{x}_g \\ \mathbf{u}_b \\ \mathbf{u}_c \end{bmatrix} \tag{5-16}$$

where **z** is the state vector, **y** is the vector of measured outputs for determing the control action, $\mathbf{u}_b$ is a vector of bearing forces, and $\mathbf{u}_c$ is a vector of control forces. For this model, the state vector consists of the displacement and velocity of each mass relative to the ground and the measured outputs for determing the control action are the absolute acceleration and control forces. The **A**, **B**, **C,** and **D** matrices can be redefined as

$$\mathbf{A} = \begin{bmatrix} \mathbf{0} & \mathbf{I} \\ -\mathbf{M}^{-1}\mathbf{K} & -\mathbf{M}^{-1}\mathbf{C} \end{bmatrix}, \mathbf{B} = -\begin{bmatrix} & \mathbf{0} & \\ \mathrm{G} & -\mathbf{M}^{-1}\mathrm{L}_b & -\mathbf{M}^{-1}\mathrm{L}_c \end{bmatrix},$$

$$\mathbf{C} = \begin{bmatrix} & \mathbf{I} & \\ -\mathbf{M}^{-1}\mathbf{K} & & -\mathbf{M}^{-1}\mathbf{C} \end{bmatrix} \text{ and } \mathbf{D} = \begin{bmatrix} & \mathbf{0} & \\ \mathbf{0} & -\mathbf{M}^{-1}\mathrm{L}_b & -\mathbf{M}^{-1}\mathrm{L}_c \end{bmatrix}$$

5.2.1 Ground Motion Records

The synthetic ground motion records used for simulation of the nonlinear bridge model are the same as those described in Section 5.1.1 for the linear bridge model. Furthermore, the Kobe and Northridge earthquakes were also considered and were scaled to 0.29g.

5.2.2 Simulation Test Cases

In the control study of the linear bridge model, described in Section 5.1, the most effective device placement case was *LocALL*. For the *LocALL* case, four total devices are utilized, with one device each placed between the left abutment and deck 1, deck 1 and deck 2,

deck 2 and deck 3, and deck 3 and the right abutment (refer to Section 5.1.2). Therefore, the *LocALL* device location case is the only case evaluated for the nonlinear bridge model.

In addition, the weighting methods used for the active and semi-active control strategies for the nonlinear bridge model are the same as those given in Table 5-2 used for the linear bridge, except for the addition of one extra weighting case. The additional weighting case used for the nonlinear bridge control study is the weighting of bridge inter-mass displacements, *ID*.

5.2.3 Evaluation Criteria

The evaluation criteria used for the control study of the nonlinear bridge model are the same as those used for the control study of the linear bridge model and are described in Section 5.1.3 and Eqs. (5-4) through (5-13). Peak uncontrolled responses for the nonlinear bridge model using synthetic time histories 1, 2, and 3 are given in Table 5-7 and using the Kobe and Northridge earthquakes are given in Table 5-8.

TABLE 5-7. Peak Uncontrolled Responses for Synthetic Time Histories

	Response	*Decks 1 & 3*	*Deck 2*
Time History 1	Displacement (in)	2.70	7.34
	Velocity (in/sec)	17.63	31.58
	Acceleration (in/sec^2)	89.0	125.5
Time History 2	Displacement (in)	2.92	6.84
	Velocity (in/sec)	15.28	27.56
	Acceleration (in/sec^2)	94.42	113.7
Time History 3	Displacement (in)	2.61	6.38
	Velocity (in/sec)	15.26	29.25
	Acceleration (in/sec^2)	90.58	111.7

TABLE 5-8. Peak Uncontrolled Responses for Recorded Earthquakes

	Response	*Decks 1 & 3*	*Deck 2*
Kobe	Displacement (in)	2.42	5.24
	Velocity (in/sec)	16.10	27.51
	Acceleration (in/sec^2)	99.17	95.80
Northridge	Displacement (in)	2.70	7.57
	Velocity (in/sec)	15.83	28.09
	Acceleration (in/sec^2)	73.33	119.18

5.2.4 Results

In order to evaluate the effectiveness of the addition of control to the nonlinear bridge model, the *LocALL* case was simulated for synthetic time histories 1, 2, and 3, and for the Kobe and Northridge earthquakes. Furthermore, four weighting methods were considered, *AA*, *AD*, *EN*, and *ID*.

Figure 5-8 shows plots of the peak normalized deck displacement versus peak total force for all weighting methods due to synthetic time history 2. As the plots demonstrate, the *EN* weighting case for the active control strategy is able to achieve roughly the same minimum peak normalized displacement when compared to the passive case at the same total force requirement. However, the peak normalized displacement is increased with active and semi-active control for the other weighting cases. Better results can be obtained when comparing peak normalized deck displacement vs. peak control force for the passive, active, and semi-active control strategies. Plots of peak normalized deck displacement vs. peak control force are presented in Figure 5-9.

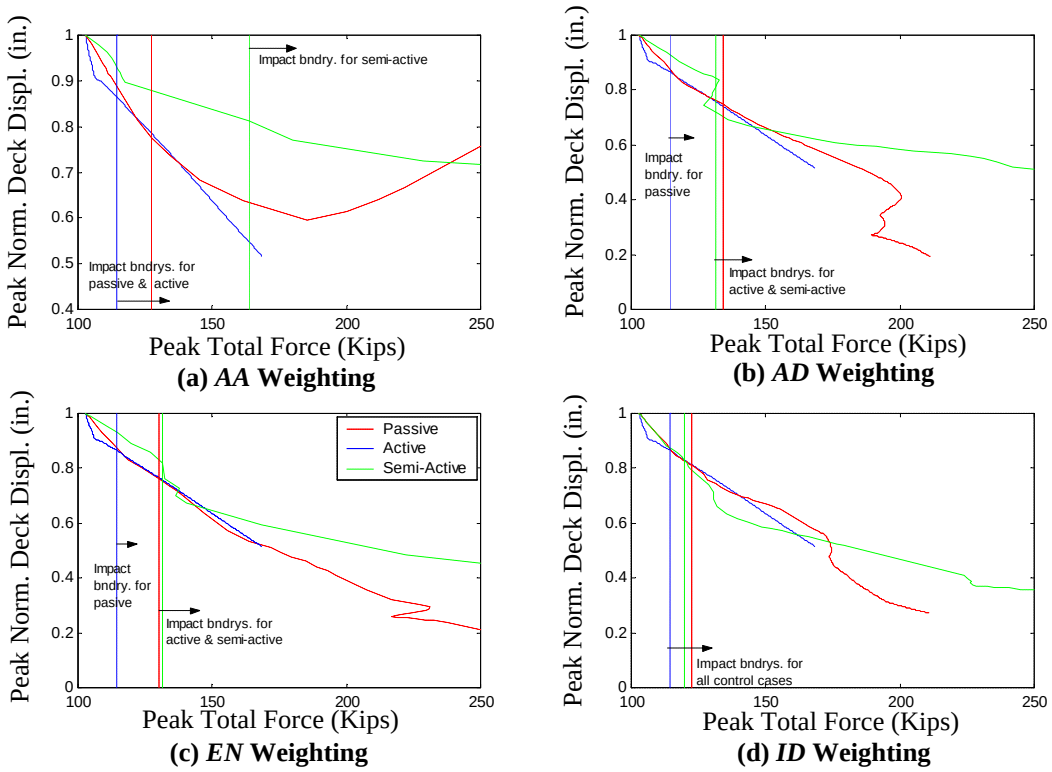

FIGURE 5-8 Peak Normalized Deck Displacement vs. Peak Total Force Due to Synthetic Time History 2 for All Weighting Cases.

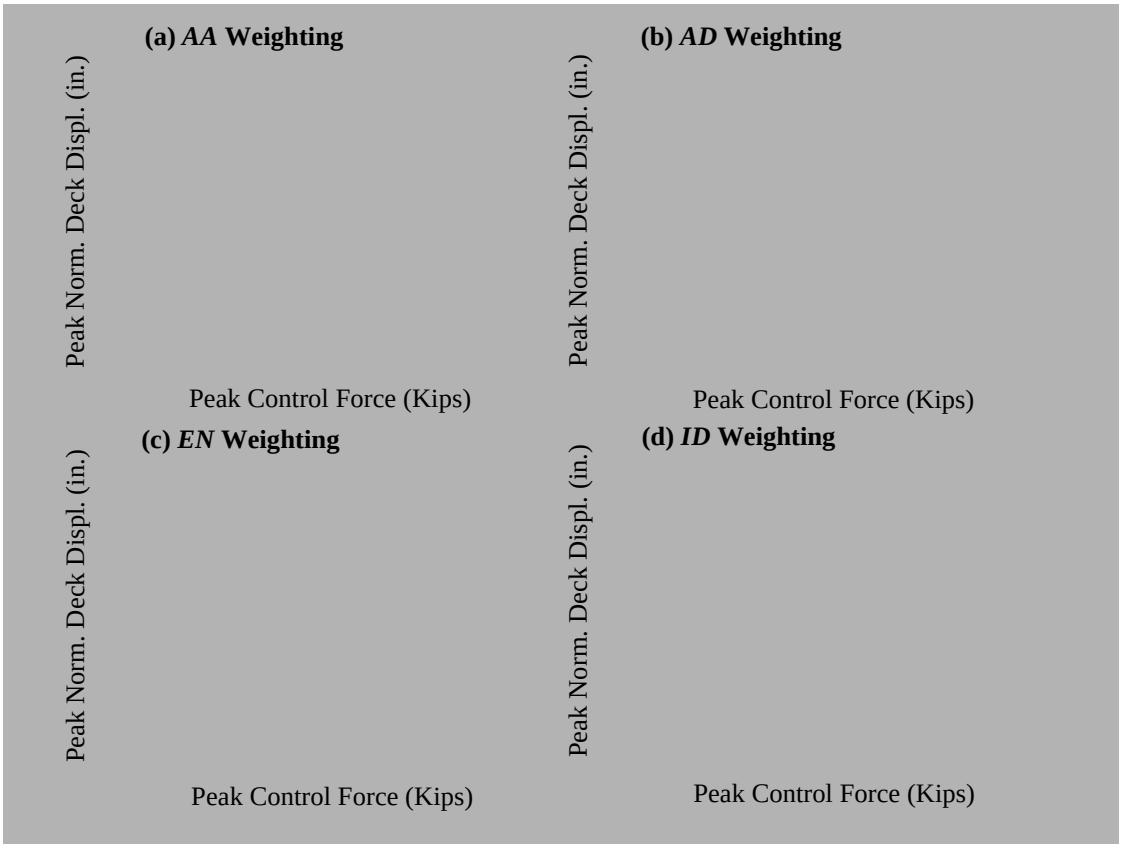

FIGURE 5-9 Peak Normalized Deck Displacement vs. Peak Control Force Due to Synthetic Time History 2 for All Weighting Cases.

From Figure 5-9, it is evident that with the *ID* weighting case the active and semi-active control strategies are able to achieve a lower minimum peak normalized deck displacement than the passive case with respect to the same control force requirement. Furthermore, the same is true for the active control strategy with the *EN* weighting case. However, for the *AA* and *AD* weighting cases, the active and semi-active control strategies are not able to out perform the passive control system.

Table 5-9 presents the bridge responses obtained for the passive, active, and semi-active control strategies for synthetic time histories 1 and 2 and the Kobe earthquake.

TABLE 5-9. Normalized Bridge Deck Responses for Nonlinear Bridge Model for Synthetic Time Histories 1 & 2 and the Kobe Earthquake.

		D_{min}	V_{min}	A_{min}	$F_{c,max}$	$F_{T,max}$
Synthetic Time History 1	Passive (c = 9.8201)	0.351	0.484	0.547	157.9	93.5
	Active (*ID*) (wt = 5600)	0.362 (+3.1%)[a]	0.477 (-1.4%)	0.587 (+7.3%)	157.9 (0%)	77.4 (-17.2)
	Semi-active (*ID*) (wt = 950)	0.468 (+33%)	0.604 (+25%)	0.653 (+19%)	156.8 (0%)	74.9 (-20%)
Synthetic Time History 2	Passive (c = 8.4101)	0.516	0.587	0.673	168.5	86.7
	Active (*ID*) (wt = 8600)	0.431 (-16%)	0.560 (-4.6%)	0.705 (+4.8%)	177.4 (+5.3%)	86.7 (0%)
	Semi-active (*ID*) (wt = 1100)	0.506 (-2%)	0.579 (-1.4%)	0.742 (+10%)	183.9 (+9.1%)	87.1 (0%)
Kobe	Passive (c = 9.8201)	0.458	0.663	0.685	183.9	119.4
	Active (*AA*) (wt = 10)	0.417 (-9%)	0.538 (-19%)	0.411 (-40%)	180.9 (-1.6%)	104.3 (-13%)
	Semi-active (*AA*) (wt = 0.37)	0.532 (+14%)	0.640 (-3.5%)	0.528 (-23%)	183.3 (0%)	111.0 (-7%)

a. Numbers in parentheses indicate percent reduction as compared to the passive case. Negative numbers correspond to a response reduction.

For the passive case, the results in the table represent the best reduction in relative deck displacement that can be achieved. Furthermore, for the active and semi-active cases, the results presented in the table for synthetic time history 1 and the Kobe earthquake represent the best relative deck displacement that can be achieved with respect to a comparable total force when compared to the total force requirement for the passive case. The results for the active and semi-active control strategies presented in the table for synthetic time history 2 represent the best relative deck displacement that can be achieved with respect a control force requirement comparable to that of the passive case. As indicated in the table, the numbers in parenthesis represent the percent reduction over the passive case.

From the results presented in Table 5-9, the greatest reduction in relative deck displacement occurred by weighting the deck inter-mass displacements (*ID*) giving a 16% and 2% reduction over the passive case, respectively, for the active and semi-active control strategies with synthetic time history 2. Furthermore, peak control force requirement for the active and semi-active cases was the same as for the passive case, while peak total force increased by a small amount for active and semi-active control. For the Kobe earthquake, the all mass acceleration weighing case (*AA*) was most effective, giving a reduction in relative displacement, velocity, and absolute acceleration for the active case of 9%, 19%, and 40%, respectively. For the same weighting case and the Kobe earthquake with semi-active control relative velocity and absolute acceleration were also reduced, however relative displacement was increased. In addition, the peak total force requirement for the active and semi-active control cases was the same as for the passive case, while peak control force for active and semi-active was decreased over the passive case.

5.3 Summary

In summary, a linear and nonlinear bridge model of a multi span simply supported bridge was controlled using passive, active, and semi-active control strategies. Several device placement location cases and weighting methods were evaluated. The results for the linear bridge model demonstrated that the use of four devices (*LocALL*) produces the best response reduction for the active and semi-active cases over the passive case. Also, for the linear bridge model the most effective response weighting for the active and semi-active control strategies when the synthetic time histories were used was found to be the case in which the total energy of the system is weighted (*EN* case). However, when using the recorded earthquake time histories, Kobe, Northridge, and El Centro, with the linear bridge model the most effective response weighting depended on the earthquake used. Moreover, for the linear bridge model the two most effective response weighting methods for the Kobe, Northridge, and El Centro earthquakes were the all mass acceleration weighting (*AA*) and the all mass displacement weighting (*AD*). The effectiveness of control for the

nonlinear bridge model was evaluated using *LocALL* and several weighting methods. The results for the nonlinear bridge model demonstrated that the active and semi-active control strategies could achieve reductions in bridge responses with the all mass acceleration weighting (*AA*) and the deck inter-mass displacement weighting (*ID*).

Chapter 6

Conclusions and Recommendations

Devastating failures, requiring costly repairs, occur in civil engineering structures as a result of seismic events. Mitigation methods, such as the use of modern control techniques, are key in reducing these earthquake induced failures in civil engineering structures. In this research, numerous control strategies have been investigated for the reduction of structural responses in buildings and bridges subjected to earthquake loading. In particular, the effectiveness of several semi-active control algorithms are compared for a building structure. Also, a bridge structure is controlled using ideal passive, active, and semi-active control and the resulting bridge responses are compared.

In the building control study, presented in Chapter 3, a variety of semi-active control algorithms for use with multiple MR dampers are presented and evaluated through a numerical example. The control algorithms examined are the Lyapunov controller, the decentralized bang-bang controller, the maximum energy dissipation controller, the clipped-optimal controller, and the modulated homogenous controller. To ensure that the algorithms would be implementable on a physical structure, measurements of absolute acceleration and device placements are used for determining the control action for each algorithm.

To compare and contrast the performance of each control algorithm, a numerical example consisting of a six-story building model with MR dampers on the bottom two floors is utilized. The MR damper behavior is modeled after an experimentally-verified phenomenological model based on the Bouc-Wen model. Furthermore, the El Centro earthquake is used, in simulation, to excite the structure and examine the reduction in drifts, accelerations, and relative displacements throughout the building structure with each proposed control algorithm.

The resulting building structural responses varied greatly depending on which semi-active control algorithm was utilized. However, each algorithm in some way produced an improvement over the best passive controller. For reductions in absolute acceleration, clipped-optimal controller A was most effective. On the other hand, Lyapunov controller B was superior in reduction of relative displacement. In addition, significant reduction in relative displacement and interstory drift was achieved with the modulated homogenous friction algorithm, although an increase in absolute acceleration was observed. Overall, the Lyapunov control algorithm, the clipped-optimal control algorithm, and the modulated homogenous friction control algorithm were found to be most suited for use with the MR damper in a multi-input control system.

In addition to building structures, bridge structures are in need of protection during seismic events. This research has investigated the use of ideal passive, active, and semi-active devices in a bridge structure. The bridge structure is modeled after a multi-span simply supported bridge with elastomeric bearings. Chapter 4 presents the linear and nonlinear bridge and bearing models developed in MATLAB (1999). For the nonlinear bridge model, two nonlinear bearing models were considered, a bilinear model and a Bouc-Wen model. Through simulation, the bridge responses, namely peak and RMS bridge mass relative displacement, velocity, and acceleration, were evaluated and compared for each bearing model. Synthetic ground motion records, generated using a modified spectrum compatible approach (Chapter 2), were used in the analysis.

In Chapter 5, the linear and nonlinear bridge model were used to evaluate the control strategies of ideal passive, active, and semi-active. Design of the ideal passive, active, and semi-active control devices was described in detail in Chapter 2. Through simulation, the effectiveness of each control device was evaluated by comparing bridge deck responses, namely relative displacement. Several device placement combinations were considered as well as different response weighting methods for the active and semiactive control algorithms. Furthermore, three synthetic earthquakes of magnitude 0.26, 0.19, and 0.21 g, respectively, were used for the simulations. The Kobe, Northridge, and El Centro earthquakes were also used.

The best results for control of the linear bridge model were achieved with the use of 4 devices (*LocALL*). When using the synthetic time histories with the linear bridge model, the most effective weighing method was total system energy weighting (*EN*). In particular, the active and semi-active control strategies were able to reduce bridge deck displacement by 29% and 19%, respectively. Furthermore, peak total force was reduced over the passive case by 12% and 10%, respectively, for the active and semi-active control strategies. With the Kobe, Northridge, and El Centro earthquakes and the linear bridge model, the most effective weighting depended on the earthquake. For example, for the Kobe earthquake the all mass acceleration weighing (*AA*) was best, whereas for the Northridge and El Centro earthquakes the all mass displacement weighing (*AD*) was most effective. In particular, active and semi-active control reductions in relative displacement were 28% and 26%, respectively, for the Kobe earthquake.

Since the *LocALL* device placement case produced the most effective results for the linear bridge model, this case was used to evaluate passive, active, and semi-active control strategies for the nonlinear bridge model. The best weighting methods for active and semi-active control with the nonlinear bridge model were the all mass acceleration weighting (*AA)* and the deck inter-mass displacement weighting (*ID*). For example, using synthetic time history 2, relative deck displacement was reduced by 16% and 2%, respectively for the active and semi-active control strategies. Furthermore, for the Kobe earthquake relative deck

displacement was decreased by 9% for active control, but slightly increased with semi-active control.

Overall, this thesis has presented research for the application of modern control strategies to building and bridge structures. Namely, the use of semi-active control algorithms with multiple magnetorheological dampers in a building structure has been investigated. Furthermore, ideal passive, active, and semi-active control strategies have been evaluated for use in a bridge structure. To expand upon the application of control to the bridge structure, further research should included the addition of control devices between the decks and columns of the bridge. Furthermore, more research needs to be conducted to evaluate the performance of the control strategies with the nonlinear bridge model.

References

Brogan, W.L. (1991). *Modern Control Theory*, Prentice Hall, Englewood Cliffs, New Jersey.

Carlson, J.D. (1994). "The Promise of Controllable Fluids," *Proc. of Actuator 94* (H. Borgmann and K, Lenz, Eds.), AXON Technoligie Consult GmbH, pp. 266–270.

Carlson, J.D. and Weiss, K.D. (1994). "A Growing Attraction to Magnetic Fluids," *Machine Design*, August, pp. 61–64.

Carlson, J.D. and Spencer Jr. B.F. (1996a). "Magneto-Rheological Fluid Dampers for Semi-Active Seismic Control," *Proc. of the 3rd Int. Conf. on Motion and Vibr. Control*, Chiba, Japan, Vol. 3, pp. 35–40.

Carlson, J.D. and Spencer Jr., B.F. (1996b). "Magneto-Rheological Fluid Dampers: Scalability and Design Issues for Application to Dynamic Hazard Mitigation," *Proc. 2nd Int. Wkshp. on Struc. Control*, Hong Kong, pp. 99–109, Dec.

Carlson, J.D., Catanzarite, D.M., and St. Clair, K.A. (1996). "Commercial Magneto-Rheological Fluid Devices," *International Journal of Modern Physics B*, Vol. 10, Nos. 23 & 24, pp. 2857–2865.

DesRoches, R., Leon, R., Choi, E., Lam, T.T., Dyke S.J., and Jansen, L. (2000). "Response Evaluation and Modification of Typical Bridges in the Central and Southwester United States," *Proc. of the 12th World Conference on Earthquake Engineering*.

DIS, Inc. (2000). "Loma Prieta Earthquake," *www.dis-inc.com/lomaprie.htm*.

Dyke, S.J., Spencer Jr., B.F., Quast, P. and Sain, M.K. (1995). "Role of Control-Structure Interaction in Protective System Design," *J. of Engrg. Mech, ASCE*, Vol. 121, No. 2, pp. 322–38.

Dyke, S.J., Spencer Jr., B.F., Quast, P., Sain, M.K., Kaspari Jr., D.C. and Soong, T.T. (1996a). "Acceleration Feedback Control of MDOF Structures," *J. of Engrg. Mech., ASCE*, Vol. 122, No. 9, pp. 907–918.

Dyke, S.J., Spencer Jr., B.F., Quast, P., Kaspari Jr., D.C., and Sain, M.K. (1996b). "Implementation of an AMD Using Acceleration Feedback Control," *Microcomputers in Civil Engrg.*, Vol. 11, pp. 305–323.

Dyke, S.J., Spencer Jr., B.F., Sain, M.K. and Carlson, J.D. (1996c). "Seismic Response Reduction Using Magnetorheological Dampers." *Proc. of the IFAC World Congress*,

San Francisco, CA, June 30–July 5.

Dyke, S.J., Spencer Jr., B.F., Sain, M.K. and Carlson, J.D. (1996d). "Modeling and Control of Magnetorheological Dampers for Seismic Response Reduction," *Smart Materials and Structures*, Vol. 5, pp. 565–575.

Dyke, S.J., Spencer Jr., B.F., Sain, M.K., and Carlson, J.D. (1996e). "Experimental Verification of Semi-Active Structural Control Strategies Using Acceleration Feedback," *Proc. of the 3rd Intl. Conf. on Motion and Vibr. Control*, Vol. 3, pp. 291–296, Chiba, JAPAN, September.

Dyke, S.J. and Spencer Jr. B.F. (1996). "Seismic Response Control Using Multiple MR Dampers," *Proc. of the 2nd Intl. Workshop on Struc. Control*, Hong Kong, pp. 163–173.

Dyke, S.J. and Spencer Jr. B.F. (1997). "A Comparison of Semi-Active Control Strategies for the MR Damper," *Proc. of the IASTED Intl. Conf. on Intelligent Info. Systems*, pp. 580–584, Bahamas, December 8–10.

Dyke, S.J., Spencer Jr., B.F., Sain, M.K., and Carlson, J.D. (1998). "An Experimental Study of MR Dampers for Seismic Protection," *Smart Materials and Structures: Special Issue on Large Civil Structures*, Vol. 7, pp. 693–703.

Dyke, S.J. Yi, F., Frech, S., and Carlson, J.D. (1999). "Application of Magnetorheological Dampers to Seismically Excited Structures," *Proc. of the Intl. Modal Anal. Conf.*, Kissimmee, Florida, February 8–11.

EQE (1999). "An EQE Briefing - 1999 Izmit, Turkey Earthquake (M7.4)," *www.eqe.com*.

Feng, Q., and Shinozuka, M. (1990). "Use of a variable Damper for Hybrid Control of Bridge Response Under Earthquake," *Proc., U.S. Nat. Workshop on Struct. Control Res.*, USC Publ. No. CE-9013, pp. 107-112.

Feng, Q., Shinozuka, M., Fujii, S., and Fujita, T. (1991). "A Hybrid Isolation System for Bridges," *Proc., 1st US-Japan Workshop on Earthquake Protection Systems for Bridges*, National Center for Earthquake Engineering, Buffalo, NY, pp. 56-58.

Ginder, J.M., Davis, L.C., and Elie, L.D. (1996). "Rheology of Magnetorheological Fluids: Models and Measurements," *International Journal of Modern Physics B*, Vol. 10, Nos. 23 & 24, pp. 3293-3303.

Gordaninejad, F., Saiidi, M., Hansen, B.C., and Chang, F. K. (1999). "Magnetorheological Fluid Dampers for Control of Bridges," *Proc. of the Second World Conference on Structural Control*, Kyoto, Japan, pp. 991-1000.

Housner, G.W., Bergman, L.A., Caughey, T.K., Chassiakos. A.G., Claus, R.O., Masri, S.F., Skelton, R.E., Soong, T.T., Spencer, B.F. and Yao, J.T.P., (1997) "Structural Control: Past, Present, and Future," *J. of Engrg. Mech.*, September, pp. 897–971.

Inaudi, J.A. (1997). "Modulated Homogeneous Friction: A Semi-active Damping Strategy," *Earthquake Engineering and Structural Dynamics,* Vol. 26, No. 3, pp. 361.

Jansen, L.M. and Dyke, S.J. (1999). "Investigation of Nonlinear Control Strategies for the Implementation of Multiple Magnetorheological Dampers," *Proceedings of the 1999 ASCE Engineering Mechanics Conference,* Baltimore, Maryland, June 16, 1999.

Jansen, L.M. and Dyke, S.J. (2000). "Semi-Active Control Strategies for MR Dampers: A Comparative Study," *J. Engrg. Mechanics*.

Kamath, G.M, and Wereley, N.M. (1995). "Distributed Damping of Rotocraft Flexbeams Using Electrorheological Fluids," *Proc. of the AIAA/ASME Adaptive Structure Forum*, New Orleans, Louisiana, April 13-14.

Kamath, G.M, Hurt, M.K., and Wereley, N.M. (1996). "Analysis and Testing of Bingham Plastic Behavior in Semi-Active Electrorheological Fluid Dampers," *Smart Materials and Structures,* Vol. 5, pp. 576-590.

Kamath, G.M, and Wereley, N.M. (1997a). "A Nonlinear Viscoelastic-Plastic Model for Electrorheological Fluids," *Smart Materials and Structures,* Vol. 6, No. 3.

Kamath, G.M, and Wereley, N.M. (1997b). "System Identification of Electrorheological Fluid-Based Dampers Using a Nonlinear Viscoelastic-Plastic Phenomenological Model," *Proc. of the AIAA Aerospace Sciences Conference*, Reno, Nevada, January 6-7.

Kamath, G.M., Wereley, N.M., and Jolly, M.R. (1997). "Analysis and testing of Model-Scale Magnetorheological Fluid Helicopter Lag Mode Damper," *Proc. of the American Helicopter Society 53rd Annual Forum,* Virginia Beach, Virginia, April 29 - May 1, Vol 53/V2.

Karnopp, D.C., Crosby, M.J., and Harwood, R.A. (1974). "Vibration Control Using Semi-Active Force Generators," *ASME Journal of Engineering for Industry*, Vol. 96, No. 2, May.

Kawashima, K. et al. (1991). "Current Research for Passive and Active Control of Highway Bridges Against Earthquake," *23rd joint meeting of US-Japan panel on wind and seismic effect,* U.J.N.R., Tsukuba, Japan.

Kawashima, K. et al. (1992). "Effectiveness of the Variable Damper for Reducing Seismic Response of Highway Bridges Against Earthquakes," *Proc of 2nd US-Japan Work-*

shop on Earthquake Protective Systems for Bridges, PWRI, Tsukuba, Japan, pp. 479-494.

Kawashima, K. and Unjoh, S. (1994). "Seismic Response Control of Bridges by Variable Dampers," *Journal of Structural Engineering*, ASCE, Vol. 120, No. 9, pp. 2583-2601.

Leitmann, G. (1994). "Semiactive Control for Vibration Attenuation," *J. of Intelligent Material Systems and Structures*," Vol. 5 September, pp. 841–846.

Liu, Y., Gordaninejad, F., Evrensel, C., Wang, X., and Hitchcock, G. (2000). "Semi-active Control of a Two-Span Bridge Using Fields-Controllable Magneto-Rheological Dampers," *Smart Structures and Materials 2000: Smart Systems for Bridges, Structures, and Highways*, Vol. 3988, pp. 199-206.

MATLAB (1999). The Math Works, Inc. Natick, Mass.

McClamroch, N.H. and Gavin, H.P. (1995). "Closed Loop Structural Control Using Electrorheological Dampers," *Proc. of the Amer. Ctrl. Conf.*, Seattle, Washington, pp. 4173–77.

Nagarajaiah, S., Riley, M., Reinhorn, A, and Shinozuka, M. (1992). "Hybrid Control of Sliding Isolated Bridges," *Proc. of 1992 Pressure Vessels and Piping Conf.*, ASME/ PVP-237, American Society of Mechanical Engineers (ASME), New York, NY, Vol. 2, pp. 83-89.

Nagarajaiah, S., Riley, M., and Reinhorn, A. (1993). "Control of Sliding-Isolated Bridge with Absolute Acceleration Feedback," *Journal of Engineering Mechanics*, ASCE, Vol. 119, No. 11, pp. 2317-2332.

Nagarajaiah, S., Sahasrabudhe, S., and Iyer, R. (2000). "Seismic Response of Sliding Isolated Bridges with MR Dampers," *Proc. of the Amer. Ctrl. Conf.*, Chicago, Illinois, June 2000, pp. 4437-4441.

Rainbow, J. (1948). "The Magnetic Fluid Clutch," *AIEE Transactions*, vol. 67, pp. 1308-1315.

Ramallo, J.C., Johnson, E.A., Spencer, B.F. Jr., and Sain, M.K. (2000). "Smart Base Isolation Systems," *Proceedings of the ACSE Structures Congress*, Philadelphia, PA.

Reinhorn, A.M., Nagarajaiah, S., Riley, M.A., and Subramanian, R. (1993a). "Hybrid Control of Sliding Isolated Structures," *Structural Engineering in Natural Hazards Mitigation*, A.H. Ang and R. Villaverde (ed.), Vol. 1, ASCE Structures Congress '93, Irvine, CA, pp. 766-771.

Reinhorn, A.M., Nagarajaiah, S., Subramanian, R., and Riley, M.A. (1993b). "Study of Hybrid Systems for Structural and Nonstructural Systems," *Proc. of Int. Workshop on Structural Control*, G.W. Houser and S.F. Masri (ed.), Honolulu, HI, pp. 405-416.

Riley, M.A., Nagarajaiah, S., and Reinhorn, A.M. (1992). "Hybrid Control of Absolute Motion in Aseismically Isolated Bridges," *Proc. of 3rd NSF Workshop on Bridge Engrg. Res.*, University of California, San Diego, CA, pp. 239-242.

Sack, R.L. and Patten, W. (1994). "Semiactive Hydraulic Structural Control." *Proceedings of the International Workshop on Structural Control*, USC Publication Number CE-9311, pp. 417–431.

Sack, R.L., Kuo, C.C., Wu, H.C., Liu, L. and Patten, W.N. (1994). "Seismic Motion Control via Semiactive Hydraulic Actuators." *Proc. of the U.S. Fifth National Conference on Earthquake Engineering*, Chicago, Illinois, Vol. 2, pp. 311–320.

SIMULINK. The Math Works, Inc. Natick, Mass.

Spencer Jr., B.F., Dyke, S.J., and Deoskar, H.S. (1997a). "Benchmark Problems in Structural Control-Part I: Active Mass Driver System," *Proc. of the ASCE Struc. Cong. XV*, Oregon.

Spencer Jr. B.F., Carlson, J.D., Sain, M.K., and Yang, G. (1997b). "On the Current Status of Magnetorheological Dampers: Seismic Protection of Full-Scale Structures," *Proc. of the Amer. Control Conf.*, pp. 458–62.

Spencer Jr., B.F., Dyke, S.J., Sain, M.K., and Carlson, J.D., (1997c). "Phenomenological Model for Magnetorheological Dampers, "*Journal of Engineering Mechanics*, ASCE, Vol. 123, No. 3, pp 230-238.

Spencer Jr., B.F. and Sain, M.K. (1997). "Controlling Buildings: A New Frontier in Feedback," *IEEE Control Systems Magazine: Special Issue on Emerging Technologies* (Tariq Samad Guest Ed.), Vol. 17, No. 6, pp. 19-35.

Spencer, Jr., B.F., Christenson, R.E. and Dyke, S.J. (1998a). "Next Generation Benchmark Control Problem for Seismically Excited Buildings," *Proceedings of the Second World Conference on Structural Control*, Kyoto, Japan, June 29–July 2, pp.1351–1360.

Spencer, Jr. B.F., Dyke, S.J., and Deoskar, H.S. (1998b). "Benchmark Problems in Structural Control: Part I – Active Mass Driver System," *Earthquake Engineering and Structural Dynamics: Special Issue on the Benchmark Structural Control Comparison*, 27, pp. 1127–1139.

Weiss, K.D., Carlson, J.D., and Nixon, D.A. (1994). "Viscoelastic Properties of Magneto-

and Electro-Rheological Fluids," *Journal of Intelligent Material Systems and Structures*, Vol. 5, pp. 772–775.

Symans, M.D. and Constantinou, M.C. (1995). "Development and Experimental Study of Semi-Active Fluid Damping Devices for Seismic Protection of Structures," *Technical Report NCEER-95-0011*.

Wen, Y.K. (1976). "Method of Random Vibration of Hysteretic Systems," *Journal of Engineering Mechanics Division*, ASCE, Vol. 102, No. EM2, pp. 249–263.

Winslow, W.M. (1947). "Method and Means for Translating Electrical Impulses into Mechanical Force," US Patent No. 2,417,850.

Yang, J.N., Li, Z., Vongchavalitkul, S. (1993a). "Hybrid Control of Seismic-Excited Bridge Structures Using Variable Dampers," *Structural Engineering in Natural Hazards Mitigation*, A.H. Ang and R. Villaverde (ed.), Vol. 1, ASCE Structures Congress '93, Irvine, CA, pp. 778-783.

Yang, J., Wu, J., Kawashima, K., and Unjoh, S. (1995). "Hybrid Control of Seismic-Excited Bridge Structures," *Earthquake Engineering and Structural Dynamics*, John Wiley & Sons, Ltd., Vol. 24, pp. 1437-1451.

Yi, F. and Dyke, S.J. (2000). "Structural Control Systems: Performance Assessment," *Proc. of the 2000 American Control Conference*, Chicago, Illinois, June 28-30.

Yi, F., Dyke, S.J., Frech, S. and Carlson, J.D. (1998). "Investigation of Magnetorheological Dampers for Earthquake Hazard Mitigation" *Proc. of the 2nd Intl. Conf. on Struc. Control*, Kyoto, JAPAN, June 30–July 2, pp. 349–358.

Yi, F., Dyke, S.J., Caicedo, J.M., and Carlson, J.D. (1999a). "Seismic Response Control Using Smart Dampers," *Proceedings of the 1999 American Control Conference*, San Diego, California, June 23–25, pp. 1022–26.

Yi, F., Dyke, S.J., Caicedo, J.M., and Carlson, J.D. (1999b). "Experimental Verification of Multi-Input Seismic Control Strategies for Smart Dampers," *Journal of Engineering Mechanics* (submitted).

VITA

Laura M. Jansen

EDUCATION

University of Missouri - Rolla, *Rolla, Missouri*, B.S. Civil Engineering (December, 1997)

Washington University, *St. Louis, Missouri*, M.S. Civil Engineering (December, 2000)

PROFFESIONAL EXPERIENCE

Research/Teaching Assistant, **Washington University,** St. Louis, MO, 8/98 - 8/00.

Structural Engineer (EIT), **Larson Engineering of Missouri,** St. Louis, MO, 2/98 - 7/98.

Engineering Intern, **Boeing,** Wichita, KS, Summer 1997.

Construction Intern, **Missouri Dept. of Transportation,** St. Louis, MO, Summer 1996.

PUBLICATIONS

L.M. Jansen and S. J. Dyke, "Semi-Active Control Strategies for the MR Damper: A Comparative Study," *Journal of Engineering Mechanics,*

L. M. Jansen and S. J. Dyke, "Investigation of Nonlinear Control Strategies for the Implementation of Multiple Magnetorheological Dampers," *Proceedings of the 1999 ASCE Engineering Mechanics Conference*, Baltimore, Maryland, June 13-16, 1999.

L. M. Jansen and S. J. Dyke, "Implications of Control-Structure Interaction in the Scaled Testing of Structural Systems," *Proceedings of the IEEE International Conference on Control Applications*, Hawaii, August 22-27, 1999.

December, 2000